

DTIC FILE COPY

ONR FINAL TECHNICAL REPORT

(2)

AD-A222 752

REPORTING PERIOD: 5 MAY 1985 - 30 APRIL 1988

LIQUID FUELED RAMJET COMBUSTION INSTABILITY:
ACOUSTICAL AND VORTICAL INTERACTIONS WITH BURNING
SPRAYS

J C
STE
8 1990 D

ONR GRANT N000-14-85-K-0658

PREPARED BY:

W.A. SIRIGNANO, PRINCIPAL INVESTIGATOR
R. BHATIA, RESEARCH ASSISTANT
K. MOLAVI, RESEARCH ASSISTANT

DEPARTMENT OF MECHANICAL ENGINEERING
UNIVERSITY OF CALIFORNIA, IRVINE

SUBMITTED TO: DR. GABRIEL D. ROY

15 MAY 1990

DISTRIBUTION STATEMENT A

Approved for public release
Distribution Unlimited

90 06 04 161

REPORT DOCUMENTATION PAGE			Form Approved OMB NO. 0704-0128
<p>Public reporting burden for this collection of information is estimated to be over 1 hour per response, including the time for reviewing instructions, searching existing data sources, gathering and maintaining the data needed, and completing and reviewing the collection of information. Send comments regarding this burden estimate or any other aspect of the collections to Washington Headquarters Services Directorate for Information Operations and Reports, 1215 Jefferson Davis Highway, Suite 1200, Arlington, VA 22202-4217, and to the Office of Management and Budget Paperwork Reduction Project (0704-0128) Washington, DC 20503.</p>			
1. AGENCY USE ONLY (Leave blank)	2. REPORT DATE	3. REPORT TYPE AND DATES COVERED	
	15 May 1990	Final - 5/5/85-4/30/88	
4. TITLE AND SUBTITLE Liquid Fueled Ramjet Combustion Instability: Acoustical and Vortical Interactions with Burning Sprays		5. FUNDING NUMBERS G - N000-14-85-K-0658	
6. AUTHOR(S) W.A. Sirignano, Principal Investigator R. Bhatia, Research Assistant K. Molavi, Research Assistant			
7. PERFORMING ORGANIZATION NAME(S) AND ADDRESS(ES) Department of Mechanical Engineering University of California, Irvine Irvine, CA 92717		8. PERFORMING ORGANIZATION REPORT NUMBER	
9. SPONSORING/MONITORING AGENCY NAME(S) AND ADDRESS(ES) Dr. Gabriel D. Roy Office of Naval Research, Code 1132P Arlington, VA 22217		10. SPONSORING/MONITORING AGENCY REPORT NUMBER	
11. SUPPLEMENTARY NOTES		DISTRIBUTION STATEMENT A Approved for public release Distribution Unlimited	
12a. DISTRIBUTION / AVAILABILITY STATEMENT Available on request. Contact Dr. W.A. Sirignano, University of California, Irvine		12b. DISTRIBUTION CODE	
13. ABSTRACT (Maximum 200 words) A theoretical/computational study of liquid-fueled ramjet instability has been performed. The roles of droplet vaporization and spray combustion processes have been determined as rate-controlling factors on the performance and stability of combustors. The effects of vaporization, mixing, turbulent transport, and chemical kinetics were evaluated. The impact of variations in geometry, initial droplet size, equivalence ratio, and various numerical factors were determined. The study had four major components: (i) individual droplet studies, (ii) a one-dimensional combustor analysis, (iii) a planar combustor study, and (iv) an axisymmetric study. A predictive capability was developed. Vaporization processes and droplet trajectories were found to affect performance and stability significantly.			
14. SUBJECT TERMS Combustion instability, liquid fuel ramjet (T&S)			15. NUMBER OF PAGES 96 16. PRICE CODE
17. SECURITY CLASSIFICATION OF REPORT Unclassified	18. SECURITY CLASSIFICATION OF THIS PAGE Unclassified	19. SECURITY CLASSIFICATION OF ABSTRACT Unclassified	20. LIMITATION OF ABSTRACT SAR

Contents

Abstract	1
I. Introduction	2
II. Technical Discussion	4
A. Oscillatory Droplet.....	4
B. One-Dimensional, Oscillatory, Liquid-Field Ramjet Model.....	9
C. Planar Configuration of Dump Combustors.....	15
D. Axisymmetric Configurations of Dump Combustors.....	25
III. Major Conclusions	40
IV. References	41
V. Appendices	45
A. Publications Resulting from Program.....	45
B. Personnel or Participating Professionals.....	46
C. Degrees Awarded.....	46

STATEMENT "A" per Dr. Gabriel Roy
ONR/Code 1132P
TELECON 6/8/90

VG

Accession For	
NTIS	CRA&I <input checked="" type="checkbox"/>
DTIC	TAB <input type="checkbox"/>
Unannounced <input type="checkbox"/>	
Justification	
By <i>per call</i>	
Distribution /	
Availability Codes	
Dist	Aval and/or Special
A-1	

Abstract

A theoretical/computational study of liquid-fueled ramjet instability has been performed. The roles of droplet vaporization and spray combustion processes have been determined as rate-controlling factors on the performance and stability of combustors. The effects of vaporization, mixing, turbulent transport, and chemical kinetics were evaluated. The impact of variations in geometry, initial droplet size, equivalence ratio, and various numerical factors were determined. The study had four major components: (i) individual droplet studies, (ii) a one-dimensional combustor analysis, (iii) a planar combustor study, and (iv) an axisymmetric study. A predictive capability was developed. Vaporization processes and droplet trajectories were found to affect performance and stability significantly.

I. Introduction

A three year effort on a theoretical/computational study of liquid-fueled ramjet instability has concluded. The general objective was to determine the role of fuel droplet vaporization and spray combustion processes as controlling factors on the performance and stability of liquid-fueled ramjets. The effects of vaporization, mixing, turbulent transport, and chemical kinetics were evaluated and their individual and relative importance were determined. Effects of geometry, initial droplet size, and equivalence ratio were examined. The impact of various numerical factors were also determined. The study continued various tasks that are reported in the next section.

A study of individual droplet behavior under oscillatory conditions and the development of improved droplet models are discussed in Section IIA. It is shown that droplet vaporization can oscillate with the proper phase and amplitude to drive combustion instability.

In Section IIB, a one-dimensional model of an oscillatory ramjet combustor is presented. Vaporization is found to be rate-controlling and a very strong correlation between the period of oscillation and the characteristic droplet heating time is found. This supports the results of Section IIA.

In Section IIC, planar combustor configurations are analyzed. Turbulent mixing and transport tend to become the slower processes. Furthermore, numerical errors tend to exaggerate the importance of mixing as a controlling factor. Vaporization is still found to be important in predicting the local mixture ratio and temperature.

Axisymmetric configurations are studied in Section IID. Vaporization is more important than it was for planar configurations; efficiencies tend to be higher on account of faster mixing. As a

result of higher efficiencies and greater energy release, the axisymmetric cases tend to have higher amplitude oscillations.

Major conclusions are presented in Section III. Lists of publications, personnel, and degrees awarded are presented in Appendices A,B, and C, respectively.

II. Technical Discussion

A. Oscillatory Droplet Vaporization

This section describes the part of the program related to the development of liquid fuel droplet vaporization models. During the 1960's and early 70's attempts were made to understand the role of fuel droplet heating and vaporization in the liquid propellant rocket combustion instability. These efforts are detailed in Harrje and Reardon (1972). During this period, no final conclusions regarding the plausibility of the unsteady vaporization process as a driving mechanism for combustion instability could be reached. A major reason was that during the early years the transient heating and vaporization of the liquid droplets was not well understood.

Since then the theory of single droplet vaporization has been intensively developed. Detailed discussions on the subject may be found in the reviews by Sirignano (1983), Law (1982) and Faeth (1977). The classical droplet vaporization model is described in many textbooks, e.g. Williams (1985). This model is based on many over-simplifications. Recently, there have been several detailed computational studies of a single droplet vaporizing into a hot gas flow, e.g. Renksizbulut and Yuen (1983), Patnaik, et. al. (1986), Chiang, Raju and Sirignano (1989), etc. However, advanced numerical models cannot be directly adopted for spray combustion calculations primarily due to the great computational time associated with a single droplet calculation. This necessitates development of a comprehensive droplet vaporization model that is sufficiently accurate for spray combustion calculations - in particular for application to combustion instability analysis. This has been the general objective of the recently completed work. In particular, in extending the classical droplet vaporization model, the effects associated with gas-phase convection, non-unitary gas-phase Lewis

number, variable thermophysical properties, internal circulation and transient heating of the droplet, Stefan flow, etc., are considered.

A ‘film theory’ based approach has been used by Abramzon and Sirignano (1987, 1989) to analyze the gas-phase. To describe the liquid-phase, Hill’s vortex solution alongwith two-dimensional energy conservation equation is employed. Also, a one-dimensional ‘effectiv. conductivity’ model is proposed. This approach simplifies the calculation procedure for internally circulating droplets by enabling transient liquid heating to be studied by a one-dimensional energy equation, making use of an effective liquid conductivity value: $k_{eff}/k_l = \chi = 1.86 + 0.86 \tanh \{2.245 \log_{10}(Pe_l/30)\}$, where Pe_l is the liquid Peclet number. This relation is shown in Figure A-1. The factor χ varies in the range of 1 to 2.72.

The following results refer to the standard cases on n-decane droplets of initial radius $r_0 = 50\mu m$, and temperature $T_0 = 300K$, which are injected into an air stream at $T_\infty = 1500K$ and $P_\infty = 10 atm$. In Figures A-2 to A-4, the dynamic and vaporization history of the droplet is illustrated for the case when the droplet with the initial velocity of 15 m/s is inserted into a quiescent air enviroment. The initial Reynolds number for the gas-phase is 105. In these figures, the curve 1 denotes the solution from the extended (two-dimensional) model, curves 2 and 3 refer to ‘infinite conductivity’ and ‘conduction limit’ models, respectively. Curve 4 represents the ‘effective conductivity’ model. Figure A-2 to A-4 show the temporal variation of the non-dimensional droplet radius, surface temperature and the instantaneous vaporization rate, respectively. As expected, the results for extended model, in general, fall between those for the ‘infinite conductivity’ and ‘conduction limit’ models. Also, the curves for the ‘effective conductivity’ model almost coincide with the extended model. Figure A-5 shows the history of the average Lewis number in the gas film. Initially, when the vapor concentration in the film is low, the Lewis number is much greater than

unity. The parameter ϕ , relating the thermal and mass transfer numbers: $B_T = (1 + B_M)^\phi - 1$ is significantly greater than unity, unlike $\phi = 1$ assumed by the classical theory. Figure A-6 shows the Reynolds numbers in the liquid and gas-phases. The gas-phase number decreases monotonically as the droplet decelerates and its diameter decreases. Figure A-7 shows the liquid Peclet number. For a substantial part of the droplet lifetime, the Peclet number remains very high, indicating that the heat transfer within the droplet is convection dominated.

To further test the proposed ‘effective conductivity’ model, the vaporization history of droplet in fluctuating flow field has been considered. The gas velocity is supposed to vary sinusoidally as: $U_\infty = \bar{U}_\infty + A_u \cos(2\pi ft)$. The results are shown in Figure A-8, which shows the gas and droplet velocities, non-dimensional droplet radius and the vaporization rate as functions of time. Curves 1 and 4 refer to the extended model of liquid heating and ‘effective conductivity model,’ respectively. The vaporization rate is affected considerably by the gas velocity oscillations. The sharp minima in the vaporization rate correspond to times when the relative gas-liquid droplet velocity is zero. Again, the ‘effective conductivity’ model is found to agree very well with the extended model.

As a part of the ONR program, Tong and Sirignano (1989) have examined the response of a vaporizing droplet to oscillating ambient pressure and velocity conditions. The work is based on their droplet vaporization model, Tong and Sirignano (1982), which involves an integral equation formulation and approximate (analytical) solutions with a quasi-steady gas-phase boundary layer assumption. This model is older and less general than the model developed by Abramzon and Sirignano. In particular, it applies only to the situation where droplet Reynolds number is large compared to unity. Both standing and travelling waves have been studied. The oscillatory rates of vaporization of an array of repetitively injected droplets in the combustor is obtained from summation of individual droplet histories. In the frequency range of interest in ramjet combustion

instabilities (100-100 Hz), the droplet lifetime and the period of oscillation are of same order of magnitude. Thus, the behavior of each droplet depends strongly upon the phase point on the pressure cycle at which the injection occurs. In the following results, the droplets are continually injected throughout the pressure cycle. A vaporization rate response function or gain is defined as:

$$G = \int_0^{2\pi} m' p' d\theta / \int_0^{2\pi} p'^2 d\theta, \text{ where } m' \text{ is vaporization rate fluctuation and } p' \text{ is normalized pressure oscillation.}$$

Tong and Sirignano (1989) report four types of calculations: (i) pressure oscillation only, (ii) velocity oscillation only, (iii) pressure and velocity oscillation in phase corresponding to a standing wave, and (iv) pressure and velocity out-of-phase corresponding to a standing wave. Figure A-9 shows case (i) with only pressure oscillation. The response throughout the frequency range is not enough to drive the instability and the response function peaks at about 200 Hz. Figure A-10 shows case (ii). It is found that the sensitivity of the response is seen to be fairly flat above 200 Hz and does not have large enough value to drive instability. Figure A-11 shows the combined sensitivity to pressure and velocity fluctuations that are in phase (case (iii)). The response function peaks at about 200 Hz and is found to be sufficiently large, through a wide range of frequency, to drive the instability. Figure A-12 shows case (iv). The response function is seen to peak at about 100 Hz, where it is marginal as a driving force for instability. At higher frequencies, it cannot drive the instability. Tong and Sirignano have also analyzed sawtooth pressure oscillations, and they obtain results similar to those for sinusoidal analysis.

A few major achievements for this part of the program are summarized below:

1. A simple but sufficiently accurate ‘effective conductivity’ model for droplet vaporization has been developed and tested for a wide range of configurations.

2. The oversimplifications of the classical droplet vaporization have been removed. The new model includes the effects of variable thermophysical properties, non-unitary Lewis number in the gas film, Stefan flow, and droplet internal circulation and transient liquid heating.
3. The model is applicable over a wide range of gas-phase Reynolds numbers, including the situations where the relative gas-droplet velocity changes sign.
4. Effects of oscillating gas pressure and velocity on the droplet vaporization were examined, and it was found that under certain conditions spray vaporization can provide the driving force in combustion instability.

B. One-Dimensional, Oscillatory, Liquid-Fueled Ramjet Model

This section describes the part of the program related to the application of the liquid fuel droplet vaporization model, briefly described in Section A, to analyze ramjet combustion instability with a one-dimensional representation of the combustion chamber. Since the 1970's there has been renewed effort to understand the mechanism of combustion instability in liquid-fueled systems. Amongst these are the efforts of Awad and Culick (1986), Crump et. al. (1986), Yang and Culick (1986), Kailasanath et. al. (1987), Hedge et. al. (1987), etc. The present work is discussed in detail in Bhatia and Sirignano (1990).

The objective of the numerical study is to gain fundamental understanding of the effects of various design parameters on the stability of the combustion process in liquid-fueled ramjets. Spray characteristics, mixture ratio profiles, and combustor geometry are amongst the more interesting parameters investigated. Effort has concentrated on computation of the unsteady solution for the gas and liquid phases, evaluation of the effects of inlet gas velocity perturbations, and the coupling between gas and liquid phases under perturbed conditions.

The physical model studied is a simplified one-dimensional approximation of a ramjet combustion chamber, Figure B-1, in which vaporization and combustion of liquid spray occurs. Monodispersed, monocomponent liquid spray is assumed. The gas-phase is taken as unsteady, subsonic, compressible, and exchanging mass, momentum and heat transfer with the liquid-phase. The basic set of equations in the Eulerian approach includes continuity, momentum, chemical species, energy and an equation of state for the gas phase. The one-dimensional, unsteady, compressible flow is described by Eulerian gas-phase conservation equations, and Lagrangian liquid-phase equations which are based on Abramzon and Sirignano (1989). The gas-phase conservation equations are solved using a

modified Implicit Continuous-fluid Eulerian (ICE) method due to Harlow and Amsden (1971) and Westbrook and Chase (1977). Dirichlet boundary conditions are used at the combustor inlet, and at the outlet Neumann boundary conditions along with the short-nozzle approximation are specified.

Results from several cases covering a wide range of parameters are obtained. In all cases, the approach is to let the combustor start from time $t = 0$ when the first droplet group is injected. After the combustor reaches a steady operating state, the inlet velocity is perturbed by forcing a sinusoidal cycle with an amplitude of $\pm 20\%$ of the mean velocity, beyond which the combustor is free to oscillate.

Several frequencies of the forcing function are used. After one forced cycle of perturbation of the inlet velocity, it is observed that in all cases, the combustor returns to its natural frequency of oscillation. Hence, it is concluded that when the combustor is free to oscillate, the frequency of oscillation is independent of the frequency of the perturbation function, and it is solely determined by the length of the combustor, the droplet size and the overall equivalence ratio. The natural frequency is found to increase with increasing overall equivalence ratio, decrease with increasing droplet radii, and decrease with decreasing length. Also, this frequency is determined to be very near the fundamental acoustic frequency of the combustion chamber. Results for equivalence ratio of 0.3 and 50 cm combustor length are summarized in Table B-1.

At the lower overall equivalence ratio of 0.3 and for combustor length of 50 cm, it has been found that the oscillations, after a cycle of perturbation, dampen and ultimately disappear for lower droplet radii of 15 and 25 μm . Figure B-2 shows temperature, velocity and pressure oscillations at different locations along the length of the combustor, for droplet radius of 25 μm . The oscillations are observed to decay completely (within $\pm 5\%$ of the mean value) in about ten cycles. For the cases of 50 and 75 μm droplets, it is seen that the startup transient oscillations themselves do not

decay completely. In these cases, limit cycle behavior is seen, with the magnitude of oscillations dependent upon droplet size. Figure B-3 shows temperature, velocity, pressure and gas flow rate oscillations for the case of $50 \mu m$ droplets.

On increasing the overall equivalence ratio to 0.5, it is seen that even the previously stable cases (15 and $25 \mu m$ radii droplets) result in weakly oscillating solution, along with 50 , 75 and $100 \mu m$ cases which are again unstable. At an equivalence ratio of 0.7, all the droplet sizes were found to result in strongly unstable solutions. This trend is similar to recent experimental observations of Yu, et. al. (1989).

Also, for the $75 \mu m$ case the presence of a "dark" region is clearly observed, which is convected downstream with the gas velocity, as shown in Figure B-4 which gives temperature and pressure oscillations for an equivalence ratio of 0.3. The dark region indicates the presence of gases at lower temperatures, in accordance with Crocco and Cheng (1956). These are local temperature oscillations (and thus local entropy oscillations) which propagate at the speed of mass motion. The amplitude of the temperature oscillations associated with these waves is very large. Similar behavior to a smaller extent, is observed with $50 \mu m$ droplet radius and to a similar extent with $100 \mu m$ droplet radius at equivalence ratios of 0.5 and 0.7.

These results are summarized in Figures B-5 to 8. These figures map the domains of stable/unstable combustion with the droplet radius, the combustor length and the overall equivalence ratio as the parameters. Figure B-5 shows the domain as determined by the droplet radius and the combustor length. It shows that, on increasing the droplet size for a fixed combustor length, the combustion passes from stable to unstable and back to stable. Also evident is the effect of the combustor length. Table B-1 estimates the characteristic time for droplet heating and thus determines the characteristic frequency corresponding to droplet heating time. On fixing the combustor

length and increasing the droplet radius, the characteristic time associated with the droplet heating increases, and at some intermediate droplet radius range, it matches with the characteristic acoustic period to excite the acoustic modes. At higher droplet radii (75 and $100 \mu m$), the low frequency oscillations begin to get excited and this phenomenon is explained below. The characteristic time associated with the acoustic frequency, $\tau_a \sim L$, and this explains the increase in the stable region on increasing the combustor length. Also shown in Table B-1 and Figure B-5 is the ratio of characteristic times for the oscillations to that for the droplet heating (τ_p/τ_{dh}). For unstable high-frequency cases, $\tau_p/\tau_{dh} \approx 0.15$. This is in agreement with the Tong and Sirignano (1989) calculation.

Figure B-6 shows the domain as determined by the droplet radii and the overall equivalence ratio. The domain for unstable operation becomes larger at higher equivalence ratios, as the overtones get excited. The situation is further complicated by the interaction of the injection frequency. For a fixed rate of injected fuel, the combustion process passes from stable to unstable at lower droplet radii, and again becomes stable at higher droplet radius. Figure B-7 shows the stability limits as a function of the combustor length and the overall equivalence ratio. For a given droplet radius, the combustion passes from stable to unstable region on increasing the equivalence ratio. Figure B-8 isolates the low frequency oscillations from the high frequency ones. The figure shows that the low frequency oscillations are important only in the cases of higher droplet radii. Also shown in the figure is the ratio of characteristic times for residence, taken as $\tau_f = 2L/u_{g,inlet}$, to the droplet heating time. It is inferred that, to excite the low frequency modes, the characteristic time for the liquid droplet heating must correspond to the residence time, or $\tau_f/\tau_{dh} \approx 1.0$.

A few major achievements for this part of the program are summarized below:

1. A one-dimensional model of ramjet combustion instability has been successfully developed.

2. Vaporization is found to be rate controlling. The combustion process can occur in either a stable or unstable mode. In the unstable mode, limit cycle behavior of pressure, temperature, velocity and gas-phase mass flow rate occurs. The magnitude of these limit cycle oscillations is determined by the combustor geometry, spray characteristics and the overall equivalence ratio.
3. Low frequency or entropy oscillations result when the characteristic time for droplet heating is close to that for the gas residence. High frequency oscillations result when the ratio of characteristic time for period of oscillation to droplet heating is close to 0.15.
4. The frequency of free oscillations is very close to the acoustic frequency of the combustor, at lower equivalence ratios. At higher equivalence ratios, overtones are present.
5. The droplet size, for the same equivalence ratio and combustor length, has a profound effect on the combustor stability. A range of droplet radii for which the combustion is unstable is observed. Below and above this range of droplet size no limit cycle behavior is present.
6. Increasing equivalence ratio enlarges the domain of unstable operation. All droplet radii and combustor length cases, in the range of the calculations, are unstable for the equivalence ratio of 0.7.

Table B-1 Frequency comparison for OER = 0.3

r_l (μm)	r.f. ^a frequency (Hz) for lengths (cm)			Frequency corresponding to Droplet Heating Time (Hz)	τ_p/τ_{dh} for lengths (cm)		
	50	100	150		50	100	150
15	820	-	-	1350	1.69	-	-
25	795	405	270	490	0.64	1.25	1.92
50	750	380	255	120	0.16	0.31	0.48
75	755	355	240	55	0.08	0.15	0.26
100	755	350	235	30	0.04	0.09	0.14

^aResonant
fundamental

C. Planar Configurations of Dump Combustors

In this section, the effects of acoustic oscillations on the fuel droplet vaporization and on the combustion process in a dump combustor configuration are studied. The flow field is approximated by a two-dimensional planar geometry and is described by the $k-\epsilon$ turbulence model. The equations are solved implicitly in an Eulerian frame using a Teach-based algorithm. The droplet vaporization rate is prescribed by the Effective Conductivity model (Abramzon and Sirignano, 1989) based on the second order accurate Improved Euler method in a Lagrangian frame of reference (Sirignano, 1986, Abramzon and Sirignano, 1987). The liquid-phase source terms are distributed over the surrounding Eulerian mesh using a second-order-accurate interpolation scheme (Aggarwal et. al., 1983). The short nozzle condition is imposed at the combustor exit. Oscillations with a range of frequencies are superimposed on the inlet velocity and, thereby, different modes of acoustic oscillations are simulated. The interaction between the flow field and the acoustic oscillations are presented for the various modes of oscillations. Initial droplet size, inlet equivalence ratio, and the chamber length are important parameters. Some of the details of this work can be found in a paper presented at an AIAA conference (Molavi and Sirignano, 1988). The derivations of the governing equations and the details of the boundary conditions are presented in the doctoral dissertation of Molavi (1990). Other details are also presented in recent publications (Molavi and Sirignano, 1990a,b).

The general form of the gas-phase equations is given as

$$\begin{aligned} \frac{\partial(\rho\phi)}{\partial t} + \frac{1}{r} \frac{\partial(r\rho u\phi)}{\partial x} + \frac{1}{r} \frac{\partial(r\rho v\phi)}{\partial y} = \\ \frac{1}{r} \left[\frac{\partial}{\partial x} \left(r\Gamma \frac{\partial\phi}{\partial x} \right) + \frac{\partial}{\partial y} \left(r\Gamma \frac{\partial\phi}{\partial y} \right) \right] + S \end{aligned} \quad (C.1)$$

The reaction rate is give by,

$$R' = \min \left\{ A \left(\frac{\rho Y_F}{W_F} \right)^\alpha \left(\frac{\rho Y_O}{W_O} \right)^\beta e^{-\frac{E}{RT}}, \frac{C_R}{W_F} g^{\frac{1}{2}} \left(\frac{\rho c}{k} \right) \right\}$$

A, E, α, β , and C_R are constants. The parameters of the individual equations are presented in

Table C.1. For the planar geometry, $r=1$ in equation (C.1) and in Table C.1. For the axisymmetric case, $r=y$. Figure C.1 presents the configuration to be studied. The corresponding boundary conditions to these equations are presented in Table C.2. The short nozzle boundary condition of Crocco and Sirignano (1966) is employed. The nozzle entrance Mach number was taken to be 0.1. The reaction rate is based on the minimum of the Arrhenius kinetics and the Eddy Breakup model. The parameters of these models are taken from the work by Westbrook and Dryer (1984). The properties of the n-decane (fuel) are recorded in the literature (Abramzon and Sirignano, 1987).

The results are presented for the planar dump combustor configuration. Here, the staggered numerical grid is chosen to have 20 nodes in the axial and 10 nodes in the radial direction. Results for other grid sizes are also presented where the number of nodes are doubled in both directions. The conversion rate is determined by the controlling effects of the chemical kinetics modeled by the Arrhenius rate, or by the turbulent mixing effects from the Eddy Breakup model. Two injection patterns are studied: droplets are injected uniformly over the inlet or equally distanced over half of the inlet, but closer to the dump step. A parametric study is performed for the effects of the inlet equivalence ratio, initial drop sizes, and combustor length on the acoustic properties of the system.

The geometry of Figure C.1 describes planar configurations. Figure C.1 presents also the stream function contours for the nonreacting planar case. The velocity vector is locally tangential to the streamlines, and is shown to be horizontal in this figure. Results are presented where continuous forced oscillation with sinusoidal shape are imposed over the inlet velocity. The frequency of the oscillations is equal to the fundamental mode of the chamber acoustics, while the amplitude is set at eight percent of the local speed of sound. The form of this velocity is as follows:

$$u_{inlet} = u_{inlet,mean} + 0.08a\sin(2\pi\nu_{osc}t)$$

The combustor length is one meter unless otherwise noted.

The simulation of the combusting flow consists of the injection of the droplets at the inlet after the steady-state situation in Figure C.1 is established. Monodisperse droplets are injected as five streams in the axial direction from points in the range of three to five centimeters away from the plane of symmetry. Here, the length of the combustor is five times its height, or one meter. The height of each dump step is a quarter of the combustor's height. With this injection pattern, the fuel is kept close to the recirculation zone. Figure C.1 together with Figure C.7 show the injection location of each characteristic. After the initial injection of the droplets, calculations are performed over a time interval equal to three residence times of the combustor without the superposition of any forced oscillations. The initial injection of the liquid fuel causes an initial rise in the fuel vapor. However, the time lag from the reaction rate causes a delay in the rise of the pressure and the energy field, after which a steady-state condition is achieved. Figure C.2 shows the steady-state results for monodisperse fuel droplets of 25 microns in initial radius, with the equivalence ratio of 1.0. Calculations indicate that, in the cases of the varying equivalence ratios with the drop radius of 25 microns, the combustion efficiency is 23.8 percent for the equivalence ratio of 1.0 and 36.9 percent for the equivalence ratio of 0.5. When the equivalence ratio is fixed at 1.0, the efficiency is 23.9 percent for the case with initial drop radius of 15 microns in radius and 23.5 percent for the radius of 50 microns. The adiabatic flame temperature is about 2850K for these cases. As the efficiency increases, the highest temperatures achieved approach this value. As the size of the droplets decrease, the effect of cooling from the vaporization becomes more pronounced downstream of the recirculation zone. The temperature in the major hot zone, downstream of the recirculation zone, decreases as more fuel vapor is added (i.e., increasing the equivalence ratio or decreasing the initial drop size). The peak temperature in the zone downstream of the inlet increases in these circumstances as the mixture approaches the stoichiometric condition.

To simulate the primary longitudinal mode of the acoustic oscillations, calculations are continued for a duration equal to one residence time of the combustor. Previous cases are repeated, with the inclusion of these oscillations, as shown in Figures C.3 and C.4. In Figure C.3, a comparison is made between the cases corresponding to the inlet equivalence ratios of 0.5 and 1.0 for the fuel droplets of 25 microns in radius. Figure C.4 shows the comparison for cases corresponding to varying droplet sizes and the equivalence ratio of 1.0. Droplets of 15, 25, and 50 microns in radius are considered for this test case. As shown, the overall rate of the combustion is increased near the peak pressure overshoot with decreasing size of the fuel droplets.

Figure C.5 shows the axial pressure, together with the velocity perturbation from the mean value, during the second free oscillation (third cycle) as a function of position along the chamber centerline. The location of the pressure node and the velocity antinode are clearly shown, demonstrating the acoustical nature of the oscillations.

Figure C.6a shows the spatial profile of the normalized overall conversion rate during the steady-state operation for the inlet equivalence ratio of 1.0, drop radius of 25 microns, and the combustor length of one meter. In Figure C.6b, a similar profile is shown where the conversion rate is controlled by Eddy Breakup rate. Clearly, the mixing is rate controlling in the recirculation zone where most of the reaction takes place, and over most of the combustor. On the other hand, chemical kinetics prevails at the inlet of the combustor where a large accumulation of the fuel vapor and oxidizer is present.

The behavior of the different liquid streams that are injected simultaneously during the steady-state calculations are shown in Figure C.7. The path of each stream is shown in Figure C.7a. The droplets which are injected closer to the dump face are deflected more than droplets injected closer to the centerline. However, the droplets paths are different from the streamlines of the flow, and the

droplets maintain a finite Reynolds number in the absence of the gas-phase oscillations. The size history of the sample droplets are presented in Figure C.7b. The lifetime of the droplets tend to vary. Here, those droplets which are injected closer to the recirculation zone, where higher mixing occurs, vaporize sooner than others. It is shown that the D^2 law is not accurate especially during the initial lifetime of the droplets which is characterized by a low rate of vaporization and a high rate of heating. Two distinct characteristic times are observed from the droplet temperature results. A steep rise in the droplet temperature occurs during its early times when most of the mass of the droplet is vaporized, and a slow rise in temperature follows during most of its remaining lifetime. Thirty percent of the mass of the droplets is vaporized during the steep-rise period. Therefore, a model which can predict the transient of the drop vaporization is needed for the correct modeling of this behavior. The droplet Reynolds numbers generally decrease and the magnitude of the droplet velocity vectors generally increase at first and later decrease during the droplet lifetimes.

Figure C.8 shows that the smaller droplets, corresponding to more fuel vapor, result in a greater amplitude of the oscillations. Much of the combustion occurs in the recirculation zone. Therefore, in the region near the inlet of the combustor, and also near the pressure anti-node, more energy is put into the oscillations from the smaller droplets than from the larger ones. For this reason, the amplitude of the pressure oscillations is larger for the smaller droplets.

The mesh size of 20 by 10 nodes was used for the results presented thus far. To see the effect of numerical diffusion, a finer mesh is chosen where 40 nodes in the axial direction and 20 nodes in the radial direction are tried. Figures C.9a, b, and c show the temperature, oxidizer, and fuel mass fraction contours for this case. Droplets are injected across one-half of the inlet closer to the dump step. The efficiency is 34 percent. To see the effect of injection pattern, another case is tried where fuel is injected uniformly over the inlet. Figures C.10a, b, and c show the temperature,

oxidizer mass fraction, and fuel mass fraction contours for this case. The hot zone downstream of the recirculation zone registers higher temperatures compared to the coarse-mesh case, partly due to the resolution of the recirculation zone by the finer mesh. Therefore, numerical diffusion has an effect similar to cooling down the flow. Another potential numerical effect is the reduction of the source term in the concentration gradient fluctuations equation due to the grid coarseness. When mixing is rate-controlling, this reduces the predicted conversion rate. The efficiency of the combustion is therefore underpredicted by the coarse mesh calculations. While 24 percent of the fuel was burned with the coarse mesh, 33 percent of the fuel is consumed over the one meter of the combustor length. The oscillations have larger amplitudes for the finer-mesh calculations. As shown in Figure C.10, the hot zone downstream of the combustor inlet also becomes more pronounced in this case. As the hot temperature zones form inside the combustor, the production of turbulence increases due to the stress between these and the surrounding colder regions. However, the effect of this mechanism is relatively insignificant over the short length of practical engines.

To study the effect of the nonhomogeneous distribution of fuel on the combustion efficiency, a case has been tried where only three drop streams, uniformly distributed over the inlet, are injected into the solution domain. Figure C.11 presents the temperature contours for this case. As the results clearly show, the hot zone downstream of the inlet has acquired higher temperature and the hot zone downstream of the recirculation zone has moved upstream. Although lower temperatures are registered in the hot zone downstream of the recirculation zone, the overall combustion efficiency is increased by four percent. Now 37 percent of the fuel is burned over the one meter of the combustor length.

A comparison is made with an axisymmetric dump combustor calculation. It is found, in the axisymmetric case, that, as the temperature increases, the mean pressure of the combustor

calculated from the nozzle equations increases. Since the mass flow rate is fixed, the conservation of mass requires that the inlet velocity decrease. It is known (Back and Roschke, 1972) that the reattachment zone at the wall downstream of the recirculation zone is a function of many parameters including the height of the step and inlet velocity. The production term in the governing equation for the turbulent kinetic energy is a function of the velocity gradients. As these gradients become larger, better turbulent mixing is achieved. The fuel entrained in the region downstream of the recirculation zone is completely consumed, while some oxidizer is still left in this region. However, the region in the vicinity of the shear layer, starting at the tip of the dump step, is rich in both the fuel and oxidizer. The largest efficiency was predicted for cases with nonuniform injection of the fuel where only 3 drop streams were considered. The resulting large gradients of the fuel mass fractions caused large production terms for the concentration fluctuations which, in turn, increased the conversion rate based on the Eddy Breakup model. The effect of the ratio of numerical mesh size (in the transverse direction) to spacing between droplet streams is seen to be a very important numerical parameter. For larger values, the mixing rate is underpredicted. Therefore, it is expected that present results generally overpredict the importance of eddy mixing as a rate-controlling factor and thereby underpredict the relative rate-controlling importance of vaporization. The transverse heat and mass diffusion coefficients did not seem to have major effects on the efficiency. The wall cooling in efficient engines is a practical problem. The particular geometry of the cylindrical combustors deserves special attention since, in the case of uniform velocity over the cross section of the combustor, the mass flow rate per unit area increases in proportion to the radius, while in the case of the planar combustors the mass flow rate per unit area is constant with the distance from the centerline. The efficiency of this axisymmetric case is 60 percent; about 30 percent better than the planar case.

From the preceding results, several conclusions can be made regarding the type of flow in the dump combustors. Variations in the initial size of the fuel droplets have pronounced effects over the combustion process and over the whole flow field. Smaller droplets cause an enhancement in the rate of the combustion during the initial transients, when compared to the larger droplets. The increased fuel vapor concentration due to the smaller droplets results in lower peak temperatures, however. An increase in the equivalence ratio has an effect similar to the decrease in the initial droplet size since it results in more fuel vapor.

Droplet heating and vaporization has been shown to be highly transient. The droplets heat up and slow down relative to the gas significantly during the early part of the droplet lifetime. The vaporization rate is faster than the conversion rate or mixing rate; droplet vaporization is completed over a fraction of the combustor length. The vaporization and, therefore, the droplet heating time, are not rate controlling in these cases. The present results consider the low efficiency cases. Accurate modeling of the droplet trajectory and vaporization rate is required to predict the local fuel vapor concentration.

When acoustical oscillations are excited, they tend to damp. Damping is more pronounced in the case of the incomplete combustion over shorter combustor lengths. Oscillations are more pronounced with the finer mesh. While the longer combustor lengths increase the efficiency, smaller drop sizes result in less damping. Larger equivalence ratio results in larger amplitude of oscillations, while concentrating the fuel-injection location near the dump step results in a few percent increase in efficiency.

Table C1: Source Terms for the Gas Phase Equations

Equation	ϕ	Γ_ϕ	Gas Source Terms S_g	Liquid Source Terms $S_l \times (\text{cell volume})$
Continuity	1	0	0	ΣM_l
Axial Momentum	u	μ_{eff}	$-\frac{\partial p}{\partial x} + \frac{\partial}{\partial x}(\Gamma_\phi \frac{\partial u}{\partial x}) + \frac{1}{r} \frac{\partial}{\partial y}(r \Gamma_\phi \frac{\partial u}{\partial x})$	$\Sigma(M_l u_l - M_l \frac{du_l}{dt})$
Transverse Momentum	v	μ_{eff}	$-\frac{\partial p}{\partial y} + \frac{\partial}{\partial y}(\Gamma_\phi \frac{\partial u}{\partial y}) + \frac{1}{r} \frac{\partial}{\partial y}(r \Gamma_\phi \frac{\partial u}{\partial y}) - \Gamma_\phi \frac{\partial v}{\partial x}$	$\Sigma(M_l v_l - M_l \frac{dv_l}{dt})$
Oxidizer Mass Fraction	Y_O	Γ_{eff}	$-s W_O R'$	0
Fuel Mass Fraction	Y_F	Γ_{eff}	$-W_F R'$	ΣM_l
Energy	h	Γ_{eff}	$W_F Q R' + \rho T \frac{D c_p}{D t}$ $- \frac{1}{r} [\frac{\partial}{\partial x} (r \Gamma_\phi T \frac{\partial c_p}{\partial x}) + \frac{\partial}{\partial y} (r \Gamma_\phi T \frac{\partial c_p}{\partial y})] + \frac{D p}{D t}$	$\Sigma M_l (h_l - L_{eff})$
Turbulent Kinetic Energy	k	Γ_{eff}	$G - C_D \rho \epsilon$	0
Dissipation Energy	ϵ	Γ_{eff}	$C_1 \frac{\epsilon}{k} G - C_2 \rho \frac{\epsilon^2}{k}$	0
Concentration Gradient	g	Γ_{eff}	$C_{g1} \mu_{eff} [(\frac{\partial f}{\partial x})^2 + (\frac{\partial f}{\partial y})^2] - C_{g2} \rho g \frac{\epsilon}{k}$	0

$$\mu_{eff} = \mu + \mu_t, \quad \mu_t = C_\mu \rho \frac{k^2}{\epsilon}, \quad \Gamma_{eff,\phi} = \frac{\mu}{\sigma_\phi} + \frac{\mu_t}{\sigma_{\phi,t}}$$

$$G = 2\mu_t [(\frac{\partial u}{\partial x})^2 + (\frac{\partial v}{\partial y})^2 + (\frac{\partial u}{r})^2] + \mu_t (\frac{\partial u}{\partial y} + \frac{\partial v}{\partial x})^2 - \frac{2}{3} \mu_t (\frac{1}{r} \frac{\partial(rv)}{\partial y} + \frac{\partial u}{\partial x})^2$$

C_D	C_1	C_2	C_μ	C_{g1}	C_{g2}
1.0	1.44	1.92	0.09	2.8	2.0

Table C2: Boundary Conditions for the Gas Phase Equations

ϕ	Top Boundary (Duct Wall)	Bottom Boundary (Plane of Symmetry)	Left Boundary		Right Boundary (Outlet)
			Inlet	Duct Face	
u	Law of the Wall	$\frac{\partial u}{\partial y} = 0$		0	$M_a = 0.1$
v	0	0	0	Law of the Wall	$\frac{\partial v}{\partial x} = 0$
Y_O	$\frac{\partial Y_O}{\partial y} = 0$	$\frac{\partial Y_O}{\partial y} = 0$	0.233	$\frac{\partial Y_O}{\partial x} = 0$	$\frac{\partial Y_O}{\partial x} = 0$
Y_F	$\frac{\partial Y_F}{\partial y} = 0$	$\frac{\partial Y_F}{\partial y} = 0$	0	$\frac{\partial Y_F}{\partial x} = 0$	$\frac{\partial Y_F}{\partial x} = 0$
h	Wall Function	$\frac{\partial h}{\partial y} = 0$	$T_{in} c_{p,in}$	Wall Function	$\frac{\partial h}{\partial x} = 0$
k	Wall Function	$\frac{\partial k}{\partial y} = 0$	k_{in}	Wall Function	$\frac{\partial k}{\partial x} = 0$
ϵ	Wall Function	$\frac{\partial \epsilon}{\partial y} = 0$	ϵ_{in}	Wall Function	$\frac{\partial \epsilon}{\partial x} = 0$
g	$\frac{\partial g}{\partial y} = 0$	$\frac{\partial g}{\partial y} = 0$	0	$\frac{\partial g}{\partial x} = 0$	$\frac{\partial g}{\partial x} = 0$
$k_{in} = 0.03(u_{in})^2$, $\epsilon_{in} = \frac{k_{in}^2}{0.005r_{in}}$, $T_{in} = 900K$					

D. Axisymmetric Configurations of Dump Combustors

The geometry, governing equations, and boundary conditions of the problem has been described in Part(C) of this report. The short nozzle assumption is employed at the exit of the combustor, while air at 900K is used as the inlet gas. The walls of the combustor are impermeable and non-slipping. The temperature of the dump wall is set at 900K, while the other walls are isothermal at 800K. The two primary zones downstream of the inlet and the recirculation zone, created by the existence of the dump step, add to the complexity of the problem. Other studies, either numerical or analytical, treat the one-dimensional case where only longitudinal acoustical waves are studied.

Quasi-One-Dimensional Results

A quasi-one-dimensional configuration and an axisymmetric configuration are compared. First, the quasi-one-dimensional case is considered wherein the dump step is removed. An axisymmetric calculation is performed. Here, one of the main sources of the production of turbulence, namely the recirculation zone, is eliminated. The effects of the diffusion terms in the momentum equations on the acoustic damping, as well as overall system behavior, are studied. The effects of the energy release of the combustion on the lifetime of the turbulent eddies and the momentum and continuity equations are also reported. The velocity is uniform over the combustor inlet area. The inlet equivalence ratio is 1.0 and the initial drop radius is 50 microns. The quasi-one-dimensional cases consider only the Arrhenius kinetics and the drops are injected uniformly at an equivalence ratio of 1.0 over the inlet for all cases. Axial velocity is plotted with time at nine centimeters downstream of the inlet in Figure D.1. Here, the combustor length is one meter, and droplets are injected uniformly at the inlet. The primary mode of the acoustics, having a wavelength twice the combustor length, is calculated to have a frequency of 300 hertz for this case. The injection frequency of

the droplets, however, is 1200 hertz. The frequency of the oscillations shown in this figure is also 1200 hertz. A forced oscillation is superimposed over the flow, when it reaches the steady-state condition, and causes an increase in the amplitude of the oscillations in the case of Figure D.1, but it causes an amplitude decrease at some other locations. To resolve the effect of the energy release on the oscillations, cases have been tried where droplets are allowed to vaporize, but no reaction takes place. Two inlet temperatures of 900 and 2000K have been tried. The pressure decreases due to the cooling of the flowfield caused by the vaporization of the droplets. The magnitude of the oscillations due to the injection of the droplets is in the noise level and insignificant in the absence of the energy release from the combustion. The decrease in pressure is more pronounced in the case with the larger temperature. Here, a higher inlet temperature causes the droplets to vaporize faster.

Generally, the numerical accuracy and resolution of the particular numerical method used in solving the governing equations is of importance. The effects of physical and numerical diffusion on the results are studied next. The diffusion terms in the axial momentum equation are examined in these cases. The effective viscosity in this momentum equation is arbitrarily increased and decreased by a factor of 100 in two test cases. The diffusion terms are found to have little effect on the longitudinal oscillations and the convective terms prevail. It is also important to distinguish between the effect of the above physical diffusion terms as opposed to the numerical diffusion that results from the error in the resolution of the convective terms. The above results were obtained for grid sizes of 40 axial nodes by 10 radial nodes. Other studies (Molavi and Sirignano, 1990) are performed to compare the effect of coarse mesh on the calculations. It is shown that the acoustic damping is less for the finer mesh.

A parametric study is performed with 100 nodes in the axial direction by 10 nodes in the radial direction. In this study, the initial radius of the droplets as well as the gas inlet temperature are varied. The inlet equivalence ratio is kept at 1.0, while the initial temperature of the droplets is 300K. The quasi one-dimensional cylindrical configuration is repeated here. The droplets are injected uniformly over the inlet at a frequency of 4800Hz, and only the Arrhenius kinetics are considered in modeling the reaction rate. The results of an analysis of the frequency spectrum are summarized in Table D.1. This parametric study includes the inlet temperature of 1000K with the initial drop radius of 50, 75, and 100 microns, inlet temperature of 900K with drop radius of 25, 50, 75, and 100 microns, and inlet temperature of 800K with the drop radius of 50 microns. The results for the inlet temperature of 900K with the drop radius of 50 microns are presented in Figures D.2 and D.3. In Figure D.2, the centerline velocity is presented in the middle of the combustor. The results of the fourier analysis of the velocity in terms of its frequency spectra is shown in Figure D.3. Axial velocity and pressure for the quasi-one-dimensional cases with the combustor length of one meter are shown in Figures D.4 and D.5 for the initial drop radius of 75 microns. The velocities are shown at the centerline and in the middle of the combustor (velocity antinode) while pressure is taken near the inlet (pressure antinode). In Table D.1, the magnitude and location of the maximum amplitude of the oscillation frequencies for each case are presented. In each entry box, the top number designates the maximum amplitude in units of meters per second, while the lower entry shows the location where that maximum occurred in terms of a fraction of the length of the combustor, measured from the inlet. The largest frequency in the table is the injection frequency. The asterisks represent the absence of certain frequencies for the specified condition.

The primary modes of the acoustics based on the combustor length of 0.5 meter and inlet temperatures of 800K, 900K, and 1000K are calculated to be 570, 600, and 630 hertz, respectively.

In these estimates, a uniform speed of sound based on the inlet temperature is assumed. However, as the combustion occurs at some distance from the inlet, the increase in the gas temperature results in an increase in the average speed of sound. The temperature in the hot zone downstream of the reaction zone can reach as high as 3000K. The size of this hot zone depends on the droplet vaporization rate, which in turn depends on the local gas-phase temperature, the drop size, and the type of fuel. Since the drops are injected uniformly over the inlet, the temperature field in this hot zone is mainly uniform except near the combustor walls where the isothermal condition is established. The primary mode of the acoustics based on the hot zone temperature of 3000K and the combustor length of 0.5 meter is calculated to be 1100Hz. However, two distinct temperature zones are distinguished. The colder zone is at the inlet temperature, while the hot zone is at the maximum temperature of the combustion products. If some spatial averaging is used to calculate the average speed of sound over the combustor length, an intermediate frequency of about 830Hz for the primary mode of the acoustics can be calculated corresponding to the combustor length of 0.5 meter. Results in Table D.1 indicate such a frequency for most of the trial cases. Also, for the inlet temperature of 900K, the largest amplitude for the velocity oscillations occurs for the initial drop size of 50 microns. The location where the maximum amplitude for this frequency occurs is also in the middle of the combustor, the velocity anti-node for the primary acoustic mode of the combustor.

The low frequency of 110Hz is indicated for the cases with the inlet temperature of 900K. Here, entropy waves travel downstream at the convective velocity of the gas, and acoustic waves reflect back upstream from the exit nozzle toward the inlet of the combustor at the speed of sound, perturbing the coupling between the liquid and gas phases and causing new entropy waves to travel downstream. These entropy waves are shown clearly in Figure D.2. At frequencies of 1000Hz and

higher, the amplitudes of the oscillations are generally greater for the smaller drops. It is shown that, at the injection frequency, the smaller drops have the largest amplitude of the oscillations. At this frequency, as the initial size of the droplets decreases, the location of the maximum amplitude of the frequencies moves closer to the inlet, since the smaller droplets vaporize at a faster rate. Since some of the higher frequencies can be the subharmonics of the injection frequency and, thus, have a numerical origin, a case is tried with a different injection frequency. Both the two rightmost columns in Table D.1 represent the cases with the initial drop radius of 50 microns and inlet temperature of 800K. The injection frequency of the column to the right is 3000Hz, while the injection frequency for its adjacent column is 4800Hz. Although differences appear between the observed frequencies for these two different injection frequencies, many frequencies are common between these two cases.

Table D.2 presents the results of another parametric study. The gas inlet temperature is set at 900K, while the combustor lengths of 0.5 and 1.0 meter are studied with the initial drop radius of 25, 50, 75, and 100 microns. The fundamental acoustic mode for the combustor length of 0.5 meter is 830Hz, while the frequency of 500Hz is the fundamental acoustic mode for the combustor length of 1.0 meter. It is shown that the amplitude of oscillations is maximum for the drop size of 50 microns for the shorter length. The maximum oscillations for the greater length, however, occurs at a drop size of 75 microns. Therefore, some sensitivity to the droplet sizes is apparent with respect to the varying length of the combustor. The amplitude of oscillations is very small for the combustor length of 1.0 meter and the drop size of 100 microns. This value, therefore, does not appear in the table. The existence of the entropy waves (110Hz, 140 Hz) are more apparent for the shorter combustor lengths. The amplitude of the oscillations are also larger for the shorter lengths.

Vaporization becomes a controlling factor as the initial size of the droplets increase. Smaller droplets vaporize near the inlet. However, larger droplets may traverse a large fraction of the

combustor length before they vaporize completely. The combustion zone varies with varying initial size of the droplets. This effect profoundly influences the behavior of the overall flow field. The acoustic behavior of the system can also change depending on the location of the energy release from the combustion relative to the pressure nodes of the acoustic modes of the chamber.

A one-dimensional computational study on the combustion instability in the ramjets has been reported in Section B (also see Bhatia and Sirignano, 1990). Although the lateral mixing can not be studied in such a one-dimensional configuration, second-order accuracy is achieved by central differencing of the governing equations. Therefore, damping is less for those results. Here, the instability is shown to be more at the drop radius of 50 to 75 microns for different combustor lengths and equivalence ratios, which compares favorably with the present results. Also, longer combustors show a tendency to become more unstable at bigger initial drop radius. This is also confirmed in the present quasi-one-dimensional results. The range of the observed frequencies for the shorter combustors is wider than for the larger combustors.

Results for Axisymmetric Dump Combustor

To obtain a qualitative comparison between the quasi-one-dimensional and the two-dimensional situations, a parametric study is performed with variations in the combustor length and the initial drop size. There is a dump step in the two-dimensional, axisymmetric configurations. The uniform grid consists of 100 nodes in the axial direction and 20 nodes in the radial direction. The inlet gas temperature is fixed at 900K, and the height of the dump step is half of the radius of the combustor. The combustor diameter is 20 centimeters, and the droplets are injected uniformly at the inlet. To study the effect of the energy release and efficiency on the combustion instability, two distinct cases are considered. Table D.3 presents the results for cases where only chemical kinetics are considered and the eddy breakup model is not considered, while Table D.4 presents the considerations of both

the turbulent mixing and the chemical kinetics. Efficiencies are higher for cases in Table D.3, than for the cases in Table D.4. Details about efficiencies are presented in Table D.5. The injection frequency for all these cases is 4800Hz. Vaporization is shown to be controlling for the results presented in Table D.5. As the initial size of the droplets increase, longer distances are traversed during the lifetime of the droplets. Since the vaporization of the largest droplets occurs over longer distances, the efficiency decreases. Changes in efficiency affect the acoustical behavior of the system. It is shown that as the efficiency increases, new frequencies appear in the frequency spectrum of like drop sizes and combustor lengths. Generally, an increase in the amplitude of the oscillations is also apparent as frequency increases. The fundamental mode of the acoustics without the eddy breakup model is 220Hz for the combustor length of 2.0 meters, and 410Hz for the 1.0 meter long combustors. The amplitude of the oscillations peaks at drop size of 75 microns for the longer length, while the same trend is obvious for the shorter combustor lengths. The magnitude of the oscillations, however, is markedly higher for the longer combustors which, as shown by Table D.5, have higher efficiencies.

Because of the lower efficiency, colder temperature fields exist in the cases of Table D.4. As a result, the average speed of sound is also lower for these cases. The fundamental acoustic mode for the cases in Table D.4 is 220 Hz for the combustor length of 2.0 meters and 350Hz for the 1.0 meter long combustors. As presented in this table, the maximum amplitudes occur at the drop size of 50 microns for the longer combustor, and at the 75 micron droplets for the shorter lengths. The presence of the entropy waves is not apparent, since the amplitude of oscillations is very small for these low efficiency cases.

Some of the unstable cases in Tables D.2 through D.4 are presented in Figures D.4 through D.11. Figures D.6 through D.11 correspond to the axisymmetric cases with the dump step included

in the geometry. The combustor length is two meters and only the chemical kinetics are considered in the conversion rates. Figure D.6 presents the axial velocity for the initial drop radius of 100 microns, Figures D.7 and D.8 present the axial velocity and the pressure for the initial drop radius of 75 microns, and Figures D.9 shows the axial velocity for the initial drop radius of 50 microns. Axial velocity and pressure for cases with the consideration of both the chemical kinetics and eddy mixing and with the initial drop radius of 75 microns are shown in Figures D.10 and D.11, respectively.

To study the effects of the geometry and the drop sizes on the combustion efficiency, The efficiency of cases presented in Tables D.1 through D.4 are tabulated in Table D.5. Results are presented for the quasi-one-dimensional cases with different inlet temperatures and drop sizes, and the combustor length of 50 centimeters. Other results pertain to the axisymmetric cases where the effects of the dump step are included in the models. The effects of chemical kinetics alone, and the turbulent mixing along with the Arrhenius kinetics on the combustion are compared for the inlet temperature of 900K and different drop sizes and combustor lengths. All the fuel droplets are vaporized and consumed over the combustor length for the quasi-one-dimensional cases. The distance that the droplets traverse over their lifetime varies slightly according to the inlet temperature. Lower efficiencies, however, are predicted for the two-dimensional cases. Higher temperatures are achieved downstream of the inlet where most of the vaporization occur for cases where only the chemical kinetics are considered in the conversion rates. Only the largest droplets of 100 microns in initial radius need a longer distance (1.1 meters) to vaporize completely for these cases. The efficiency is higher for the smaller droplets. This is due to the short life of these droplets which vaporize closer to the inlet and, in the gas phase, follow the streamlines of the flow field. The path of the fuel droplets in the liquid phase tend to be different from the gas streamlines, since the droplets maintain a Reynolds number greater than zero over most of their life. The lowest efficiency

is predicted for cases with the consideration of the eddy mixing model. The primary combustion zone is downstream of the recirculation zone. However, droplets vaporize mainly in the colder zone downstream of the inlet. Both the vaporization and mixing are important in these cases. Since the rate of the drop vaporization is lower for these cases, droplets larger than 50 microns in their initial radius need a distance longer than 1.0 meter to vaporize completely. The 100 micron droplets vaporize over a distance of more than 2.0 meters.

The conclusions for this group of results can be summarized as follows.

The efficiencies and the amplitudes of oscillation are higher for the finer mesh. The efficiencies are less when the dump step is added. Here, only the chemical kinetics are included in modeling the conversion rates for the case without a step. The Eddy mixing model is considered only in geometries with the dump step, where mixing effects are important. With no mixing delays in the quasi-one-dimensional cases, the Arrhenius kinetics predicts higher rates of conversion.

In the quasi-one-dimensional cases, the shorter combustors demonstrated a larger variety of low-amplitude, high-frequency oscillations. In the two-dimensional cases, many of the higher frequencies dissipated quickly near the combustor inlet for the smaller droplets. The lower frequency oscillations in the longer combustors, however, had larger amplitudes. The injection frequency is more important in the quasi-one-dimensional cases. These frequencies excite several of their subharmonics in the shorter combustors where the fundamental modes are higher. These frequencies dissipated with distance from the inlet in the two-dimensional cases. The larger droplet case required longer distances for dissipation. Only the frequencies corresponding to the entropy waves and to the fundamental modes are observed inside the combustor for the two-dimensional cases.

Although the Eddy breakup model may underpredict the conversion rates and efficiencies, and more accurate model-constants are required for the particular geometries under study, the qualitative features of the flowfield are predicted by this model. Consideration of only the chemical kinetics causes unrealistic prediction of high temperatures downstream of the inlet for the two-dimensional cases.

The physical diffusion, both axial and lateral, has little effect in these high Reynolds number flows.

Vaporization is shown to be controlling, especially for the larger droplets. Tabulated results indicate that the distance that the droplets traverse to vaporize completely varies with the initial size of droplets. The life-time of the larger droplets can be of the same order of magnitude as the residence time of the chamber. Smaller droplets vaporize near the inlet. However, larger droplets may traverse a large fraction of the combustor length before they vaporize completely. The combustion zone varies with varying initial size of the droplets. This effect profoundly influences the behavior of the overall flow field. The acoustic behavior of the system can also change depending on the location of the energy release from the combustion relative to the pressure nodes of the acoustic modes of the chamber.

Table D.1: Magnitude and Location of the Maximum Amplitude of the Oscillations
Quasi-One-Dimensional Chamber, Length=0.5 meter, Equiv. Ratio=1.0

Inlet Temperature, K	1000			900				800	
	Droplet Radius, μ	50	75	100	25	50	75	100	50
Frequency, Hz									
80	***	***	0.1	***	***	***	***	***	***
	***	***	0.8L	***	***	***	***	***	***
110	***	***	***	0.4	0.25	0.27	0.13	***	***
	***	***	***	0.4L	0.3L	0.4L	0.3L	***	***
400	***	***	***	***	***	***	***	0.45	0.6
	***	***	***	***	***	***	***	0.1L	0.3L
500	***	***	***	***	***	***	***	1.0	***
	***	***	***	***	***	***	***	0.3L	***
650	0.8	0.7	0.4	***	***	***	***	***	***
	0.3L	0.3L	0.3L	***	***	***	***	***	***
700	***	***	***	***	***	***	***	0.4	0.5
	***	***	***	***	***	***	***	0.3L	0.3L
830	1.0	0.7	0.24	1.0	1.5	0.6	***	0.5	***
	0.5L	0.4L	0.5L	0.3L	0.5L	0.5L	***	0.5L	***
890	***	***	***	***	***	***	***	0.5	***
	***	***	***	***	***	***	***	0.3L	***
950	***	***	***	***	***	***	***	***	1.1
	***	***	***	***	***	***	***	***	0.5L
1000	0.6	0.25	0.3	1.5	0.9	***	***	***	***
	0.5L	0.4L	0.8L	0.5L	0.6L	***	***	***	***
1150	***	***	***	***	***	***	***	0.4	0.35
	***	***	***	***	***	***	***	0.5L	0.6L
1400	***	***	***	***	***	***	***	***	0.22
	***	***	***	***	***	***	***	***	0.7L
1500	0.5	0.4	0.25	***	***	***	***	***	***
	0.7L	0.2L	0.8L	***	***	***	***	***	***
1650	***	***	***	***	***	***	***	1.4	0.55
	***	***	***	***	***	***	***	0.1L	0.3L
1700	0.8	0.5	0.6	***	***	***	***	***	***
	0.2L	0.2L	0.8L	***	***	***	***	***	***
2100	1.25	0.6	0.3	***	***	***	***	1.4	***
	0.3L	0.5L	0.3L	***	***	***	***	0.1L	***
2190	***	***	***	***	***	***	***	0.9	1.1
	***	***	***	***	***	***	***	0.1L	0.3L
2400	***	***	***	2.0	***	***	0.9	***	***
	***	***	***	0.1L	***	***	0.8L	***	***
2600	***	***	***	***	***	***	***	***	0.85
	***	***	***	***	***	***	***	***	0.2L
2700	0.8	0.4	***	***	0.5	1.4	***	0.85	***
	0.1L	0.1L	***	***	0.2L	0.2L	***	0.2L	***
Inj. Freq. 3000	***	***	***	***	***	***	***	***	6.6
	***	***	***	***	***	***	***	***	0.1L
3100	1.8	1.1	1.0	***	***	***	***	***	***
	0.1L	0.2L	0.8L	***	***	***	***	***	***
Inj. Freq. 4800	8.5	2.9	1.85	18.0	4.6	3.8	1.8	6.5	***
	0.1L	0.2L	0.3L	0.1L	0.1L	0.2L	0.3L	0.1L	***

Table D.2: Frequency Spectrum, Quasi-one-dimensional,
Inlet Temp. = 900K, Equiv. Ratio=1.0

Combustor Length,m	1				0.5			
	Droplet Radius, μ	25	50	75	100	25	50	75
Frequency,Hz								
110	***	***	***	***	0.4	0.25	0.27	0.13
	***	***	***	***	0.4L	0.3L	0.4L	0.3L
140	1.1 0.2L	***	***	***	***	***	***	***
	***	***	***	10.3	***	***	***	***
410	***	***	***	0.5L	***	***	***	***
	***	***	***	0.5L	***	***	***	***
500	1.8 0.6L	16.0	25.0	***	***	***	***	***
	0.5L	0.5L	0.5L	***	***	***	***	***
850	***	0.8	***	***	1.0	1.5	0.6	***
	***	0.2L	***	***	0.3L	0.5L	0.5L	***
1000	***	0.6	2.3	***	1.5	0.9	***	***
	***	0.3L	0.3L	***	0.5L	0.6L	***	***
2400	***	0.7	***	***	2.0	***	***	0.9
	***	0.1L	***	***	0.1L	***	***	0.8L
2700	***	***	***	***	***	0.5	1.4	***
	***	***	***	***	***	0.2L	0.2L	***
4800	13.0	1.2	2.3	1.4	18	4.6	3.8	1.8
	0.1L	0.1L	0.1L	0.1L	0.1L	0.1L	0.2L	0.3L

Table D.3: Frequency Spectrum, Dump Combustor,
Only Arrhenius Kinetics Used, Equiv. Ratio=1.0

Combustor Length,m	2				1		
	25	50	75	100	50	75	100
Droplet Radius, μ							
Frequency,Hz							
220	29.0 0.6L	22.0 0.5L	26.5 0.4L	22.0 0.5L	*** ***	*** ***	*** ***
410	*** ***	*** ***	*** ***	*** ***	1.6 0.5L	4.7 0.3L	3.0 0.6L
500	9.3 0.7L	9.5 0.7L	5.5 0.7L	4.0 0.2L	*** ***	*** ***	*** ***
700	4.0 0.5L	3.0 0.5L	2.5 0.5L	2.8 0.2L	*** ***	*** ***	*** ***
800	*** ***	*** ***	*** ***	*** ***	*** ***	*** ***	1.9 0.7L
900	*** ***	*** ***	*** ***	*** ***	*** ***	0.8 0.7L	*** ***
950	2.0 0.6L	2.0 0.6L	*** ***	2.0 0.4L	*** ***	*** ***	*** ***
2400	*** ***	*** ***	*** ***	*** ***	3.7 0.2L	4.5 0.2L	1.7 0.2L
4800	5.0 0.1L	15.0 0.1L	12.7 0.1L	4.0 0.2L	18.0 0.2L	20.0 0.2L	4.5 0.2L

Table D.4: Frequency Spectrum, Dump Combustor,
Eddy Mixing and Arrhenius Kinetics Considered, Equiv. Ratio=1.0

Combustor Length,m	2				1			
	Droplet Radius, μ	25	50	75	100	50	75	100
Frequency,Hz								
220		3.9	7.5	2.1	0.6	1.3	1.0	***
	0.6L	0.5L	0.3L	0.5L	0.2L	0.1L		***
350	***	***	***	***	***	0.6	0.2	
	***	***	***	***	***	0.6L	0.6L	
500	***	1.4	0.3	***	0.6	***	***	
	***	0.8L	0.5L	***	0.3L	***	***	
4800		0.3	0.2	0.2	0.2	1.4	0.9	0.7
	0.1L	0.1L	0.1L	0.1L	0.1L	0.1L	0.1L	

Table D.5: Combustion Efficiency, Equiv. Ratio=1.0

Axisymmetric Combustor	Inlet Temp, K	Combustor Length,M	Drop Radius, μ	Distance to Vaporize,M	Exiting Radius, μ	Efficiency
Quasi- One- Dimensional	1000	0.5	50	0.135	0	0.99
	1000	0.5	75	0.25	0	0.99
	1000	0.5	100	0.39	0	0.99
	900	0.5	25	0.054	0	0.99
	900	0.5	50	0.14	0	0.99
	900	0.5	75	0.25	0	0.99
	900	0.5	100	0.39	0	0.99
	800	0.5	50	0.14	0	0.99
2-D with Arrhenius Kinetics	900	1.0	50	0.37	0	0.73
	900	1.0	75	0.75	0	0.60
	900	1.0	100	>1.0	47	0.58
	900	2.0	25	0.12	0	0.93
	900	2.0	50	0.35	0	0.80
	900	2.0	75	0.69	0	0.68
	900	2.0	100	1.1	0	0.65
	900	1.0	50	>1.0	25	0.32
Eddy Breakup and Arrhenius Kinetics	900	1.0	75	>1.0	57	0.40
	900	1.0	100	>1.0	83	0.45
	900	2.0	25	0.3	0	0.69
	900	2.0	50	0.92	0	0.64
	900	2.0	75	1.27	0	0.57
	900	2.0	100	>2.0	40	0.60

III. Major Conclusions

The isolated droplets study and the one-dimensional spray combustor study jointly indicate that transient droplet vaporization is rate-controlling and provides a very plausible mechanism for liquid-fueled combustion instability. Droplet heating times do correlate with the time periods of oscillations in unstable situations. These conclusions are generally supported by axisymmetric calculations in the special quasi-one-dimensional case where there is no dump step.

In the planar and axisymmetric cases where a dump step is present, mixing within a turbulent eddy and transport in the transverse direction tends to become significant factors in the control of the conversion rate and in the driving mechanism for the instability. Vaporization is still one of the controlling factors. Initial droplet size also affects droplet trajectories and therefore the local mixtures ratio and conversion rate. Poor resolution of mixing details or (in other words) a large ratio of transverse mesh size to droplet stream spacing tends to underpredict the mixing rate and thereby overpredict its importance in control of the conversion rate. The injection frequency is a numerical factor that can lead to some artificial oscillatory behavior.

In summary, there is very convincing evidence about the important role of transient droplet heating and vaporization in liquid-fueled ramjet instability. As design changes lead to more rapid mixing, comparable with rocket motors or gas turbine combustors, vaporization should become more important compared to turbulent mixing as a rate-controlling factor. Increased computational resources in the future should lead to a decrease in the underprediction of mixing rates.

References

1. Abramzon, B. and Sirignano, W. A., "Approximate Theory of a Single Droplet Vaporization in a Convective Field: Effects of Variable Properties, Stefan Flow and Transient Liquid Heating." *Proc. 2nd ASME-JSME Thermal Eng. Joint Conf.*, Hawaii, Vol. 1, 1987.
2. Abramzon, B. and Sirignano, W. A., "Droplet Vaporization Model for Spray Combustion Calculations," *Int. J. Heat Mass Transfer*, Vol. 32, No. 9, 1989.
3. Aggarwal, S. K., Fix, G. J., Lee, D. N., and Sirignano, W. A., "Numerical Optimization Studies of Axisymmetric Unsteady Sprays," *J. Computational Physics*, Vol. 50, No. 1, April 1983.
4. Awad, E. and Culick, F. E. C., "On the Existence of Stability of Limit Cycles for Longitudinal Acoustic Modes in a Combustion Chamber," *Combustion Sci. and Tech.*, Vol. 46, 1986.
5. Back, L. H., and Roschke, E. J., "Shear-Layer Flow Regimes and Wave Instabilities and Reattachment Lengths Downstream of an Abrupt Circular Channel Expansion," *J. Applied Mechanics*, September 1972, pp. 677-680.
6. Bhatia, R., and Sirignano, W. A., "A One-Dimensional Model of Ramjet Combustion Instability," *AIAA 28th Aerospace Sciences Meeting*, Reno, Nevada, Preprint No. 90-0271, 1990. Submitted to *J. Propulsion and Power*.
7. C. H. Chiang, M. S. Raju and W. A. Sirignano, "Numerical Analysis of Convecting, Vaporizing Fuel Droplet with Variable Properties," *AIAA Aerospace Sciences Meeting*, Paper 89-0834, 1989.
8. Crocco, L. and Cheng, Sin-I, "Theory of Combustion Instability in Liquid Propellant Rocket Motors," *Butterworths Scientific Publications*, 1956.

9. Crocco, L., and Sirignano, W. A., "Effects of the Transverse Velocity Component on the Nonlinear Behaviour of Short Nozzles," *AIAA Journal*, Vol. 4, No. 8, August 1966.
10. Crump, J. E., Schadow, K. C., Yang, V., and Culick, F. E. C., "Longitudinal Combustion Instability in Ramjet Engines: Identification of Acoustic Modes," *J. Propulsion*, Vol. 2, No. 2, 1986.
11. Faeth, G. M., "Current Status of Droplet and Liquid Combustion," *Progress in Energy and Combustion Science*, Vol. 3, 1977.
12. Harlow, F. H. and Amsden, A. A., "A Numerical Fluid Dynamics Calculation Method for All Flow Speeds." *Journal of Computational Physics*, 8, 1971.
13. Harrje D. T. and Reardon, F. A., editors. "Liquid Propellant Rocket Combustion Instability." NASA, 1972.
14. Hedge, U. G., Reuter, D., Daniel, B. R., and Zinn, B. T., "Flame Driving of Longitudinal Instabilities in Dump Type Combustors," *Combustion Sci. and Tech.*, Vol. 55, 1987.
15. Kailasanath, K., Gardner, J. H., Boris, J. P., and Oran, E. S., "Numerical Simulations of Acoustic-Vortex Interactions in a Central-Dump Ramjet Combustor," *J. Propulsion*, Vol. 3, No. 6, 1987.
16. Law, C. K., "Recent Advances in Droplet Vaporization and Combustion," *Progress in Energy and Combustion Science*, Vol. 8, 1982.
17. Molavi, K., "Acoustic Oscillations in the Dump Combustor Configurations," Ph.D Dissertation, Department of Mechanical Engineering, University of California at Irvine, 1990.
18. Molavi, K., and Sirignano, W. A., "Unsteady Ramjet Combustor Computations, Part I. Planar Configuration," to be published, 1990a.

19. Molavi, K., and Sirignano, W. A., "Unsteady Ramjet Combustor Computations, Part II. Axisymmetric Configuration," to be published, 1990b.
20. Molavi, K., and Sirignano, W. A., "Computational Analysis of Acoustic Instabilities in Dumb Combustor Configuration," AIAA/ASME/SAE/ASEE 24th Joint Propulsion Conference, Boston. Massachusetts, Preprint No. 88-2856, 1988.
21. Patnaik, G., Sirignano, W. A., Dwyer, H. A. and Sanders, B. R., "A Numerical Technique for the Solution of a Vaporizing Fuel Droplet," *Dynamics of Reaction Systems, Prog. Astronaut. Aeronaut.*, 105, 1986.
22. Renksizbulut, M. and Yuen, M. C., "Numerical Study of Droplet Evaporation in a High Temperature Stream," *J. Heat Transfer*, 105, 1983.
23. Sirignano, W. A., "Fuel Droplet Vaporization and Spray Combustion Theory," *Progress in Energy and Combustion Science*, Vol. 9, 1983.
24. Sirignano, W. A., "The Formulation of Spray Combustion Models: Resolution Compared to Droplet Spacing," *Journal of Heat Transfer*, Vol. 108, 1986, pp. 633-639.
25. Tong, A. Y. and Sirignano, W. A., "Analytical Solution for Diffusion and Circulation in a Vaporizing Droplet," *19th Symp. Int. on Comb.*, 1982.
26. Tong, A. Y. and Sirignano, W. A., "Oscillatory Vaporization of Fuel Droplet in Unstable Combustor," *J. Propulsion and Power*, Vol. 5, No. 3, 1989.
27. Westbrook, C. K. and Chase, L. L., "A One-Dimensional Combustion Model," *UCRL-52297, Lawrence Livermore Laboratory*, Livermore, 1977.
28. Westbrook, C. K., and Dryer, F. L., "Chemical Kinetic Modeling of Hydrocarbon Combustion," *Prog. Energy Combust. Sci.*, Vol. 10, 1984, pp. 1-57.

29. Williams. F. A., *Combustion Theory*, Benjamin/Cummings, Menlo Park, California, 1985.
30. Yang, V., and Culick, F. E. C., "Analysis of Low Frequency Combustion Instabilities in a Laboratory Ramjet Combustor," *Combustion Sci. and Tech.*, Vol. 46, 1986.
31. Yu, K., Keanini, R., Bauwens, L. and Daily, J., "Low Frequency Pressure Oscillations in a Model Ramjet Droplet Combustor, The Nature of Frequency Selection", *AIAA 27th Aerospace Sciences Meeting*, Reno, Nevada, 1989.

Appendices

A. Publications Resulting from Program

1. Abramzon, B. and Sirignano, W. A., "Approximate Theory of a Single Droplet Vaporization in a Convective Field: Effects of Variable Properties, Stefan Flow and Transient Liquid Heating." *Proc. 2nd ASME-JSME Thermal Eng. Joint Conf.* Hawaii, Vol. 1, 1987.
2. Abramzon, B. and Sirignano, W.A., "Droplet Vaporization Model for Spray Combustion Calculations." *Int. J. Heat Mass Transfer* Vol. 32, No. 9, 1989.
3. Bhatia, R. and Sirignano, W.A.. "A One-Dimensional Model of Ramjet Combustion Instability." AIAA 28th Aerospace Sciences Meeting. Reno, Nevada, Preprint No. 90-0271. 1990. Also submitted to *Journal of Propulsion and Power*.
4. Molavi, K. and Sirignano, W.A., "Unsteady Ramjet Combustor Computations, Part I. Planar Configuration." to be published. 1990a.
5. Molavi, K. and Sirignano, W.A., "Unsteady Ramjet Combustor Computations, Part II. Asymmetric Configuration," to be published , 1990b.
6. Molavi, K. and Sirignano, W.A., "Computational Analysis of Acoustic Instabilities in Dump Combustor Configuration," AIAA/ASME/SAE/ASEE 24th Joint Propulsion Conference, Boston, Massachusetts, Preprint No.88-2856, 1988.
7. Molavi, K., "Acoustic Oscillations in the Dump Combustor Configuration," PH.D Dissertation, Department of Mechanical Engineering, University of California at Irvine, 1990.
8. Tong, A.Y. and Sirignano, W.A., "Oscillatory Vaporization of Fuel Droplet in Unstable Combustor," *J. Propulsion and Power*, Vol. 5, No. 3, 1989.

9. Sirignano, W.A. and Molavi, K., "Spray Combustion Driving Mechanism for Ramjet Instability." presented at the 25th JANNAF Combustion Meeting, Huntsville, AL, October 1988.
10. Bowman, C.T. Law, C.K. and Sirignano, W.A., "Spray Combustion Processes in Ramjet Combustion Instability," presented at the 25th JANNAF Combustion Meeting, Huntsville, AL. October 1988.
11. Sirignano, W.A., Riva, G., Tong, A., Abramzon, B. and Molavi, K., "Spray Combustion: A Driving Mechanism for Ramjet Combustion Instability," 23rd JANNAF Combustion Meeting. Langley, VA, October 1986.

B. Personnel

B. Abramzon. Postdoctoral Researcher

R. Bhatia. Graduate research assistant

K. Molavi, Graduate research assistant

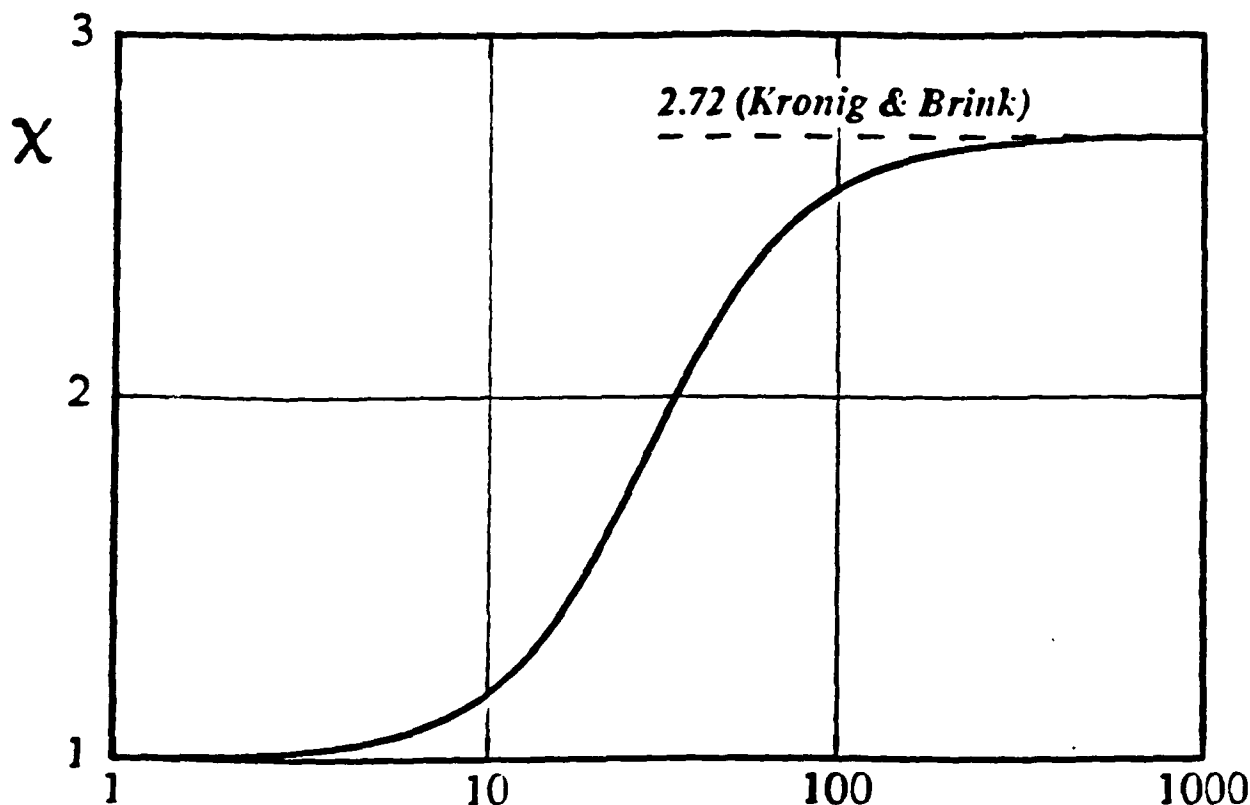
G. Riva, Visiting Researcher

W. A. Sirignano, Principal Investigator

A. Y. Tong, Visiting Faculty

C. Degrees Awarded

K. Molavi, Ph.D. degree 1990



$$\text{Liquid Peclet number, } Pe_L = 2U_s r / \alpha_L$$

Fig. A-1 Effective thermal conductivity factor vs liquid Peclet number.

NONDIMENSIONAL RADIUS

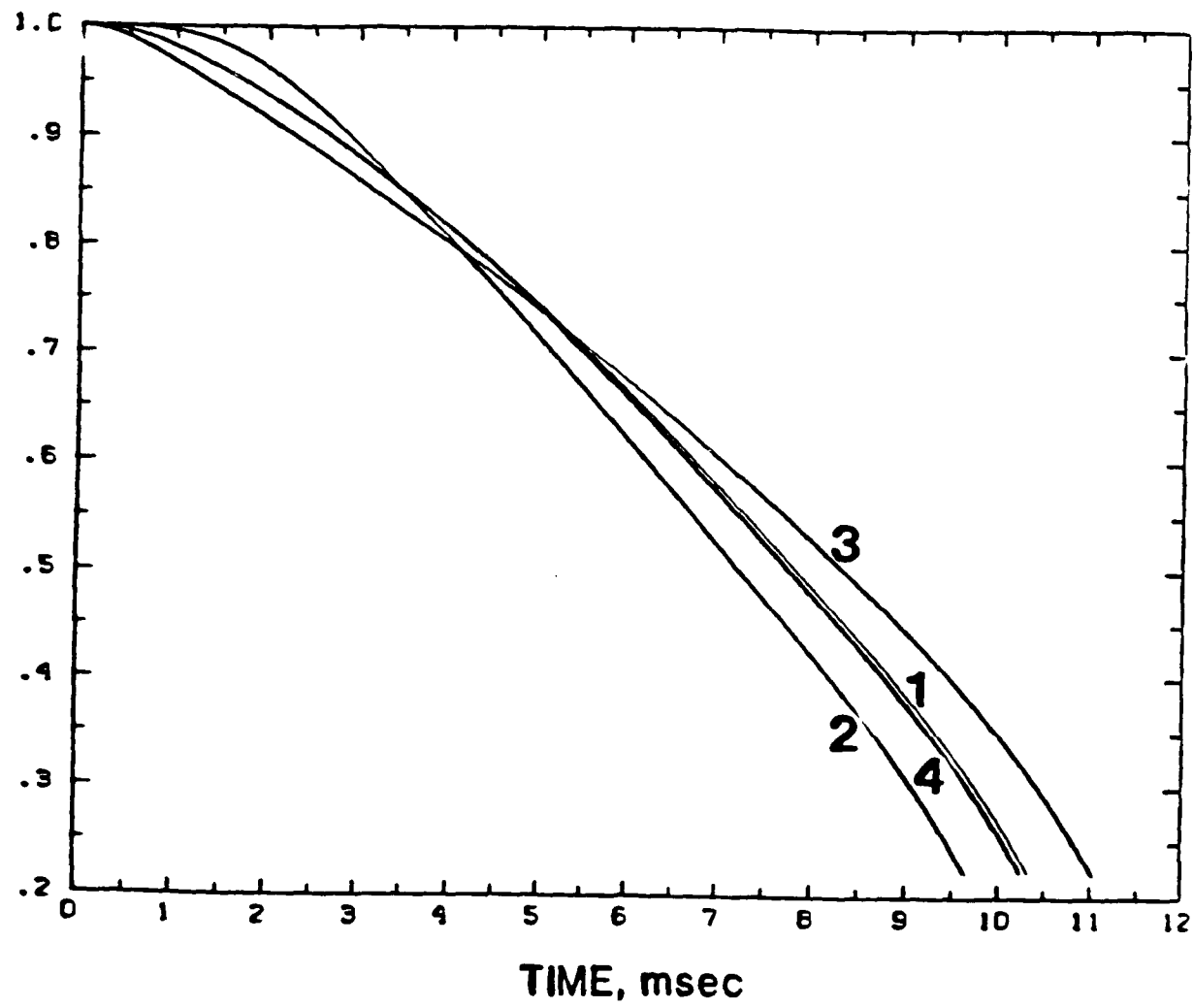


Fig. A-2 Non-dimensional droplet radius vs time: extended model (curve 1), infinite conductivity model (curve 2), conduction limit model (curve 3), and effective conductivity model (curve 4).

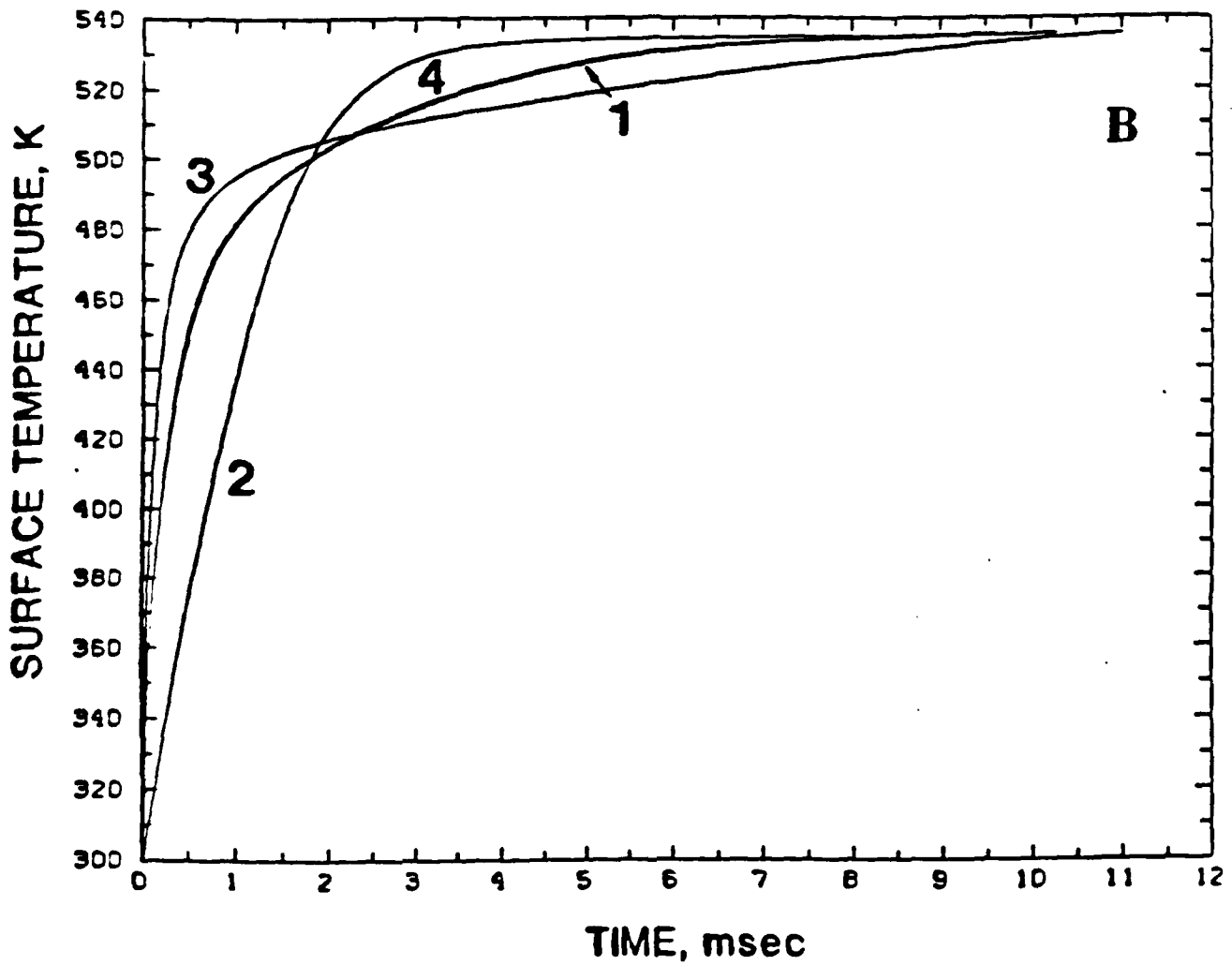


Fig. A-3 Surface temperature (K) vs time: various models.

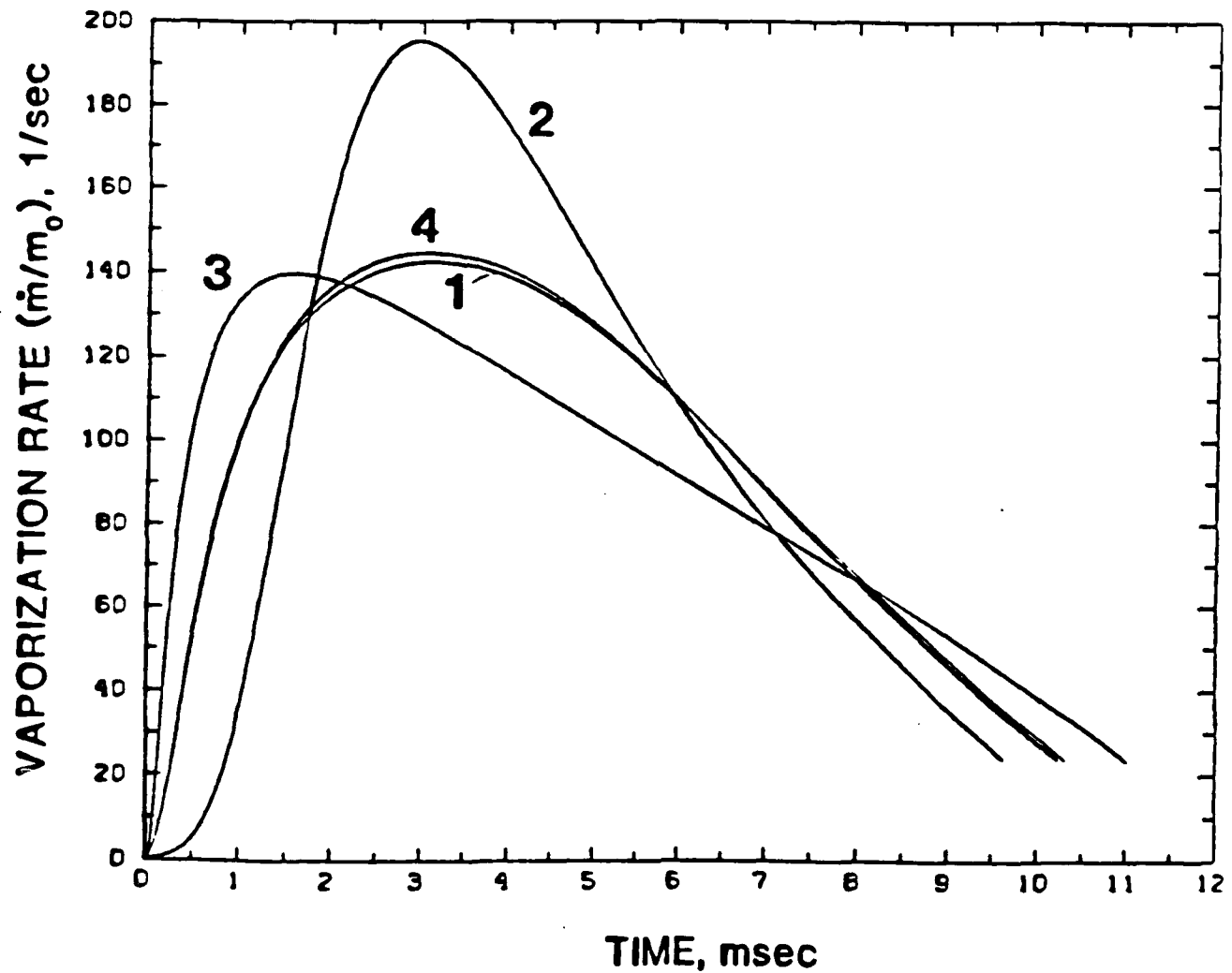


Fig. A-4 Vaporization rate vs time: various models.

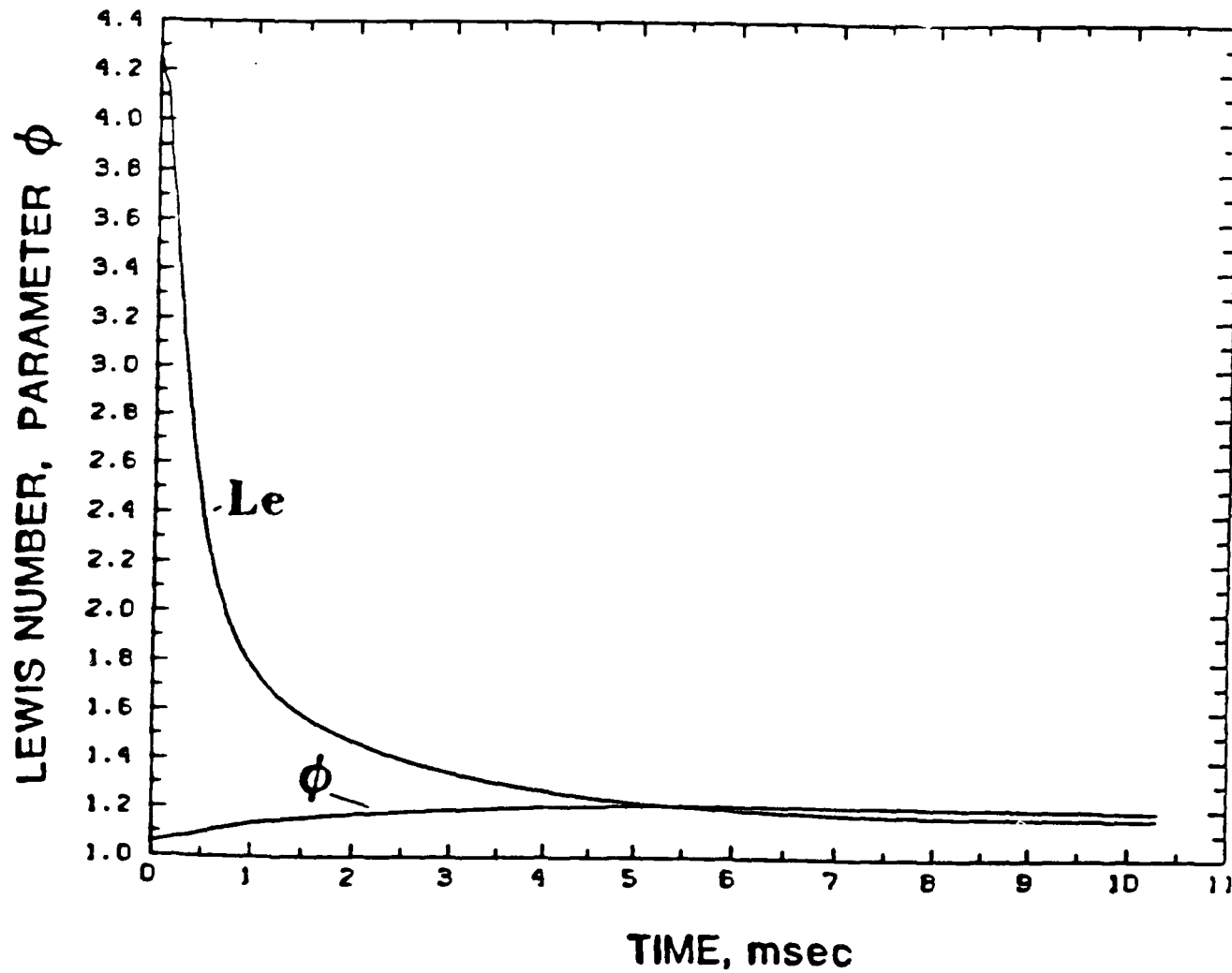


Fig. A-5 Lewis number vs time and parameter ϕ vs time.

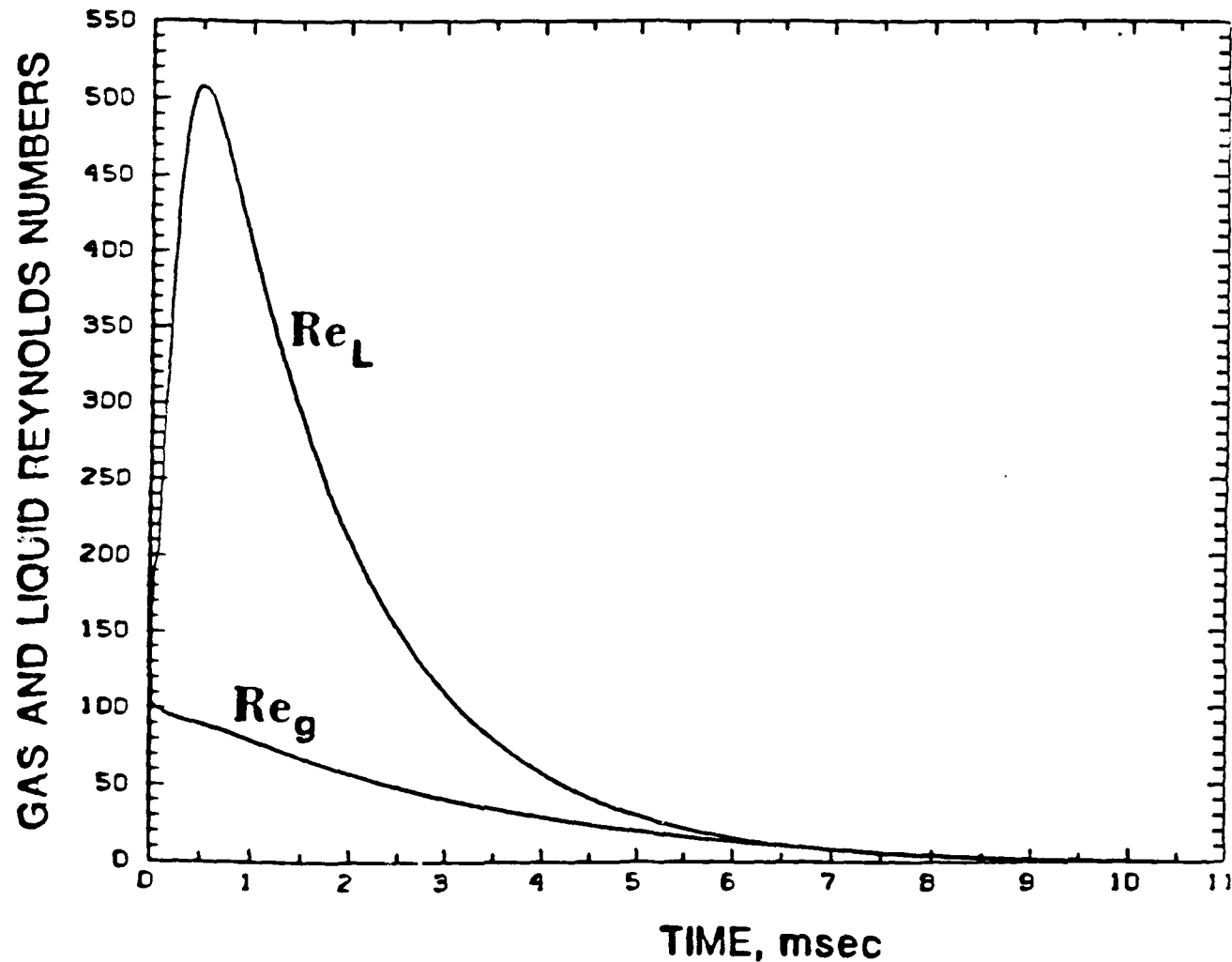


Fig. A-6 Gas and liquid Reynolds numbers vs time.

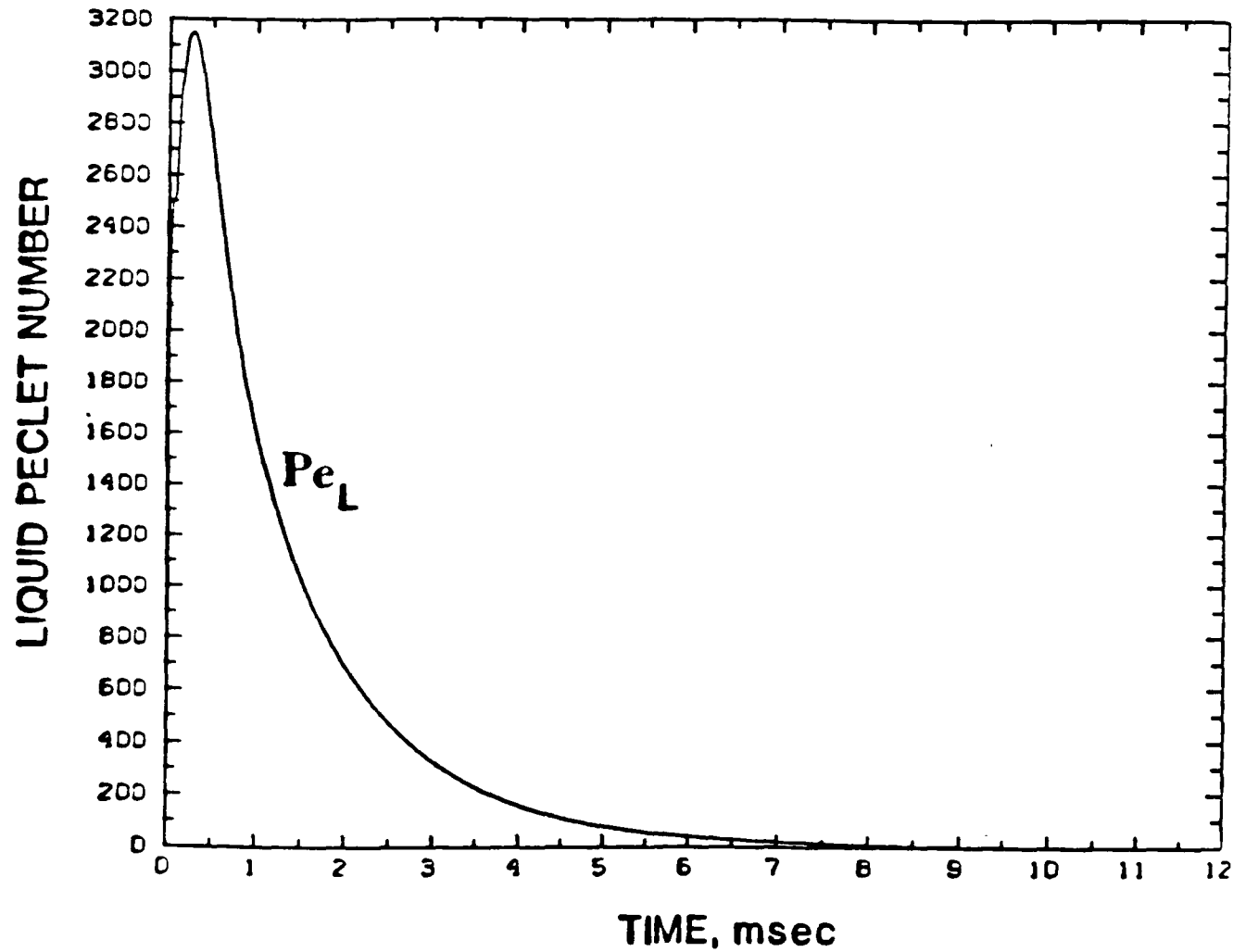


Fig. A-7 Liquid Peclet number vs time.

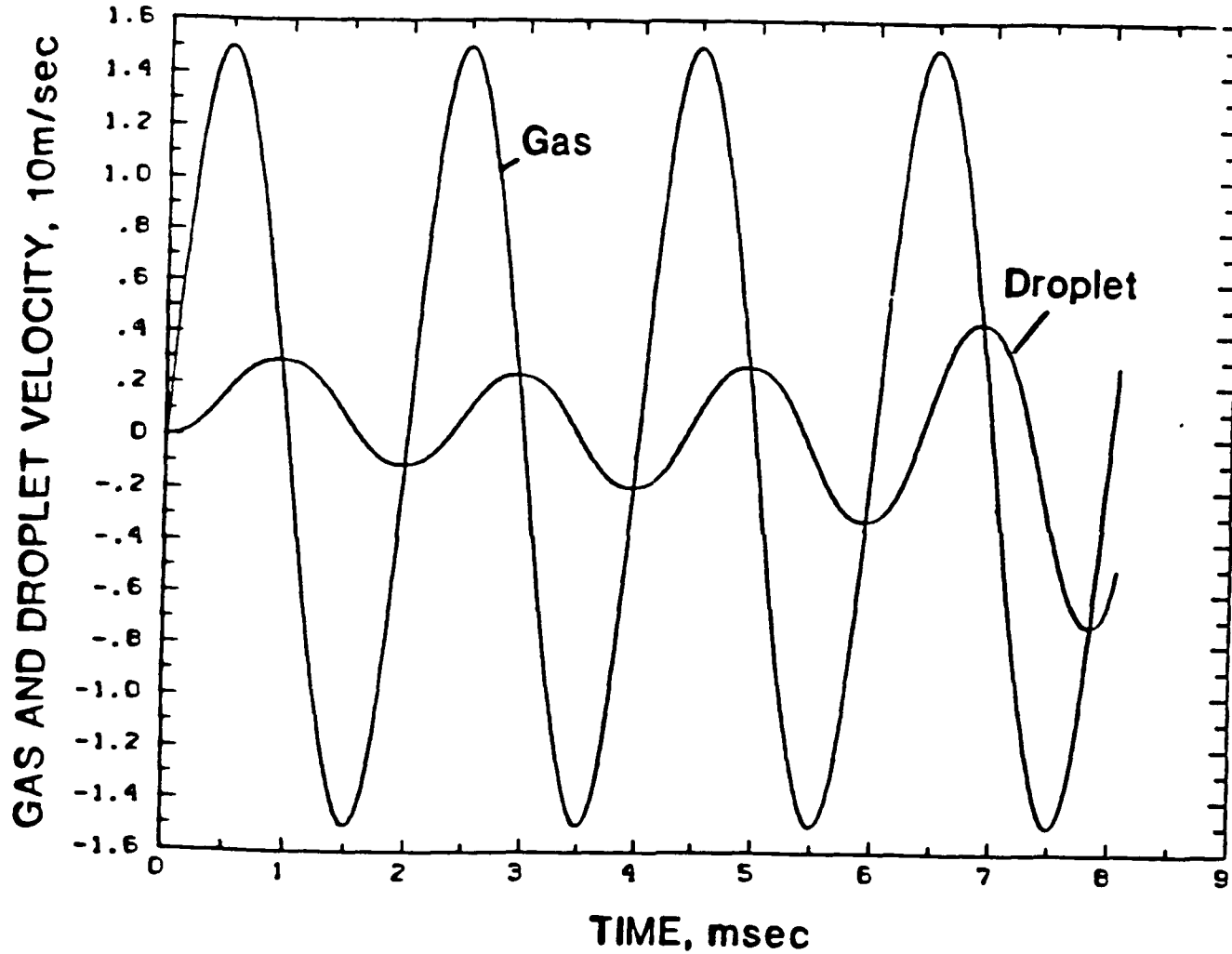


Fig. A-8(a) Gas and Droplet velocities vs time.

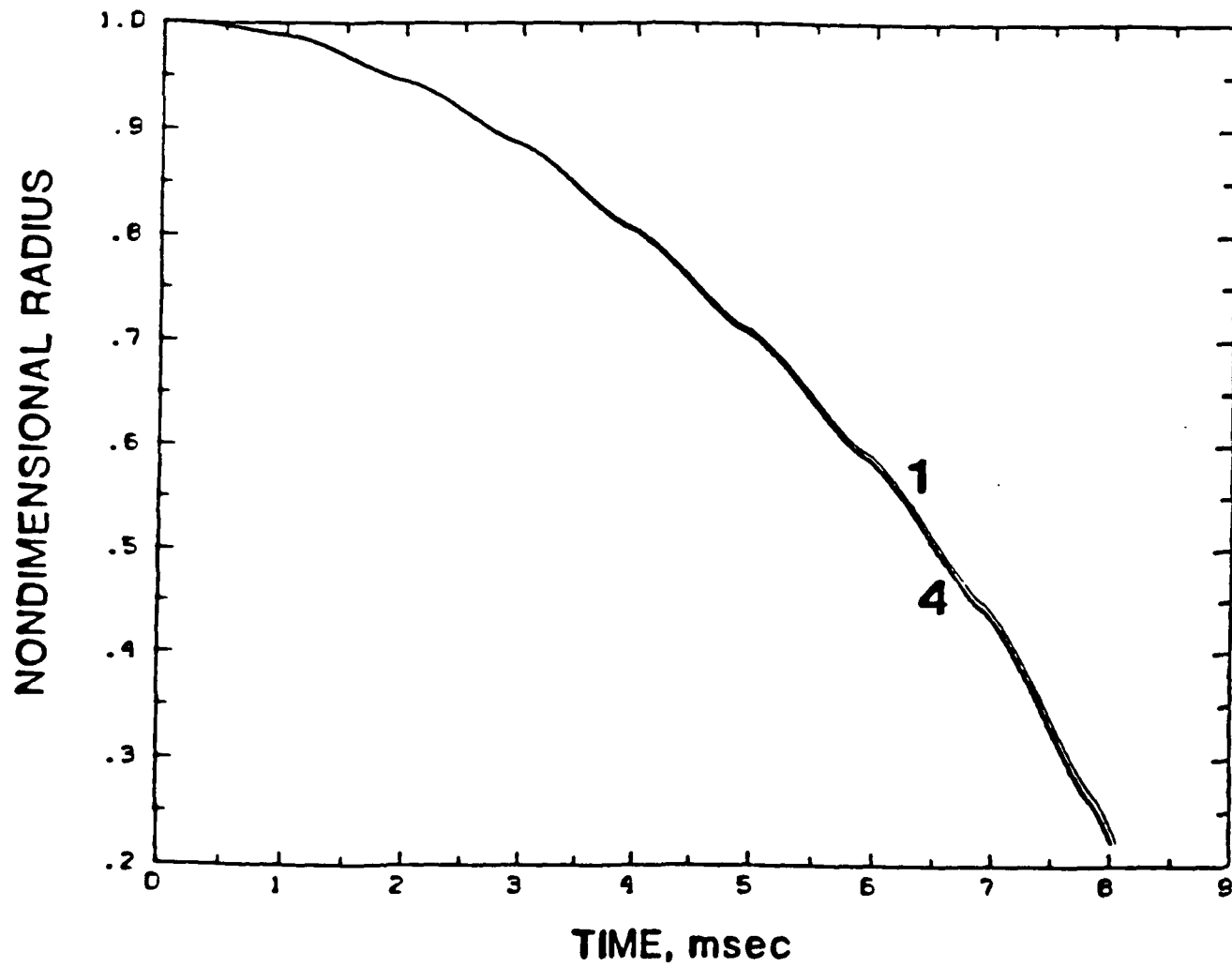


Fig. A-8(b) Non-dimensional droplet radius vs time.

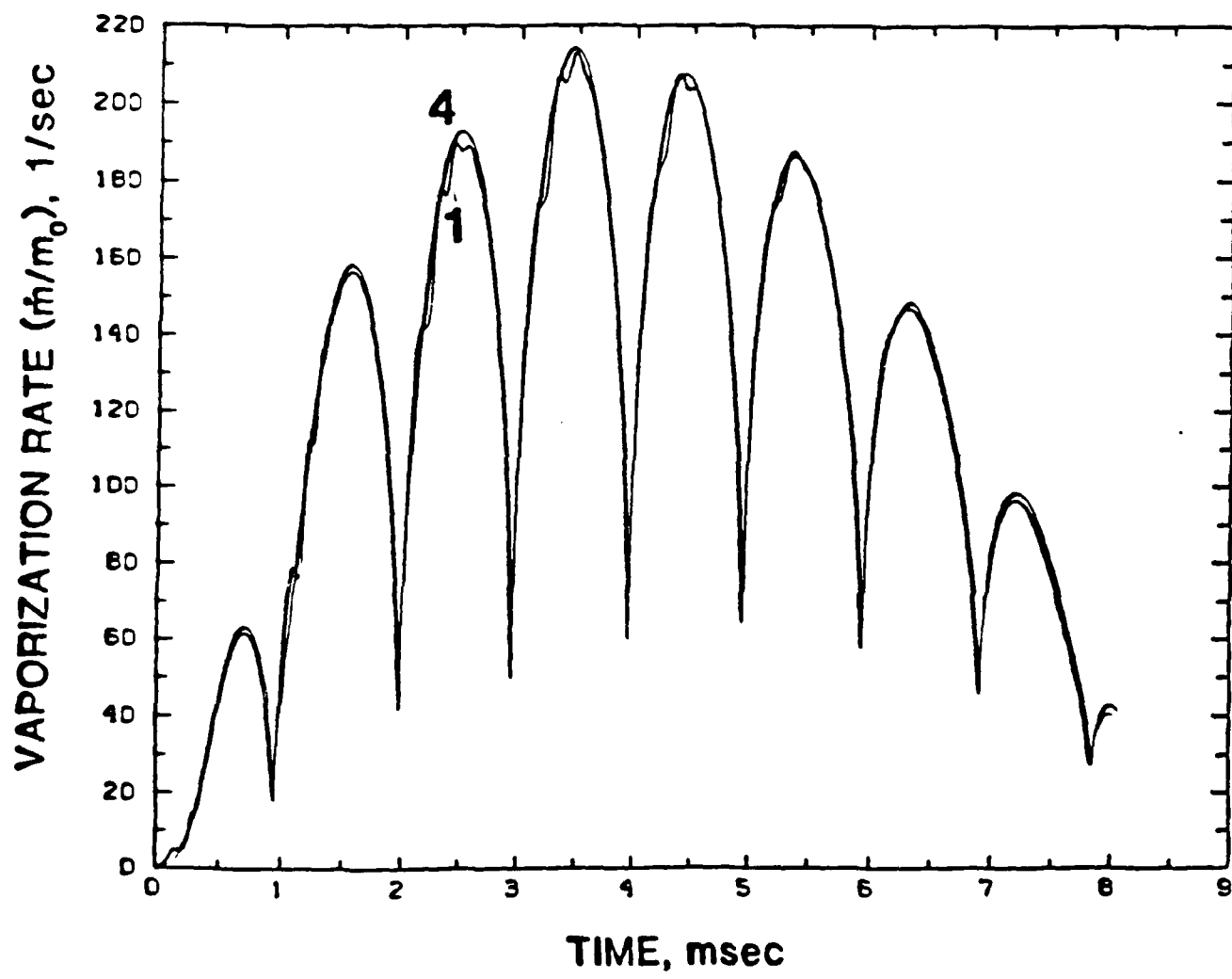


Fig. A-8(c) Vaporization rate vs time.

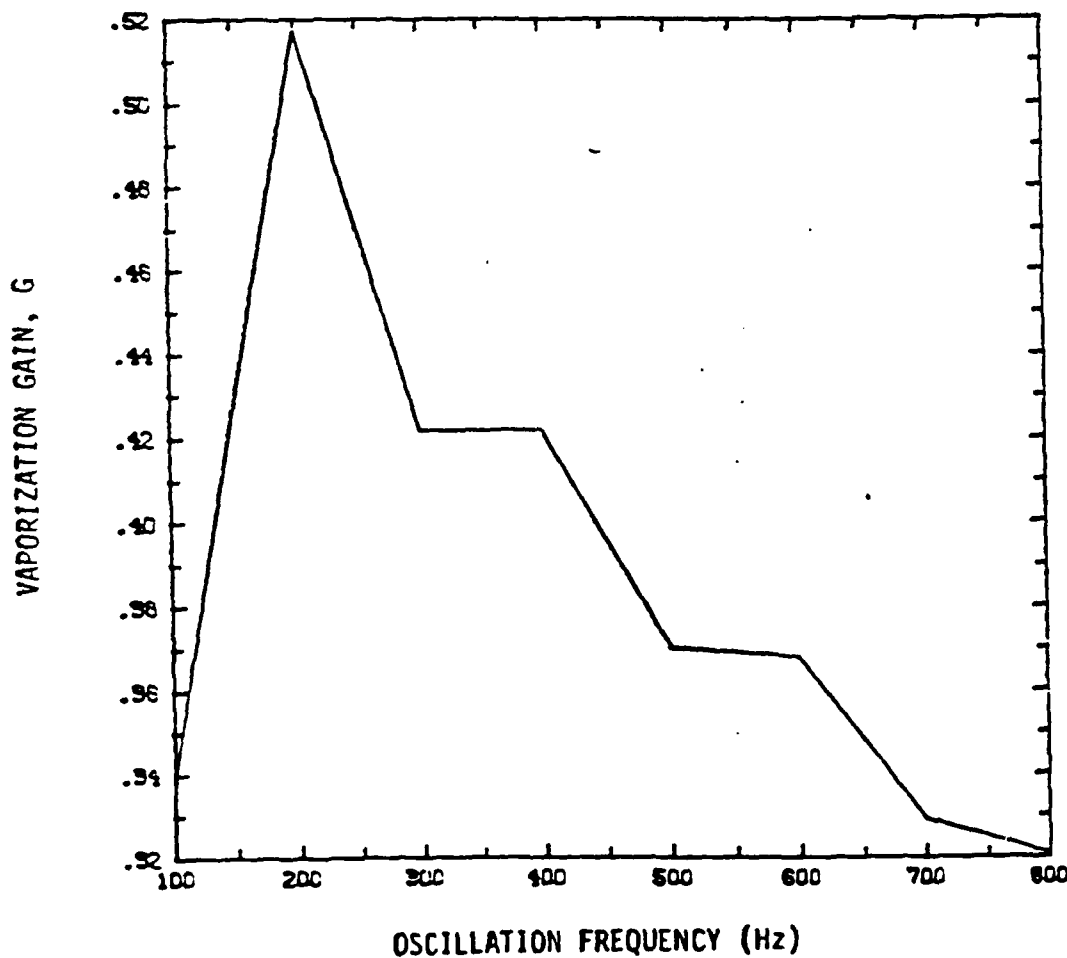


Fig. A-9 Vaporization rate gain versus oscillation frequency: pressure sensitivity only.

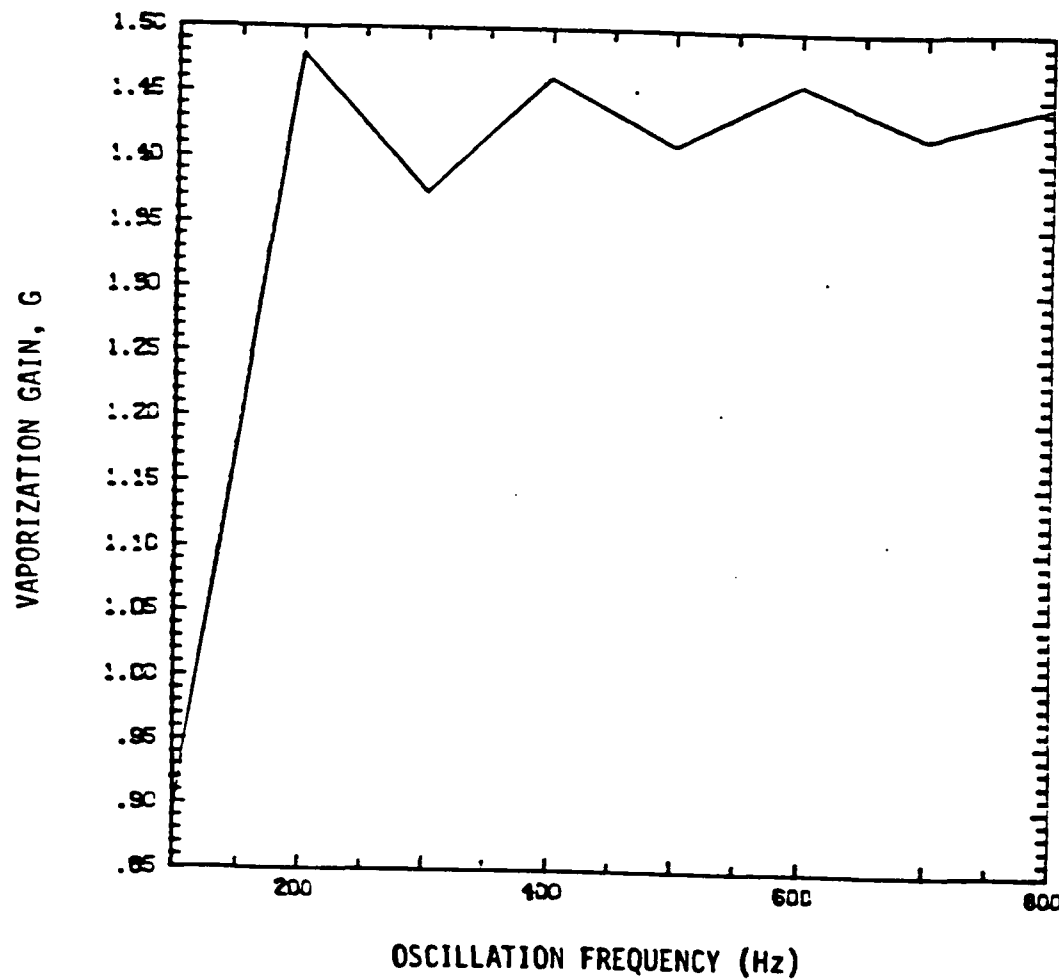


Fig. A-10 Vaporization rate gain versus oscillation frequency: velocity sensitivity only.

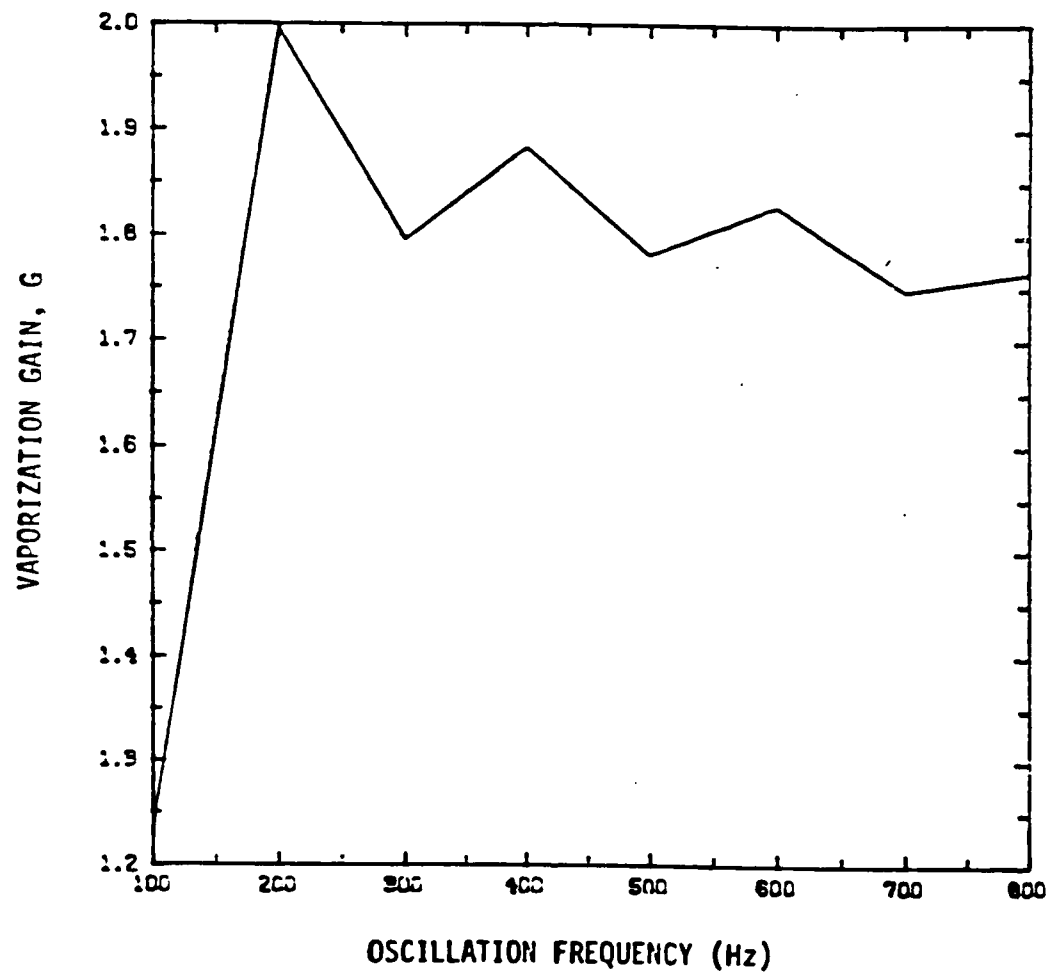


Fig. A-11 Vaporization rate gain versus oscillation frequency: pressure and velocity in phase (travelling waves).

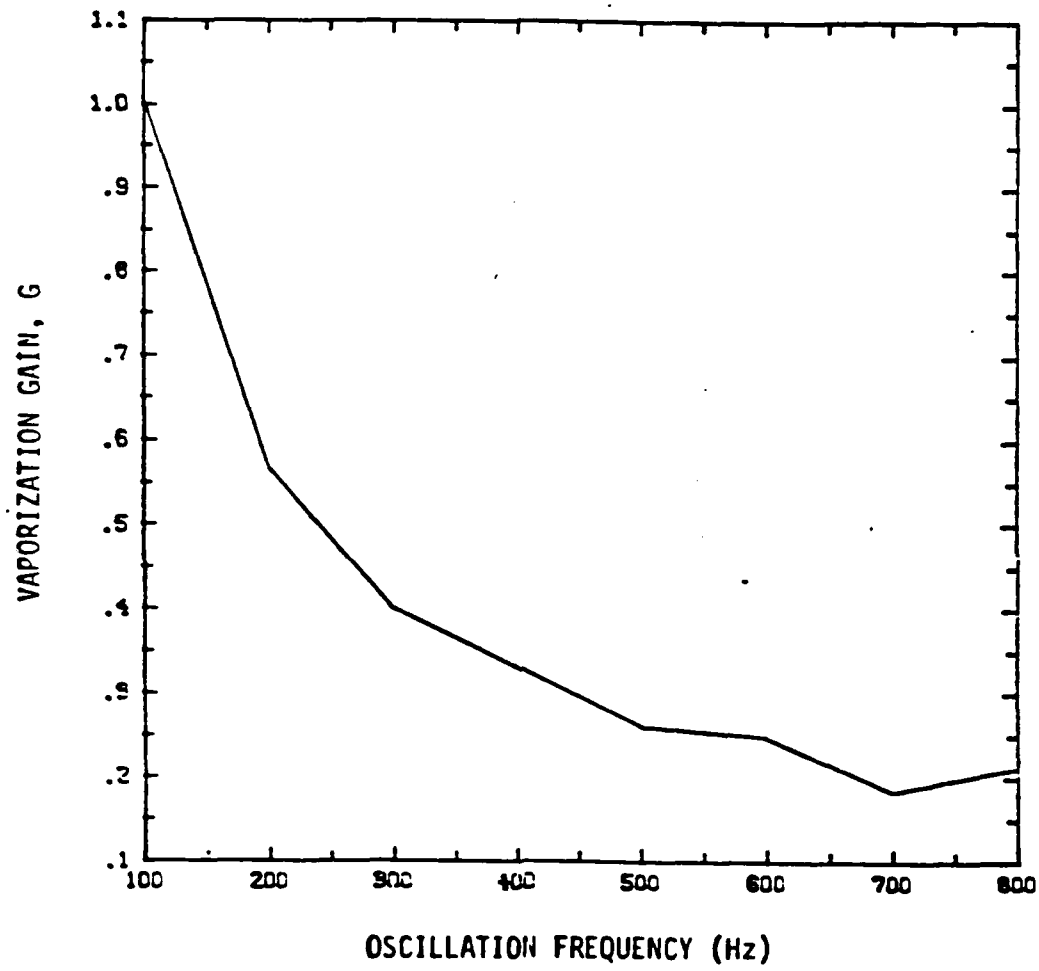
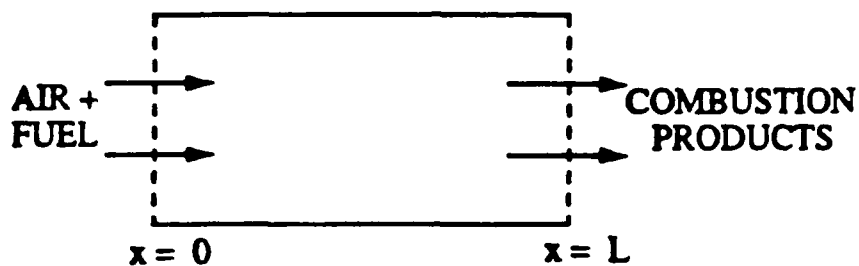


Fig. A-12 Vaporization rate gain versus oscillation frequency: pressure leads velocity by 90° (standing wave).



Combustor Lengths (L) = 25, 50, 100, 150 cm

Inlet Gas Velocity = 5000 cm/s

Inlet Liquid Velocity = 2000 cm/s

Inlet Gas Temperature = 1000 K

Inlet Liquid Temperature = 350 K

Inlet Gas Pressure = 10 atm

Exit Mach Number = 0.08

Fig. B-1 Physical model of the combustor.

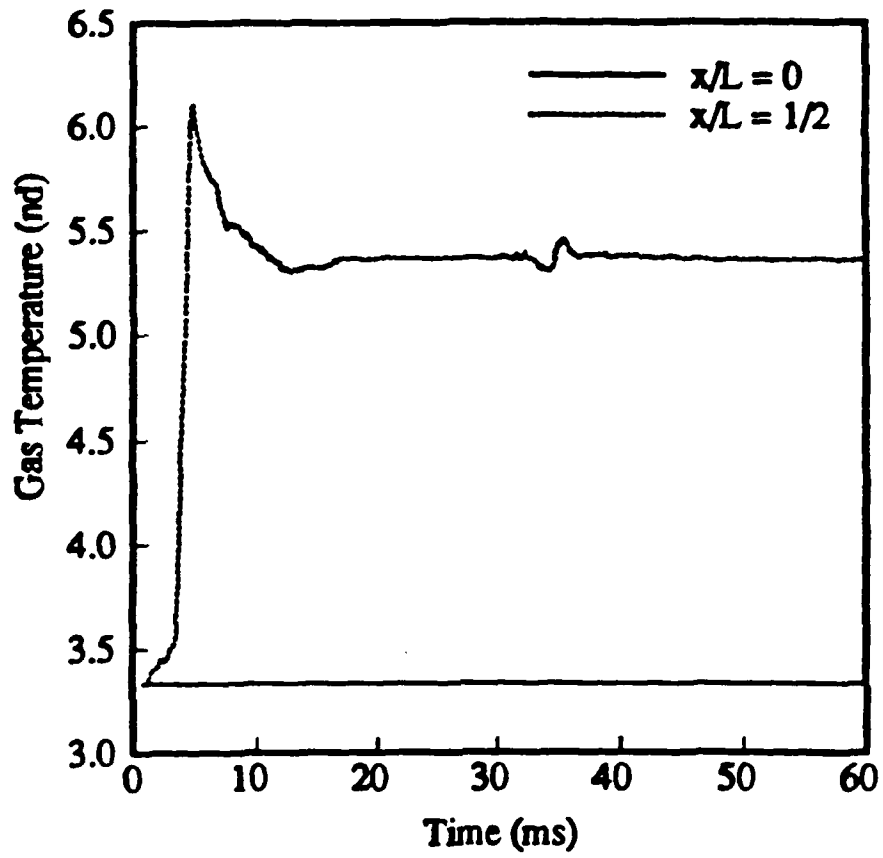


Fig. B-2(a) Temperature: For $L = 50$ cm, OER = 0.3, $r_i = 25\mu m$

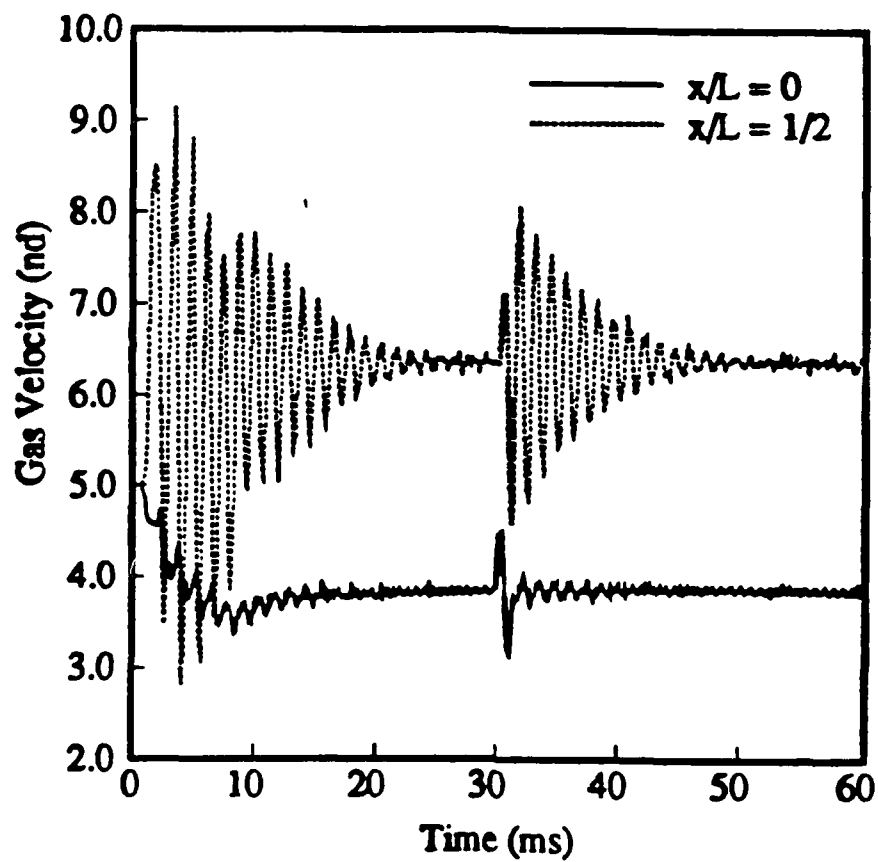


Fig. B-2(b) Velocity: For $L = 50$ cm, OER = 0.3, $r_i = 25\mu m$

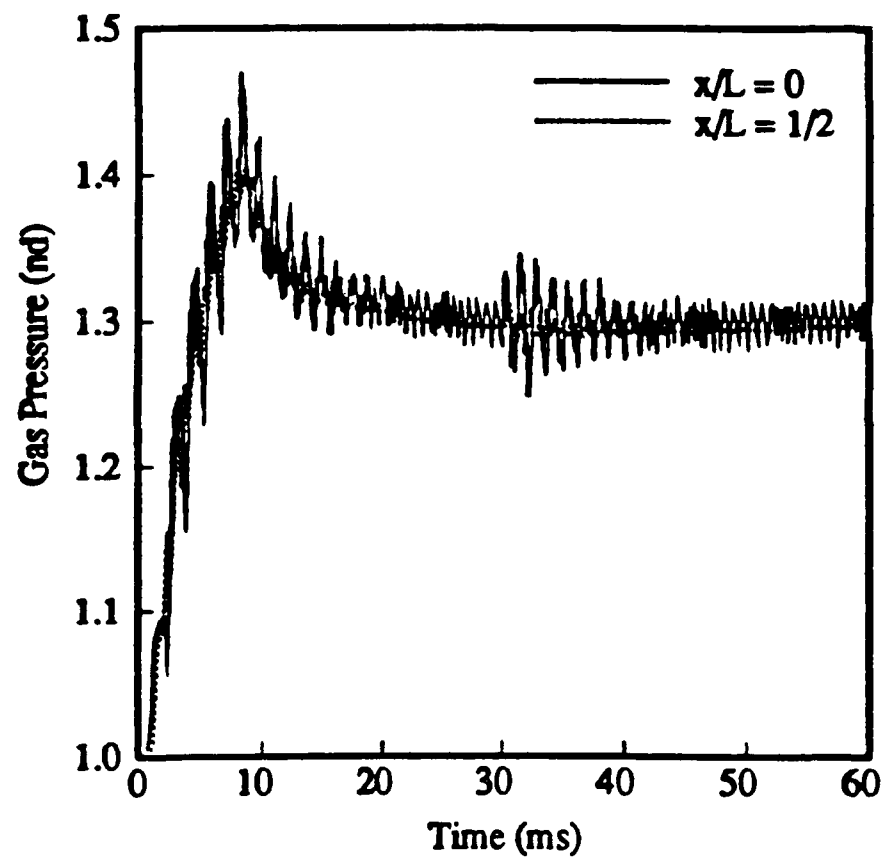


Fig. B-2(c) Pressure: For $L = 50$ cm, OER = 0.3, $r_i = 25\mu m$

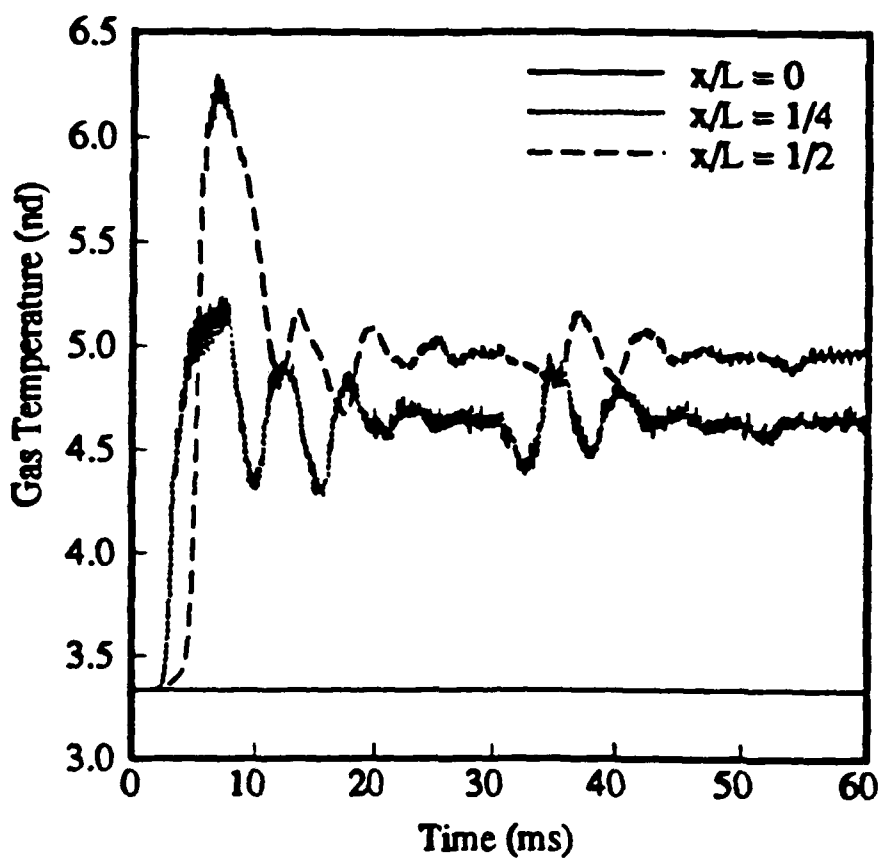


Fig. B-3(a) Temperature: For $L = 50$ cm, OER = 0.3, $r_i = 50\mu m$

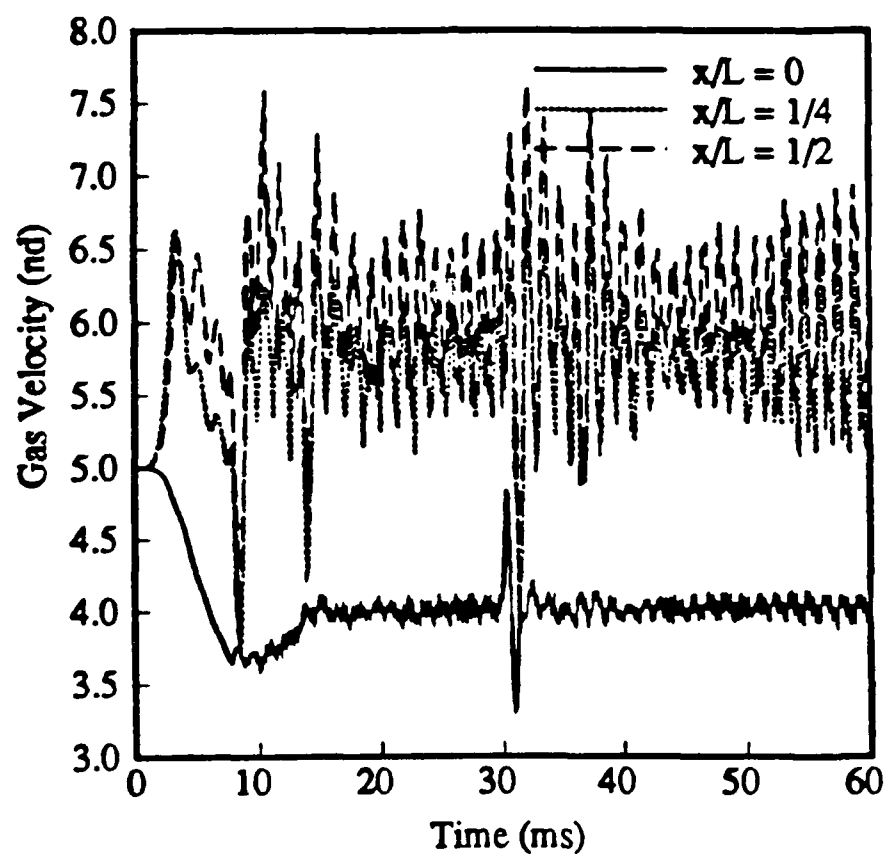


Fig. B-3(b) Velocity: For $L = 50$ cm, OER = 0.3, $r_i = 50\mu m$

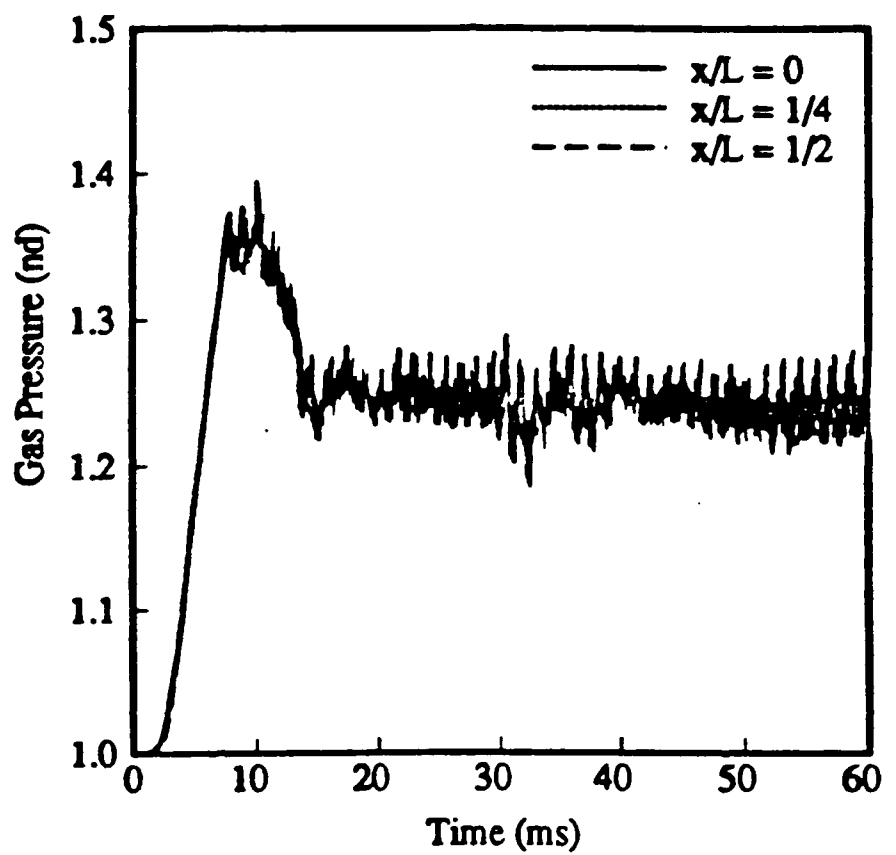


Fig. B-3(c) Pressure: For $L = 50$ cm, OER = 0.3, $r_i = 50\mu m$

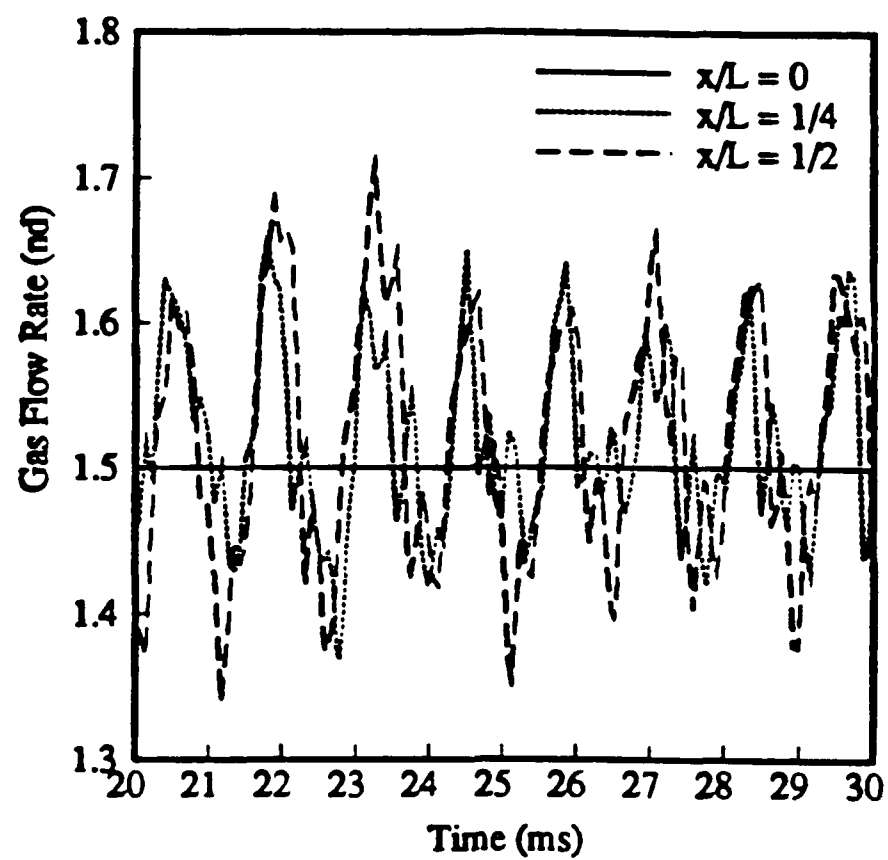


Fig. B-3(d) Gas Flow Rate: For $L = 50$ cm, OER = 0.3, $r_i = 50\mu m$

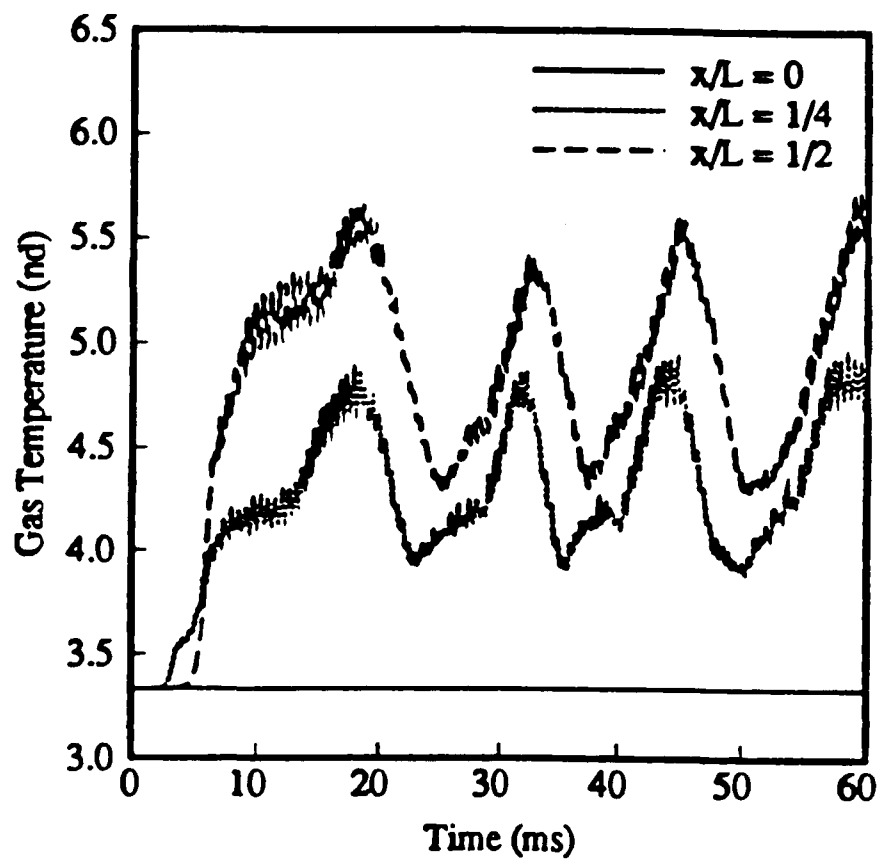


Fig. B-4(a) Temperature: For $L = 50$ cm, OER = 0.3, $r_i = 75\mu m$

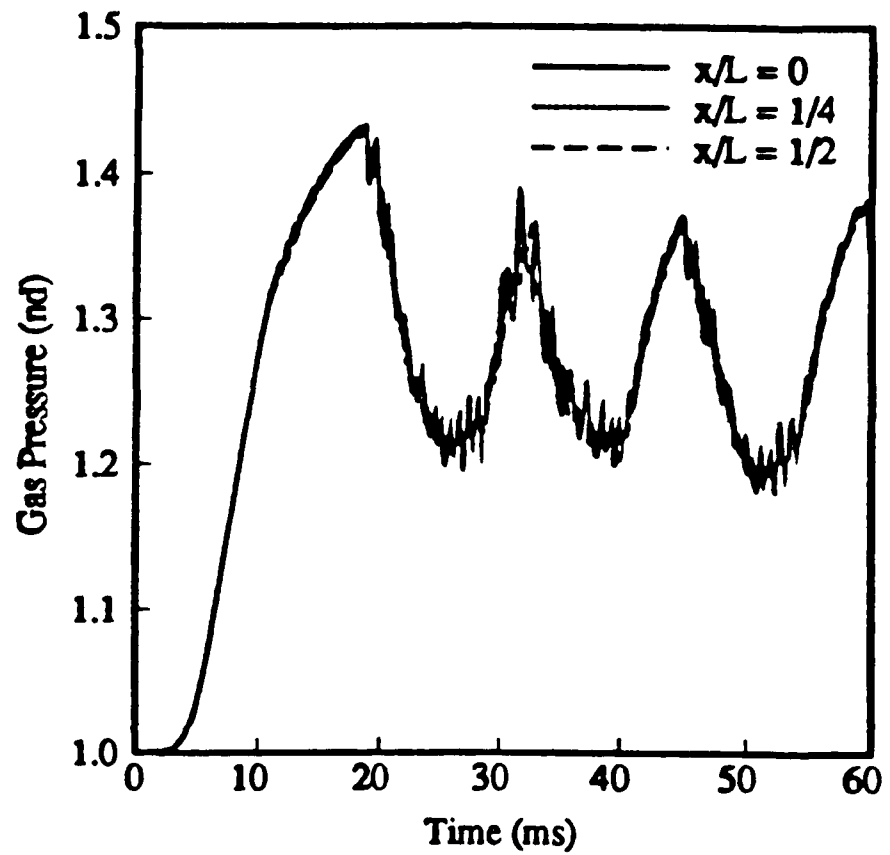


Fig. B-4(b) Pressure: For $L = 50$ cm, OER = 0.3, $r_i = 75\mu m$

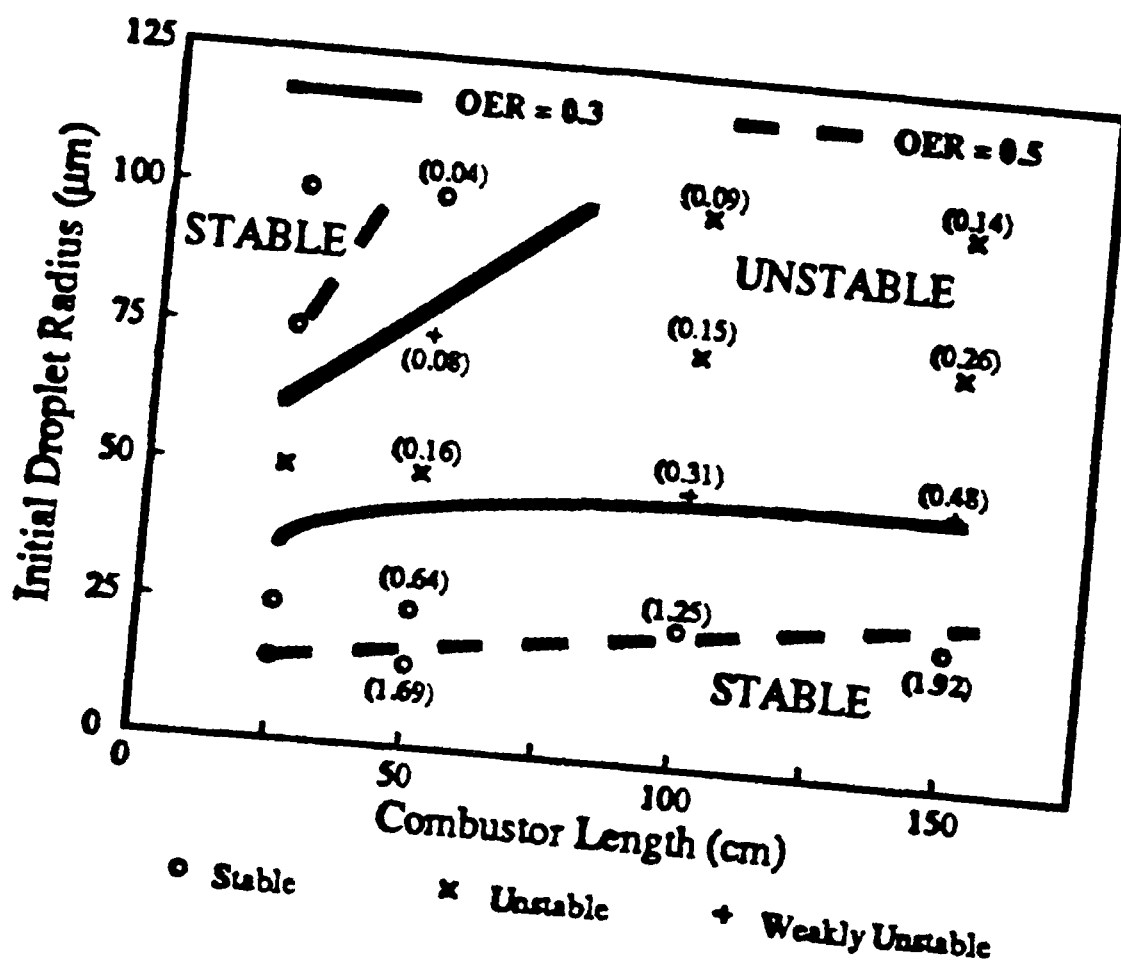


Fig. B-5

Domain of stable/unstable operation: droplet radius and combustor length
Points shown correspond to OER = 0.3. Numbers in parenthesis indicate r_p/r_{dh}

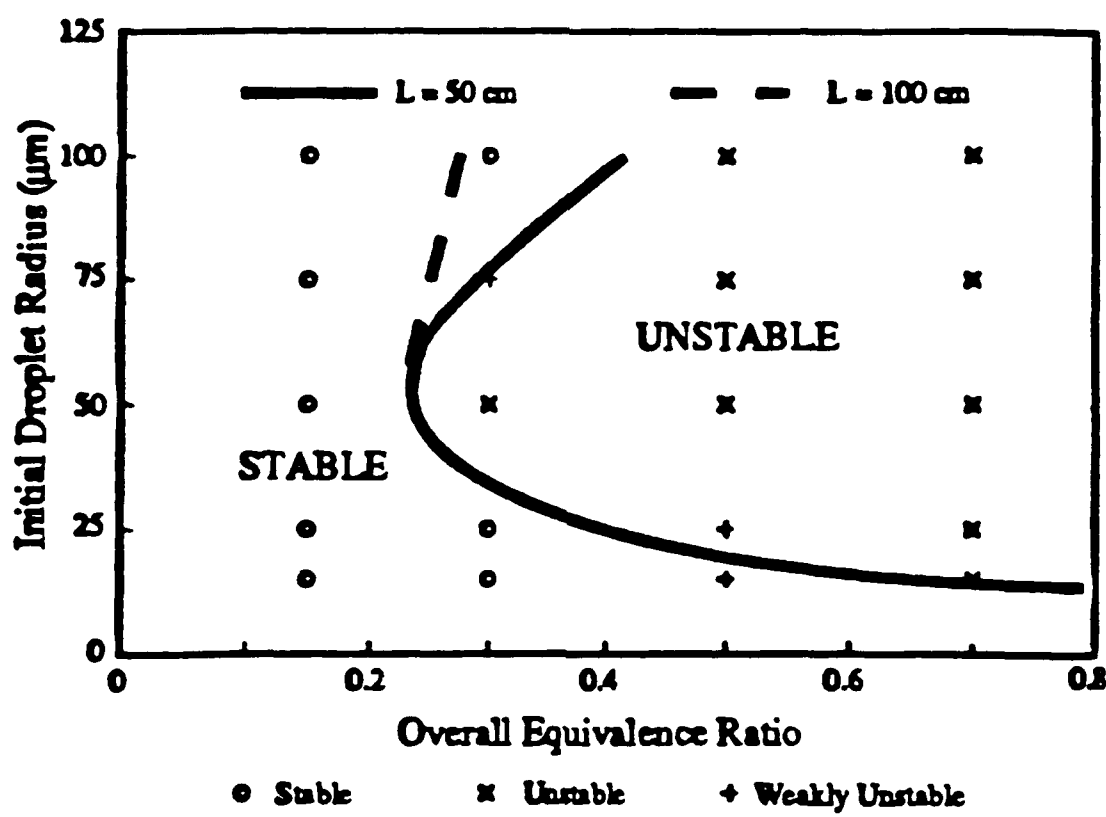


Fig. B-6 Domain of stable/unstable operation: droplet radius and equivalence ratio
Points shown correspond to $L = 50 \text{ cm}$

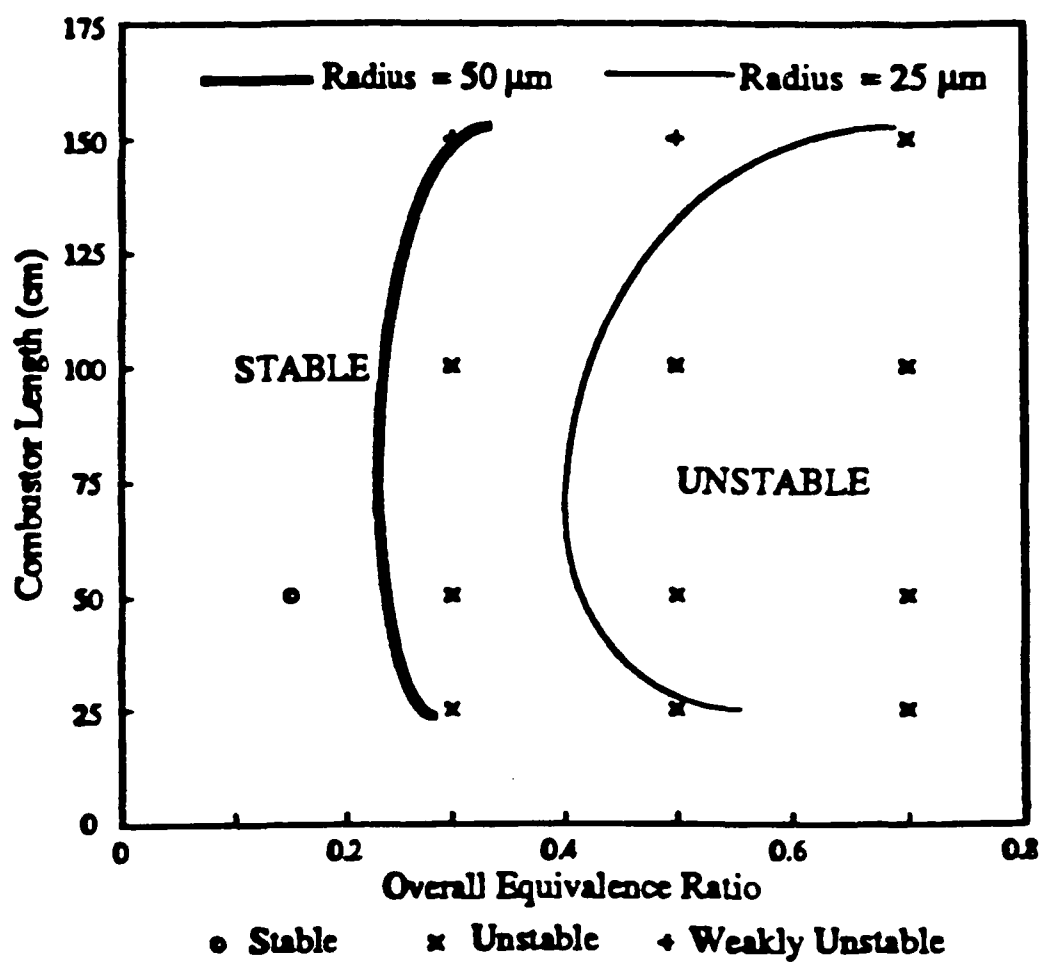


Fig. B-7 Domain of stable/unstable operation: combustor length and equivalence ratio
Points shown correspond to $r_i = 50 \mu\text{m}$

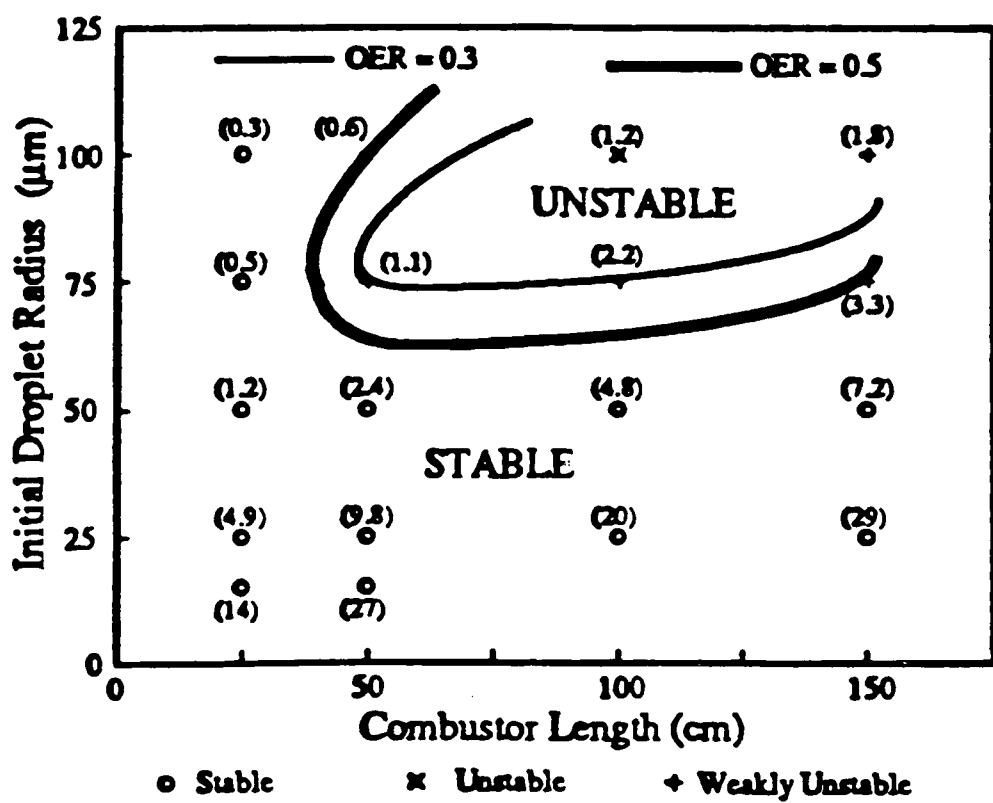


Fig. B-8 Domain of Stable/Unstable Operation for Low Frequency Oscillations only:
Droplet Radius and Combustor Length
Points shown correspond to OER = 0.3. Numbers in parenthesis indicate τ_f/τ_{dh}

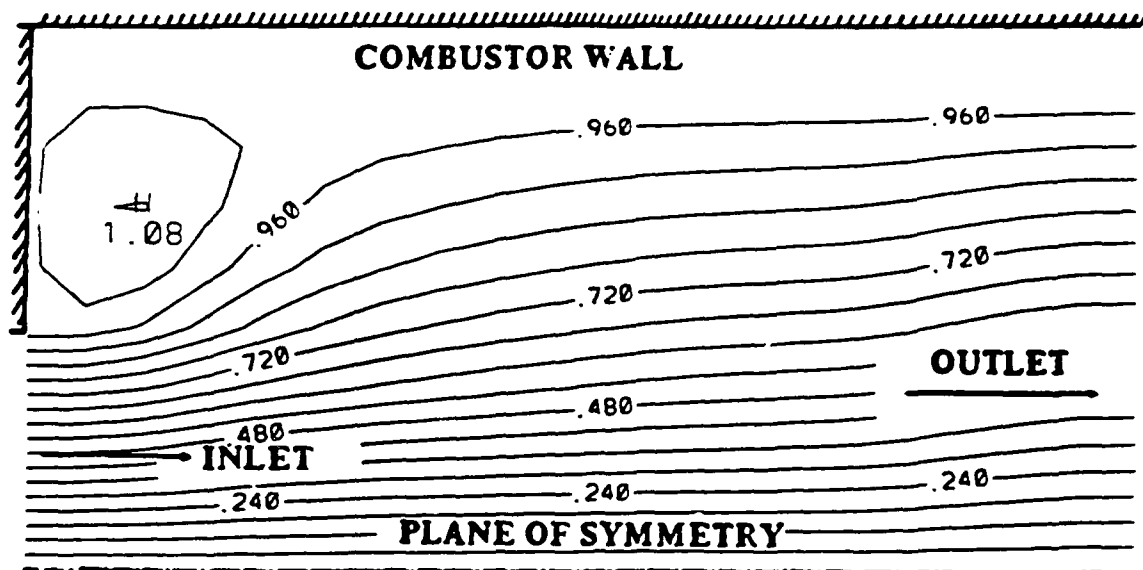


Figure C.1: Geometry of the problem and stream function for the cold, planar case.

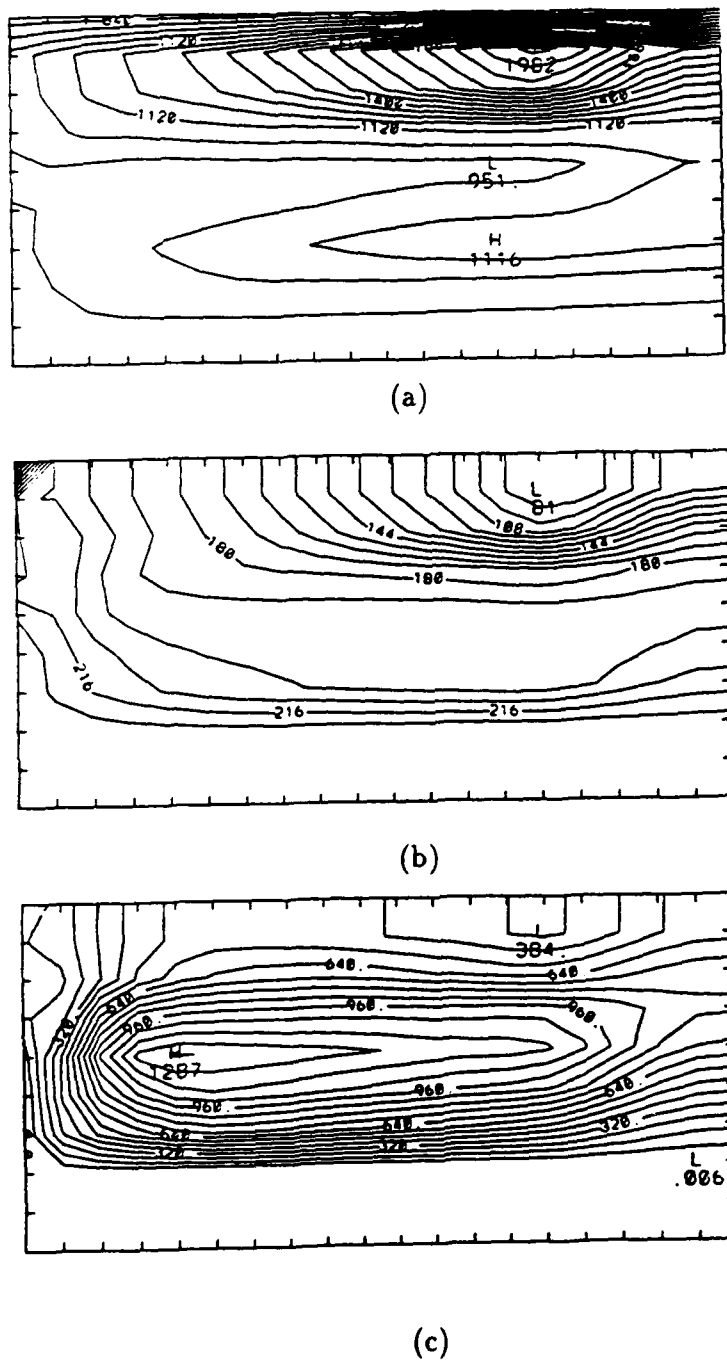


Figure C.2: Steady-state a)temperature contour, b)oxygen mass fraction contour values times 10^3 , and c)fuel mass fraction contour values times 10^4 for inlet equivalence ratio of 1.0 and initial drop radius of 25 microns.

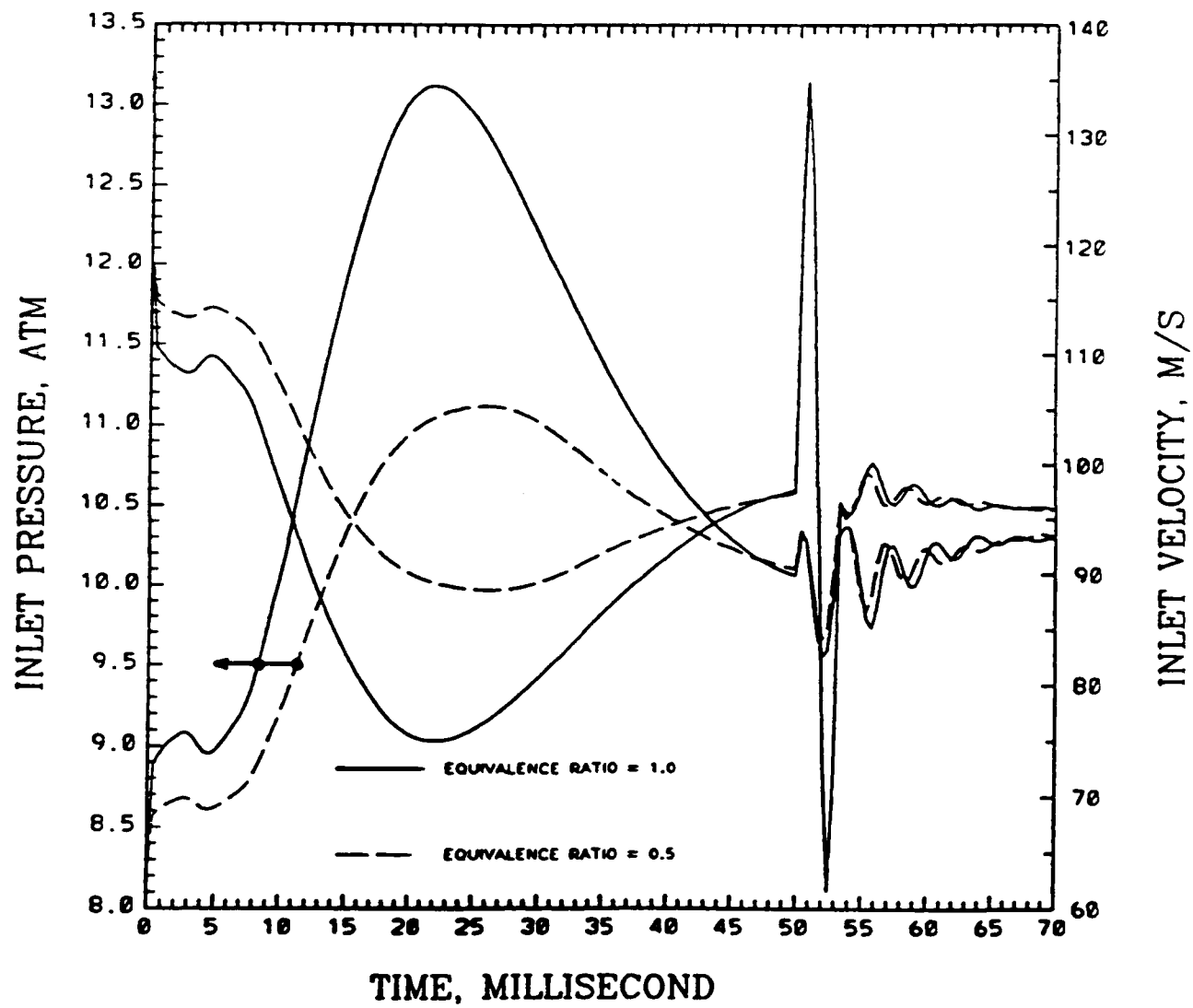


Figure C.3: Inlet pressure and velocity vs. time for the inlet equivalence ratios of 0.5 and 1.0 and initial drop radius of 25 microns.

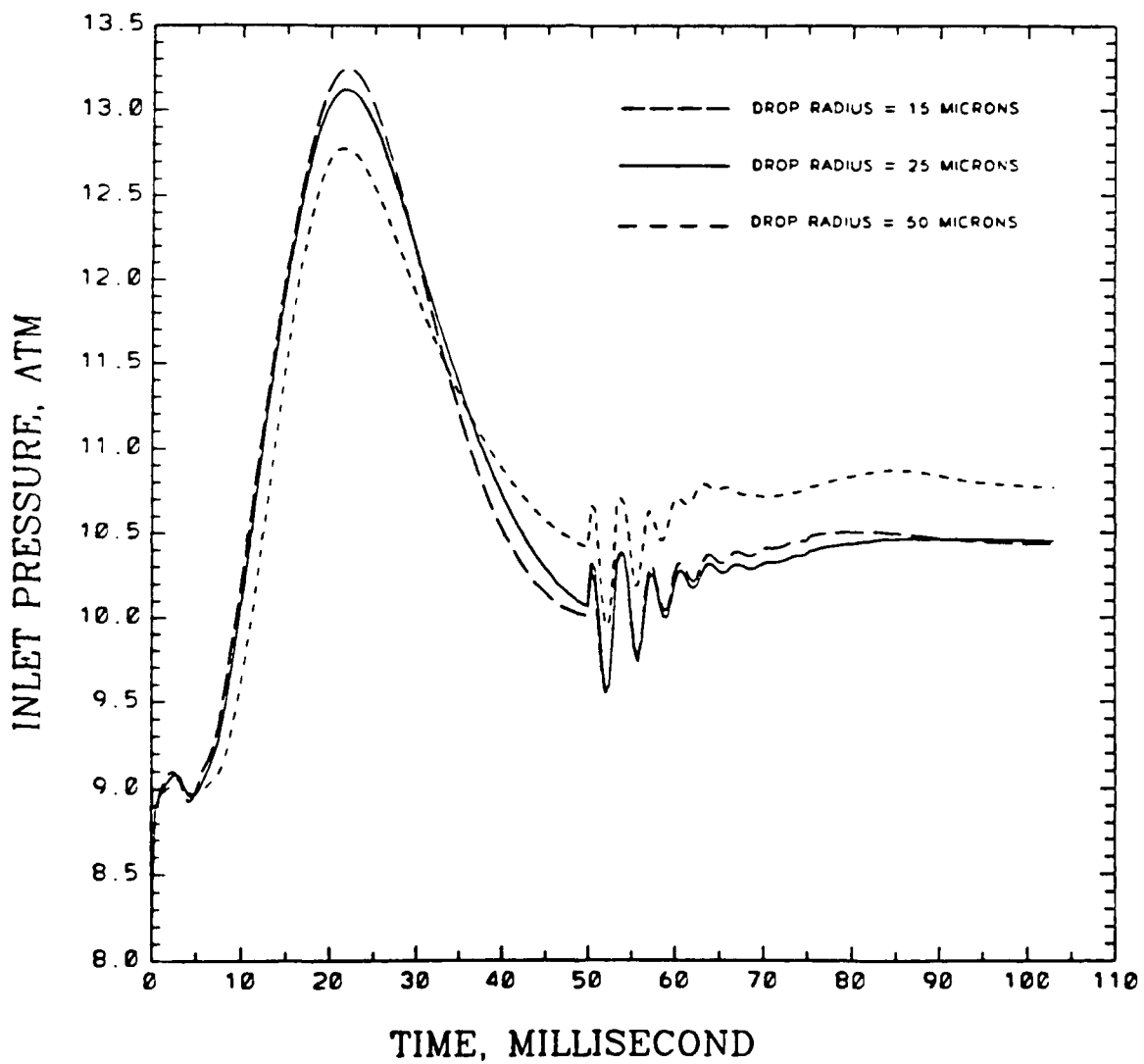


Figure C.4: Inlet pressure vs. time for the inlet equivalence ratio of 1.0 and different initial drop radius.

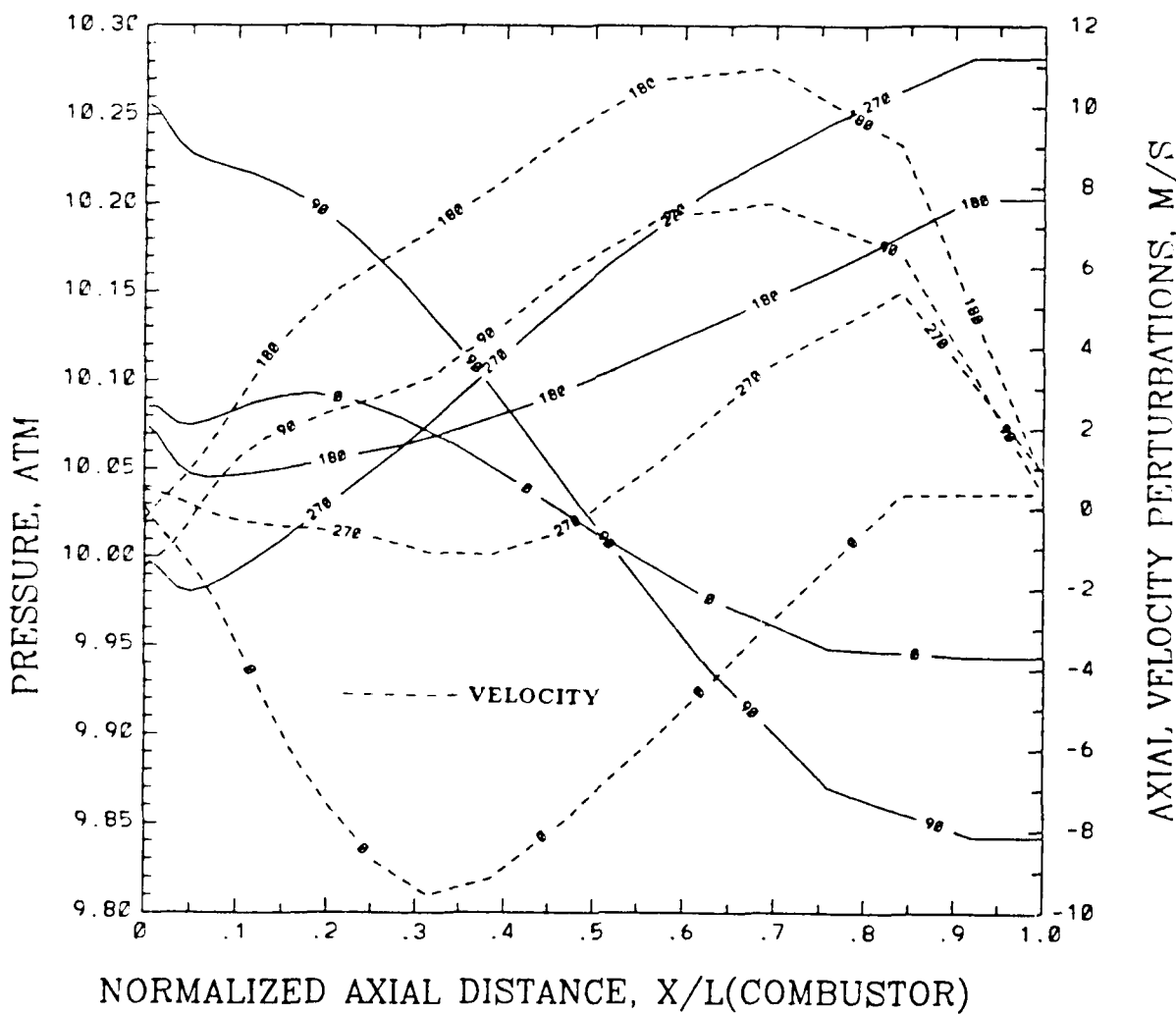
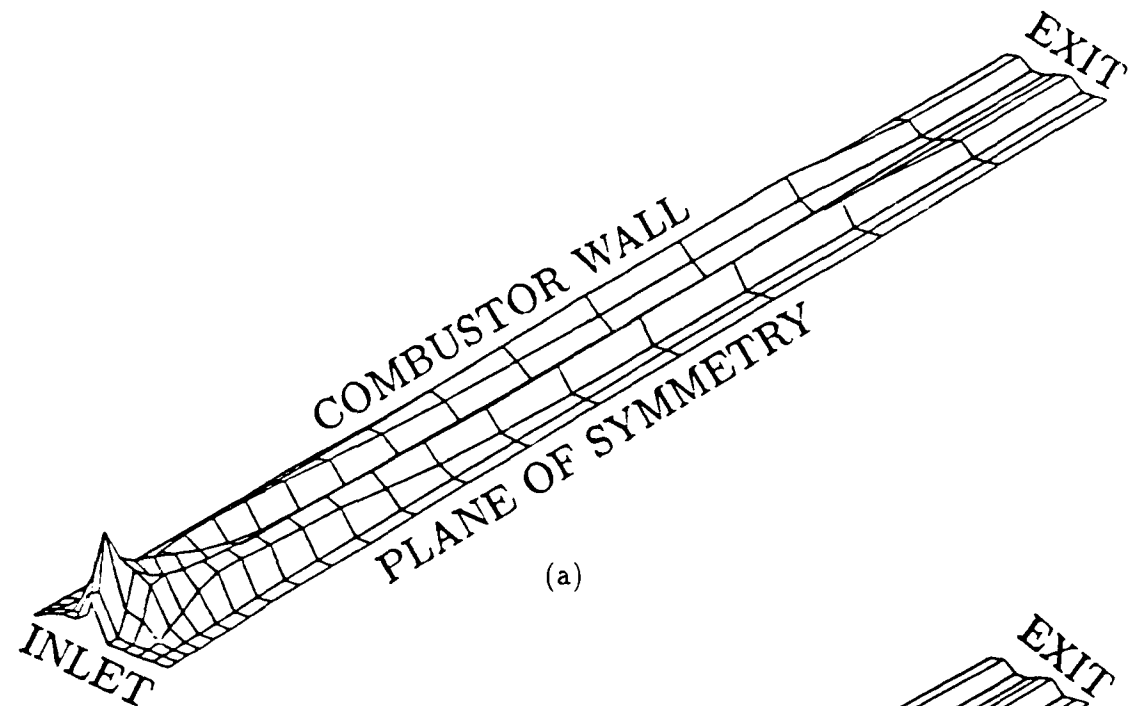
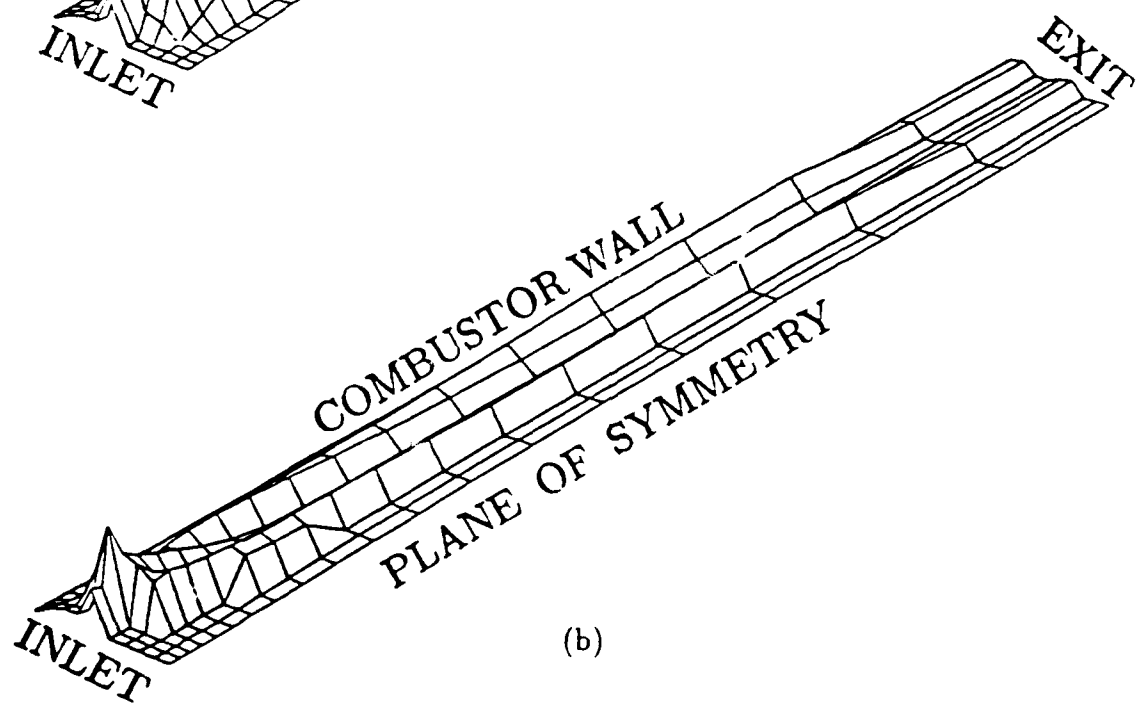


Figure C.5: Centerline pressure and perturbations to the mean centerline velocity profiles for the inlet equivalence ratio of 1.0 and initial drop radius of 25 microns at different phase angles during the second free oscillations.

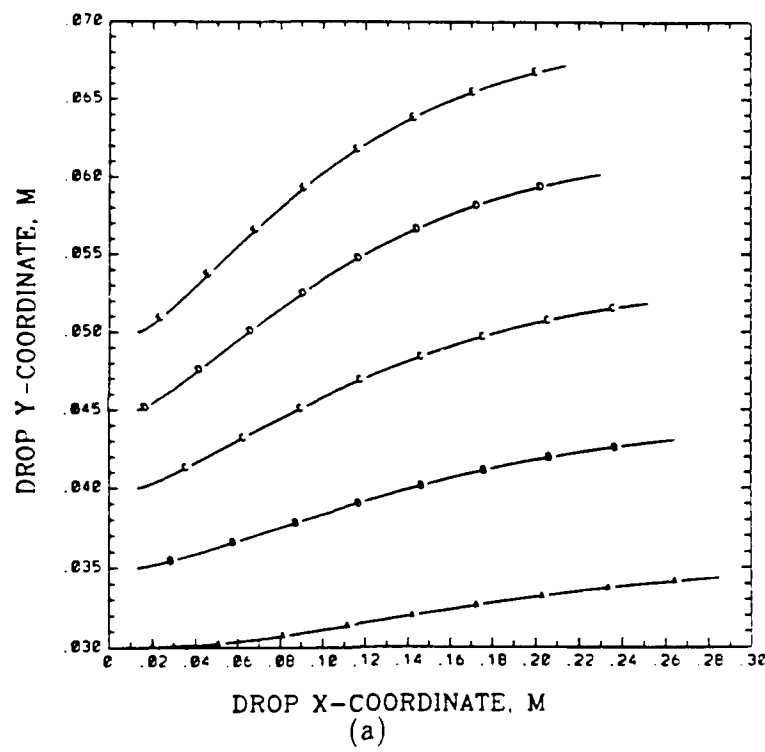


(a)

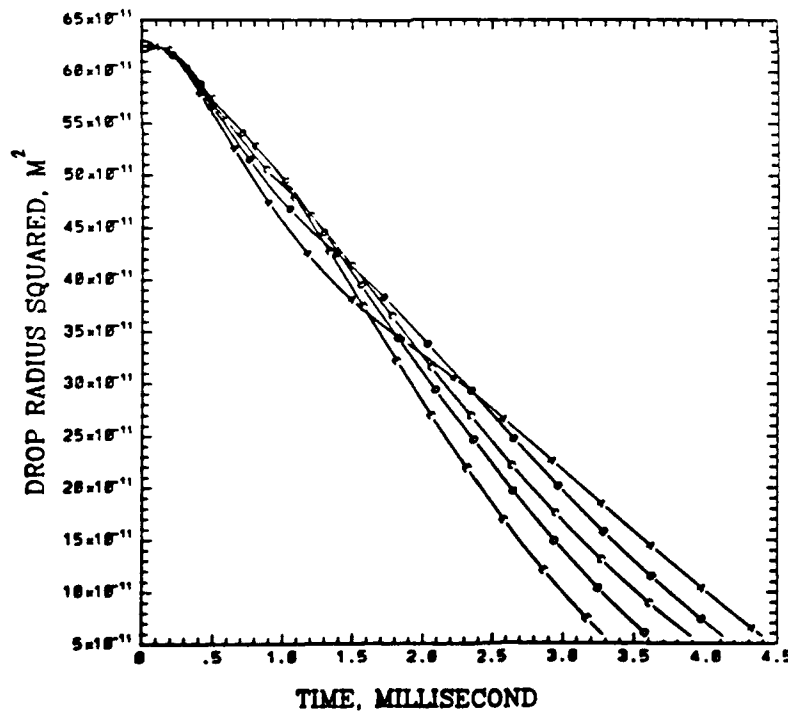


(b)

Figure C.6: Spatial profiles of the normalized a)overall conversion rate (minimum of the Arrhenius kinetics and eddy mixing) and b)conversion rate where eddy mixing is controlling for the inlet equivalence ratio of 1.0, initial drop radius of 25 microns, and combustor length of 1 meter.



(a)



(b)

Figure C.7: a) Trajectories and b) radius squared vs. time for the sample characteristics injected during the steady-state operations with inlet equivalence ratio of 1.0, initial drop radius of 25 microns, and combustor length of 1 meter.

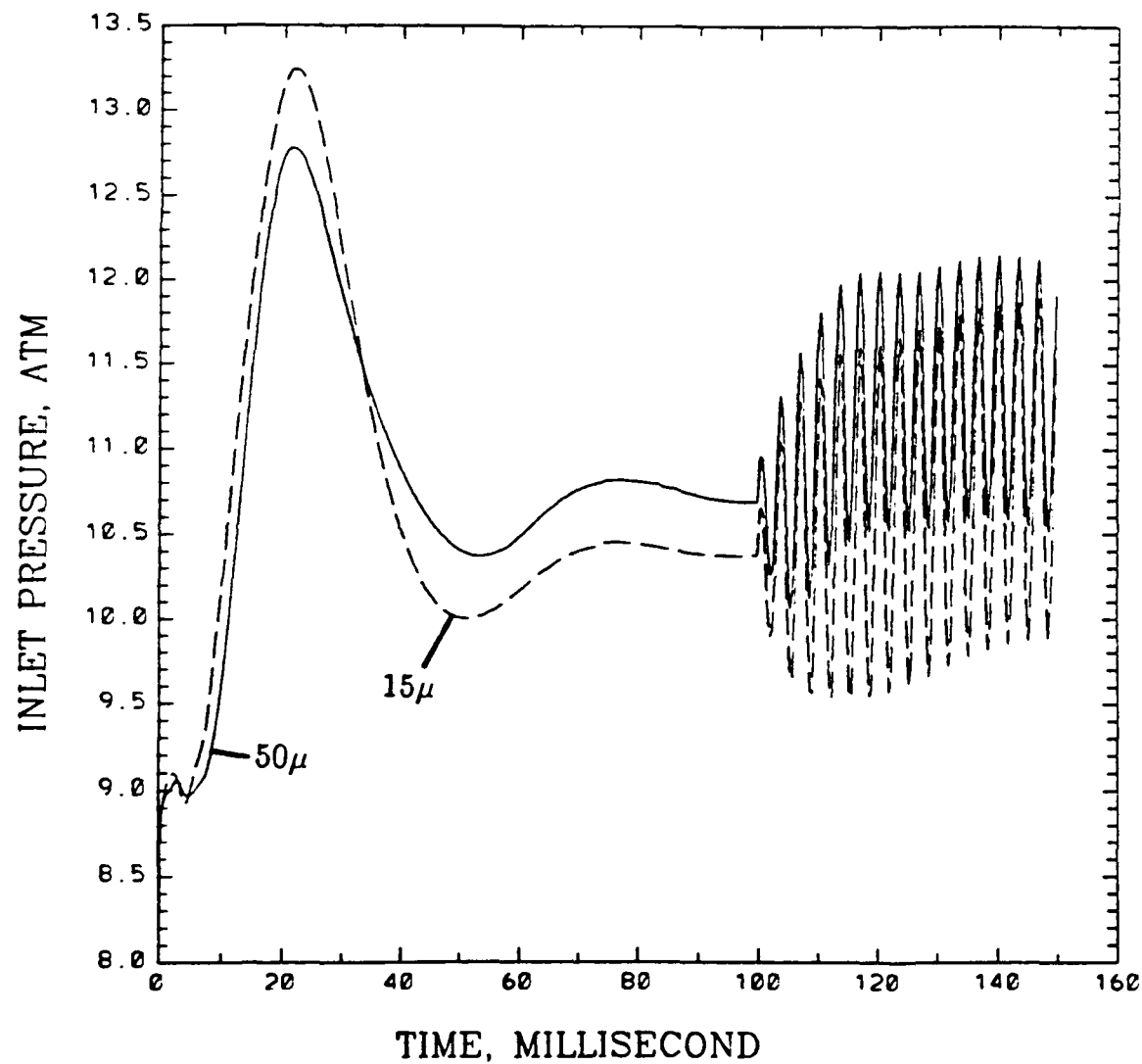
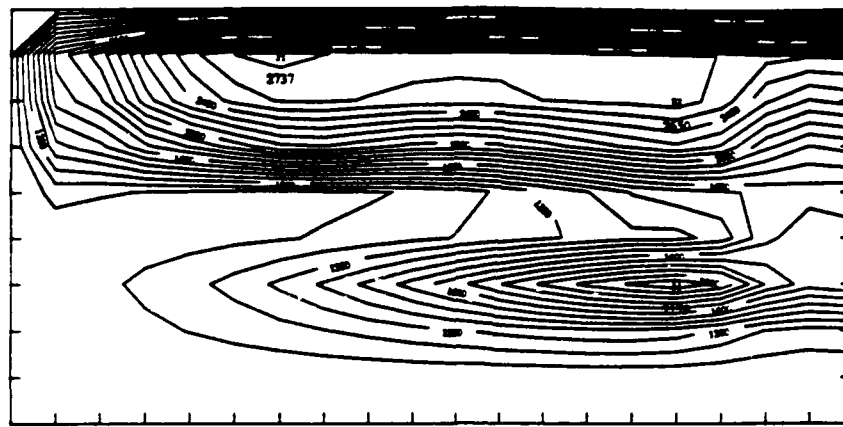
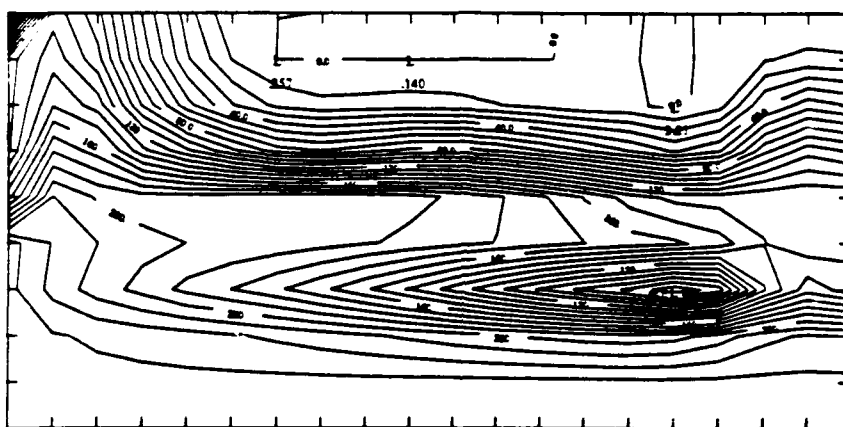


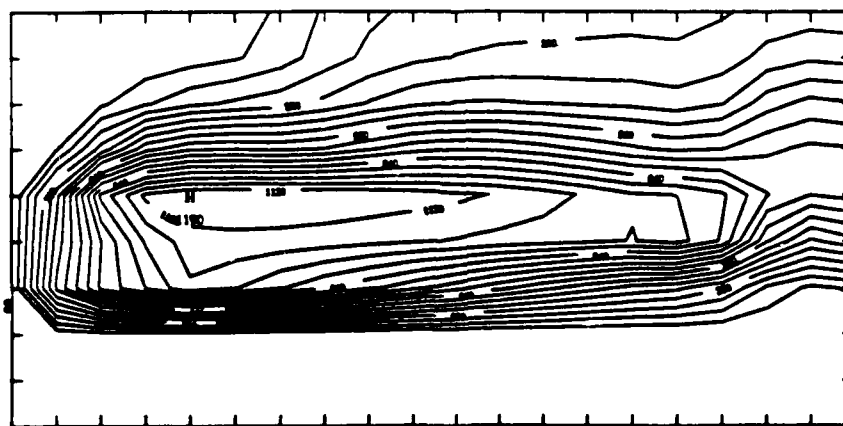
Figure C.8: Inlet pressure vs. time for the continuous forced oscillations with inlet equivalence ratio of 1.0, different initial drop sizes, and combustor length of 1 meter.



(a)



(b)



(c)

Figure C.9: Steady-state a)temperature contour, b)oxygen mass fraction contour values times 10^3 , and c)fuel mass fraction contour values times 10^4 for inlet equivalence ratio of 1.0, initial drop radius of 25 microns, and fine mesh (40*20), fuel is injected half way over the inlet.

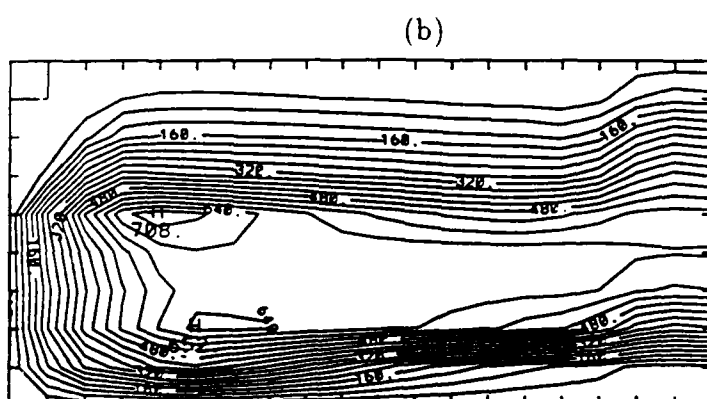
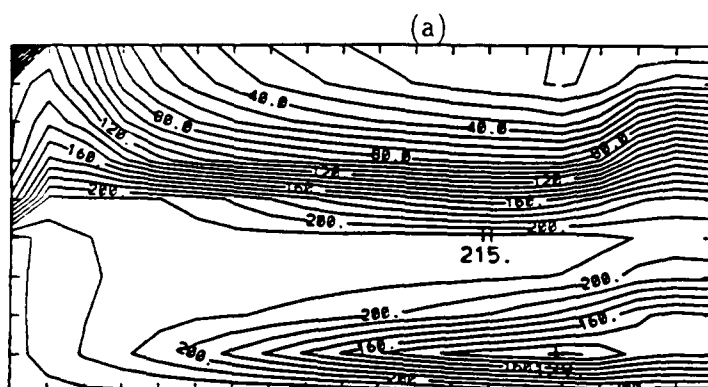
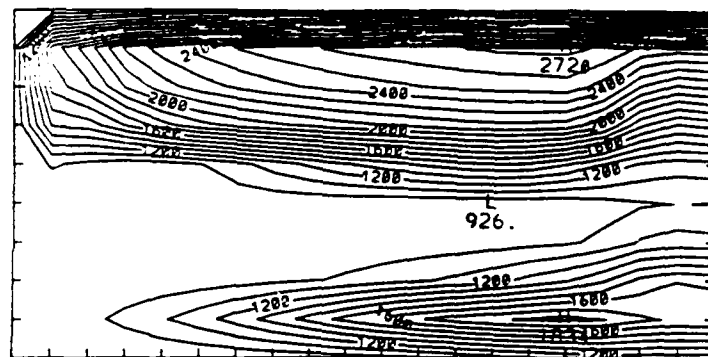


Figure C.10: Steady-state a)temperature contour, b)oxygen mass fraction contour values times 10^3 , and c)fuel mass fraction contour values times 10^4 for inlet equivalence ratio of 1.0, initial drop radius of 25 microns, and fine mesh (40*20), uniform injection.

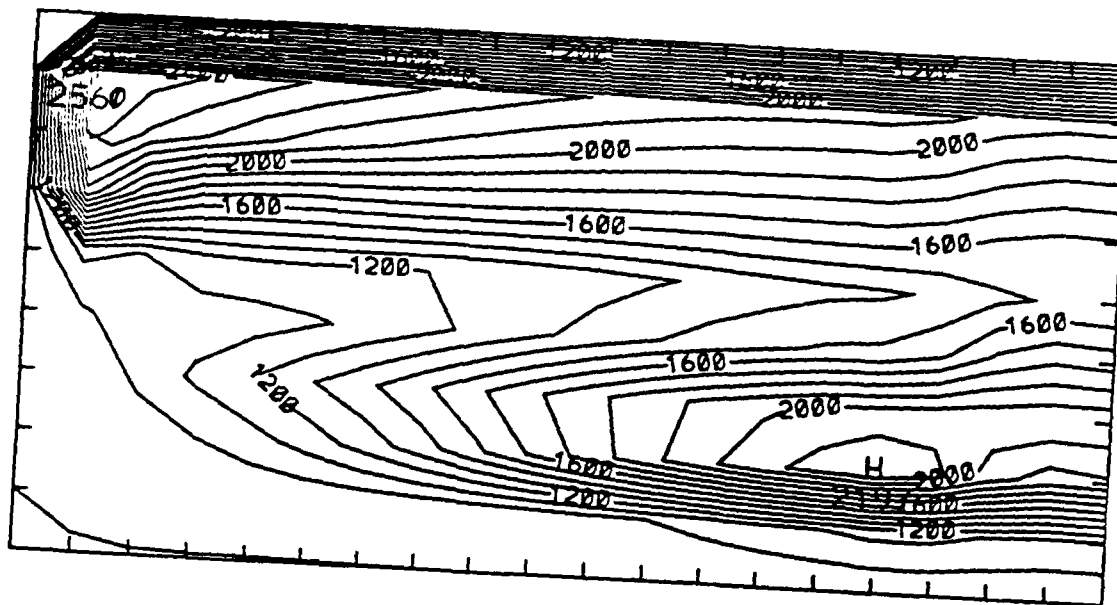


Figure C.11: Steady-state temperature contour for inlet equivalence ratio of 1.0 and initial drop radius of 25 microns, only 3 drop streams.

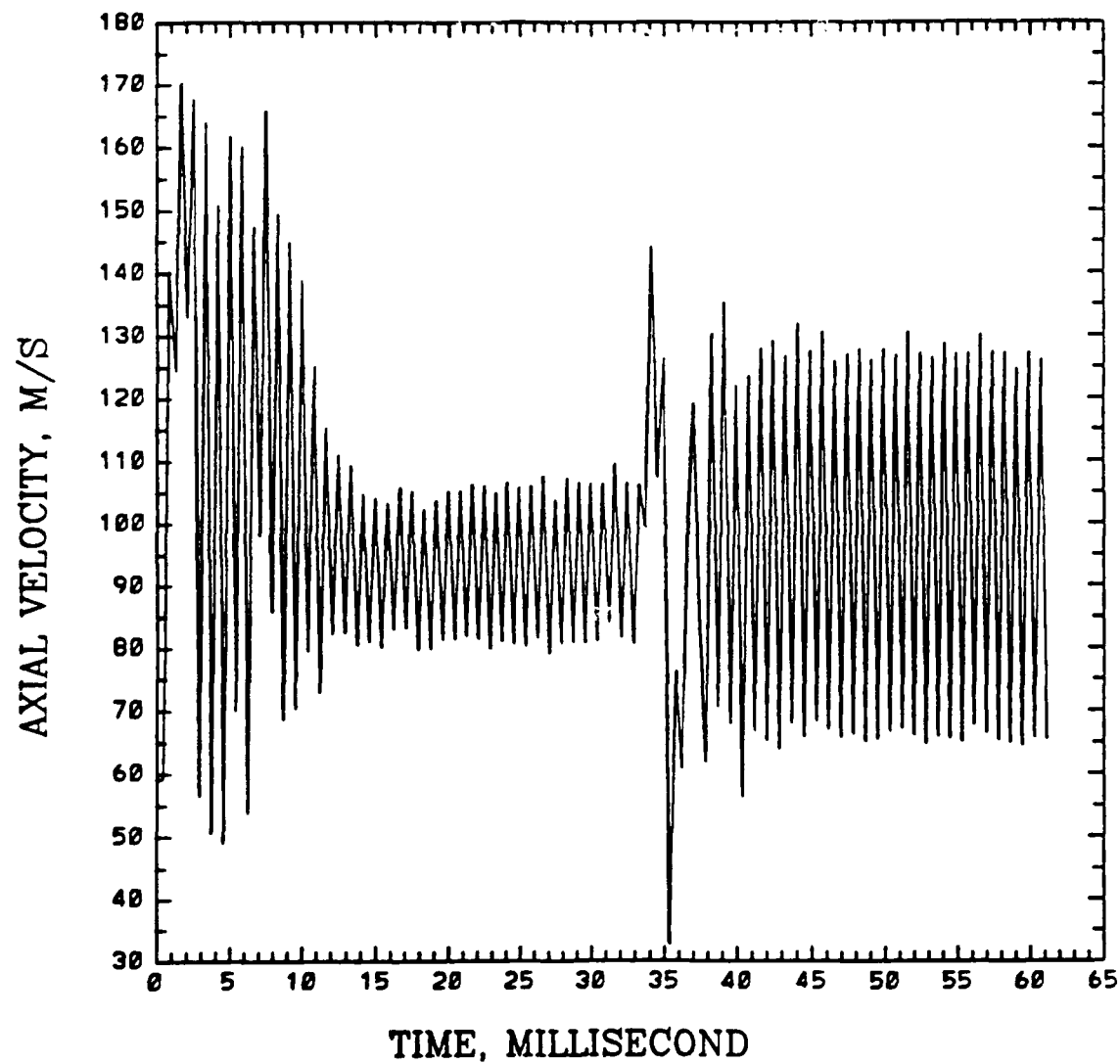


Figure D.1: Velocity vs. time for the quasi-one-dimensional case with one forced cycle, $x=.09L$.

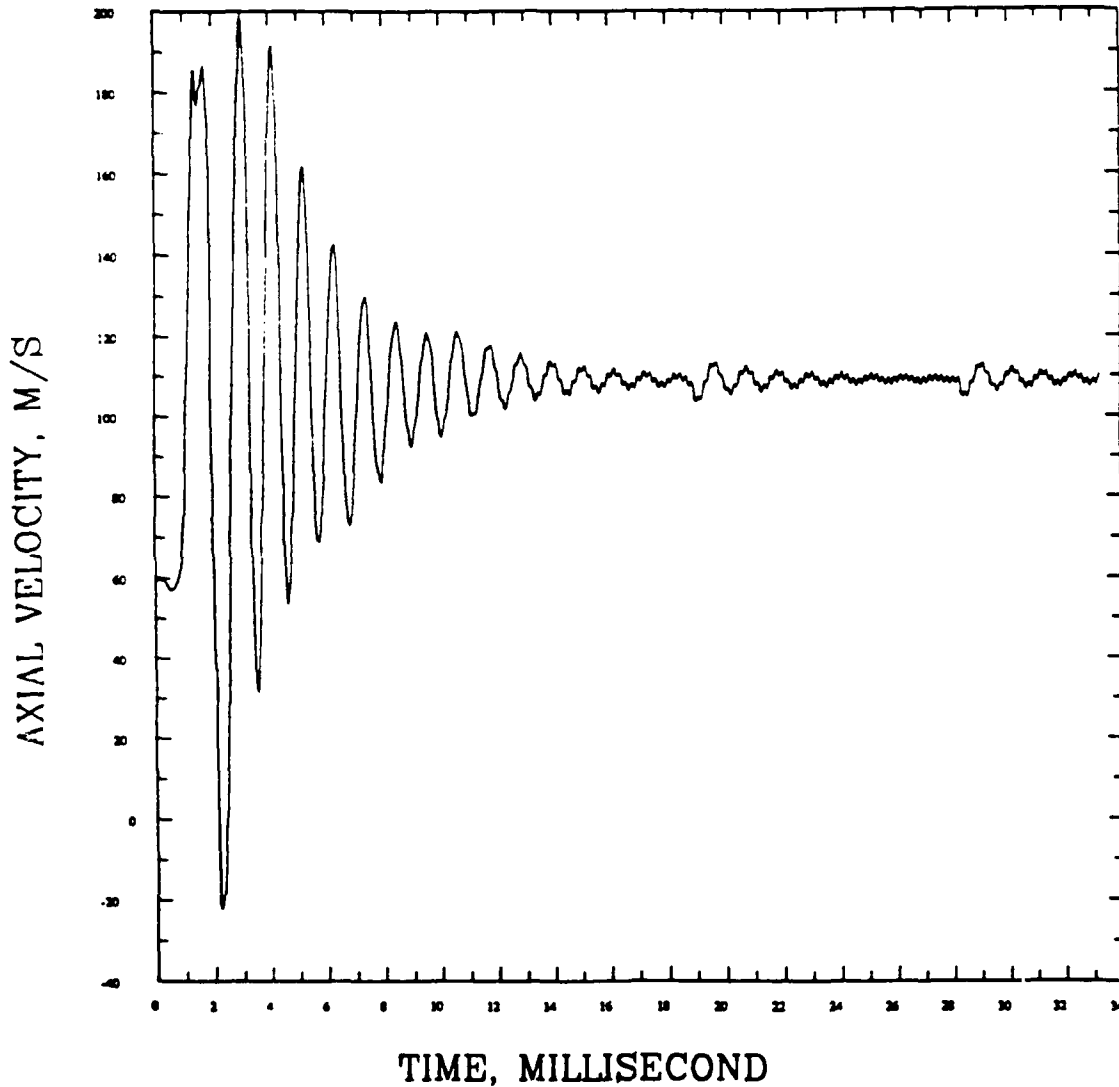


Figure D.2: Axial velocity vs. time for the quasi-one-dimensional case, mesh size of 100 by 10, initial drop radius of 50 microns, combustor length of 0.5 meter, inlet temperature=900K, $x=0.5L$.

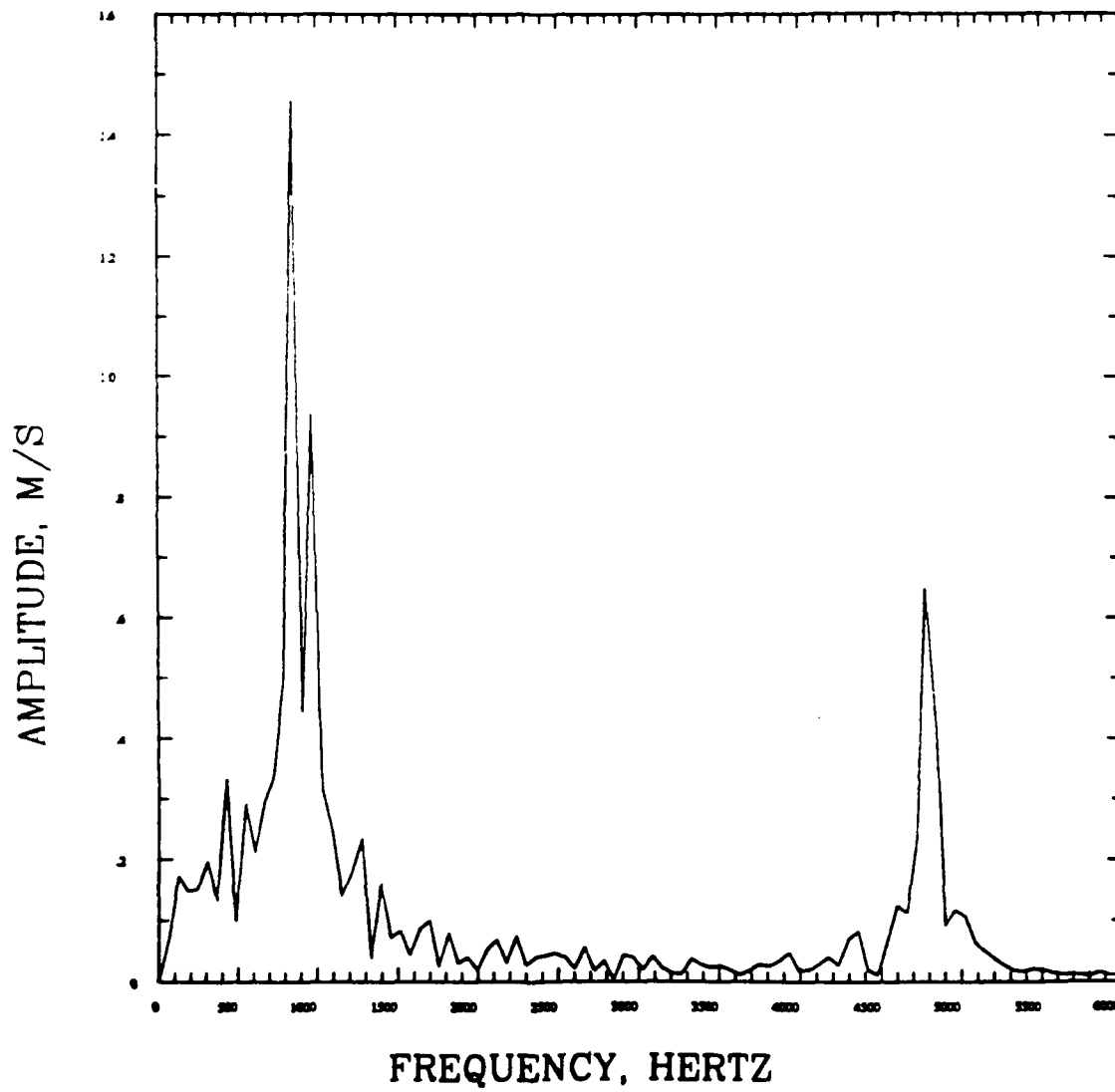


Figure D.3: Frequency spectrum of velocity for the quasi-one-dimensional case, mesh size of 100 by 10, initial drop radius of 50 microns, combustor length of 0.5 meter, inlet temperature=900K, $x=0.5L$.

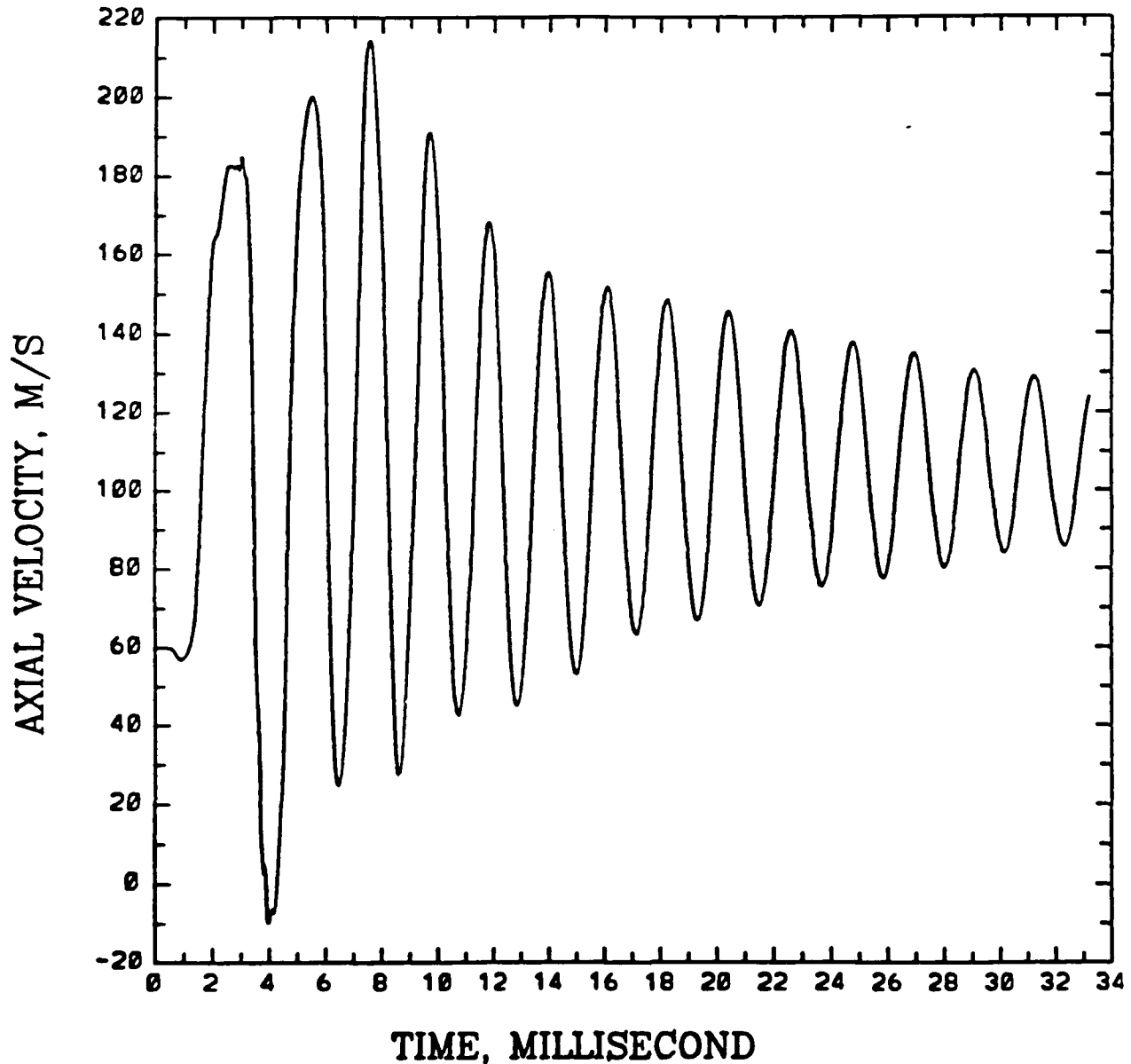


Figure D.4: Axial velocity vs. time for the quasi-one-dimensional case, mesh size of 100 by 10, initial drop radius of 75 microns, combustor length of 1.0 meter, inlet temperature=900K, $x=0.5L$.

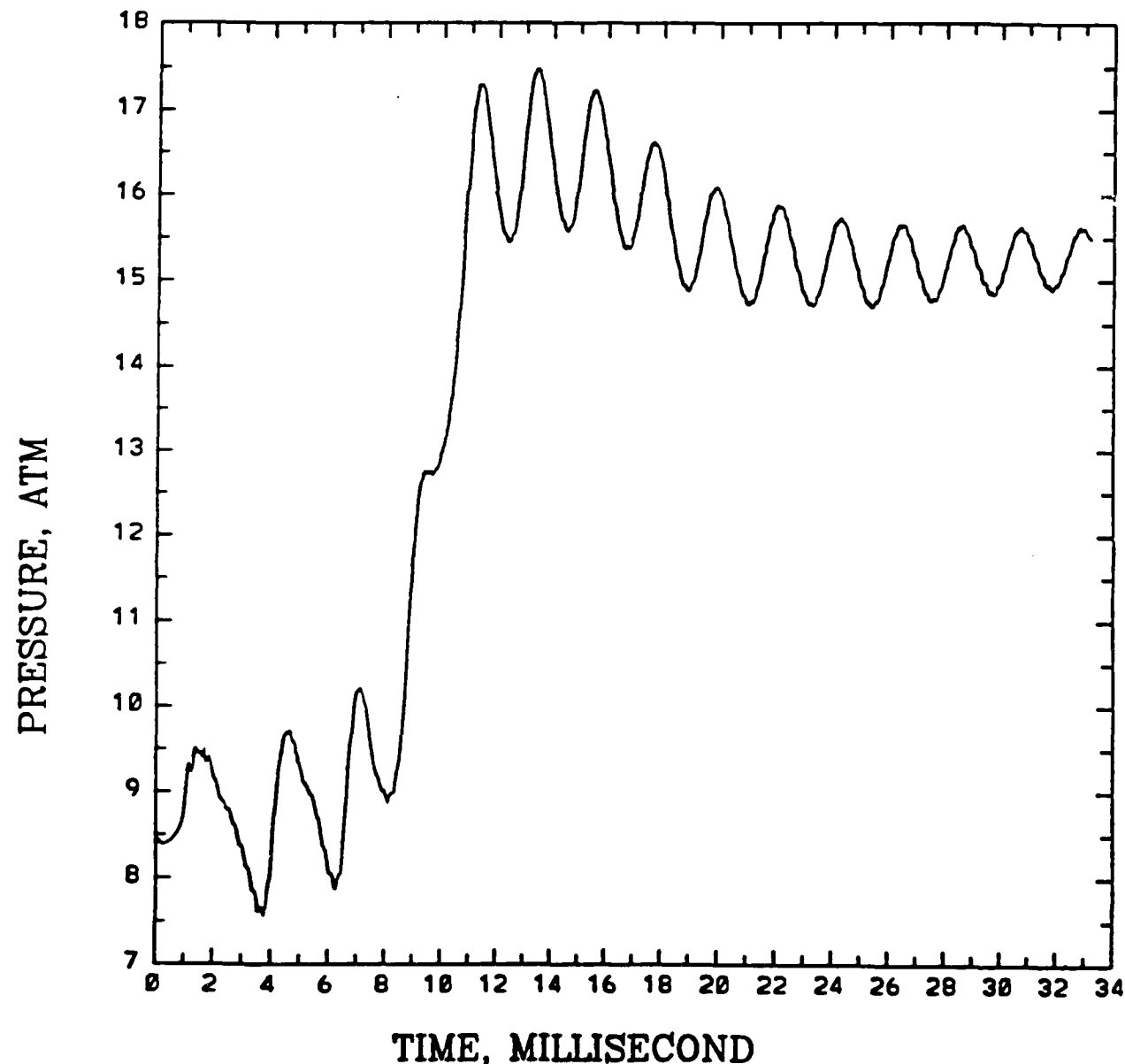


Figure D.5: Pressure vs. time for the quasi-one-dimensional case, mesh size of 100 by 10, initial drop radius of 75 microns, combustor length of 1.0 meter, inlet temperature=900K, $x=0.1L$.

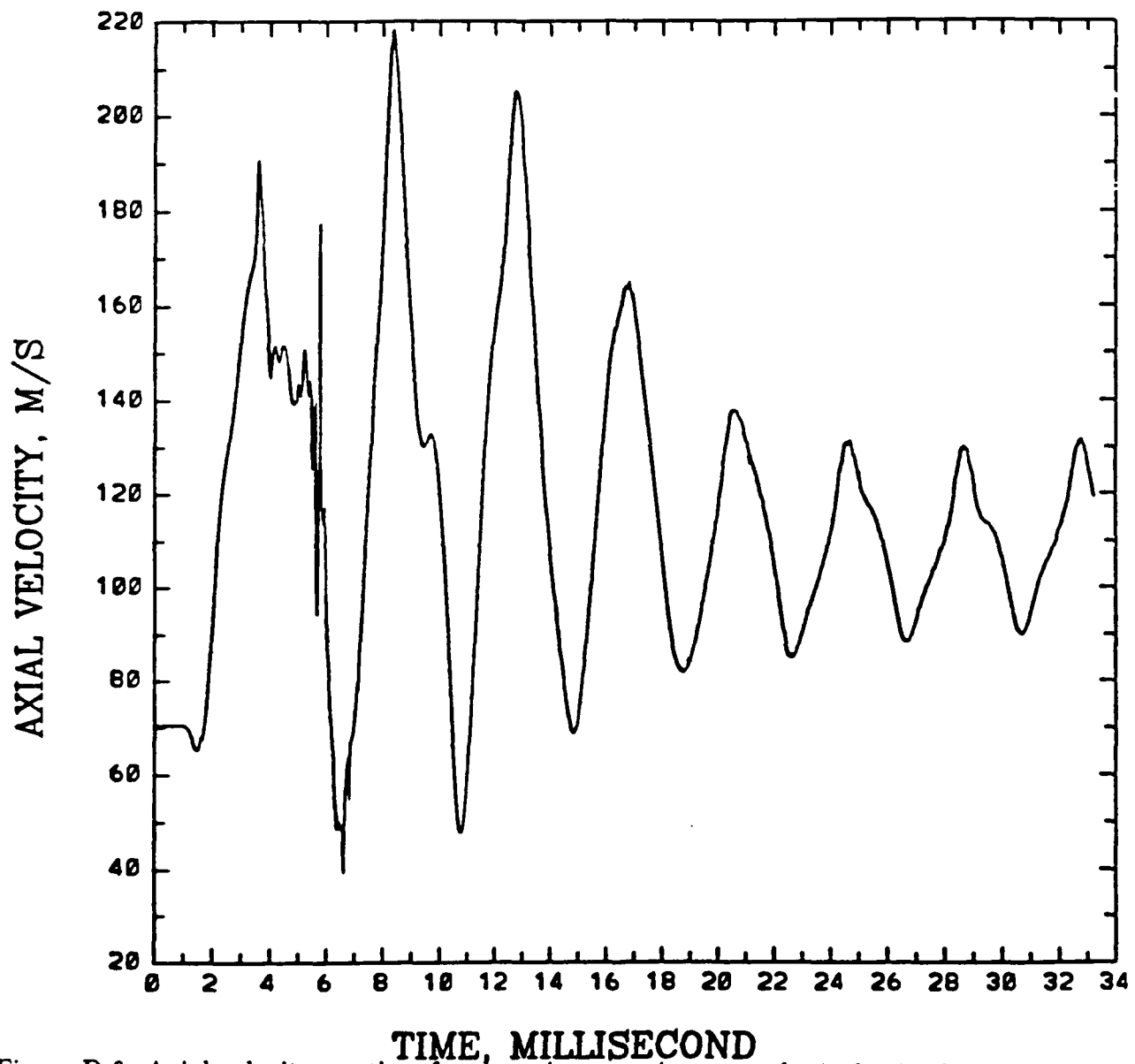


Figure D.6: Axial velocity vs. time for the axisymmetric case, only Arrhenius kinetics considered, mesh size of 100 by 20, initial drop radius of 100 microns, combustor length of 2.0 meters, inlet temperature=900K, $x=0.5L$.

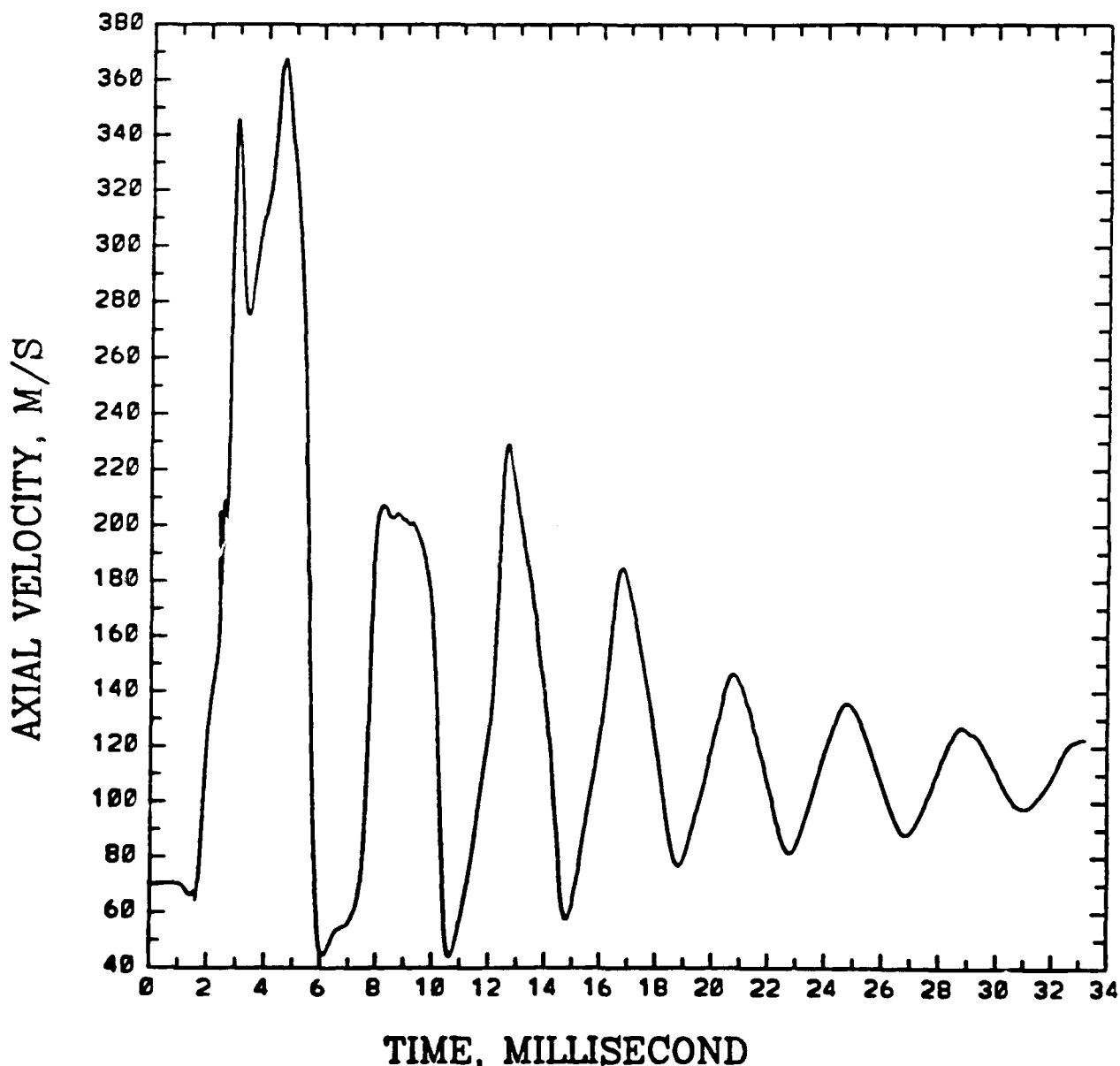


Figure D.7: Axial velocity vs. time for the axisymmetric case, only Arrhenius kinetics considered, mesh size of 100 by 20, initial drop radius of 75 microns, combustor length of 2.0 meters, inlet temperature=900K, $x=0.5L$.

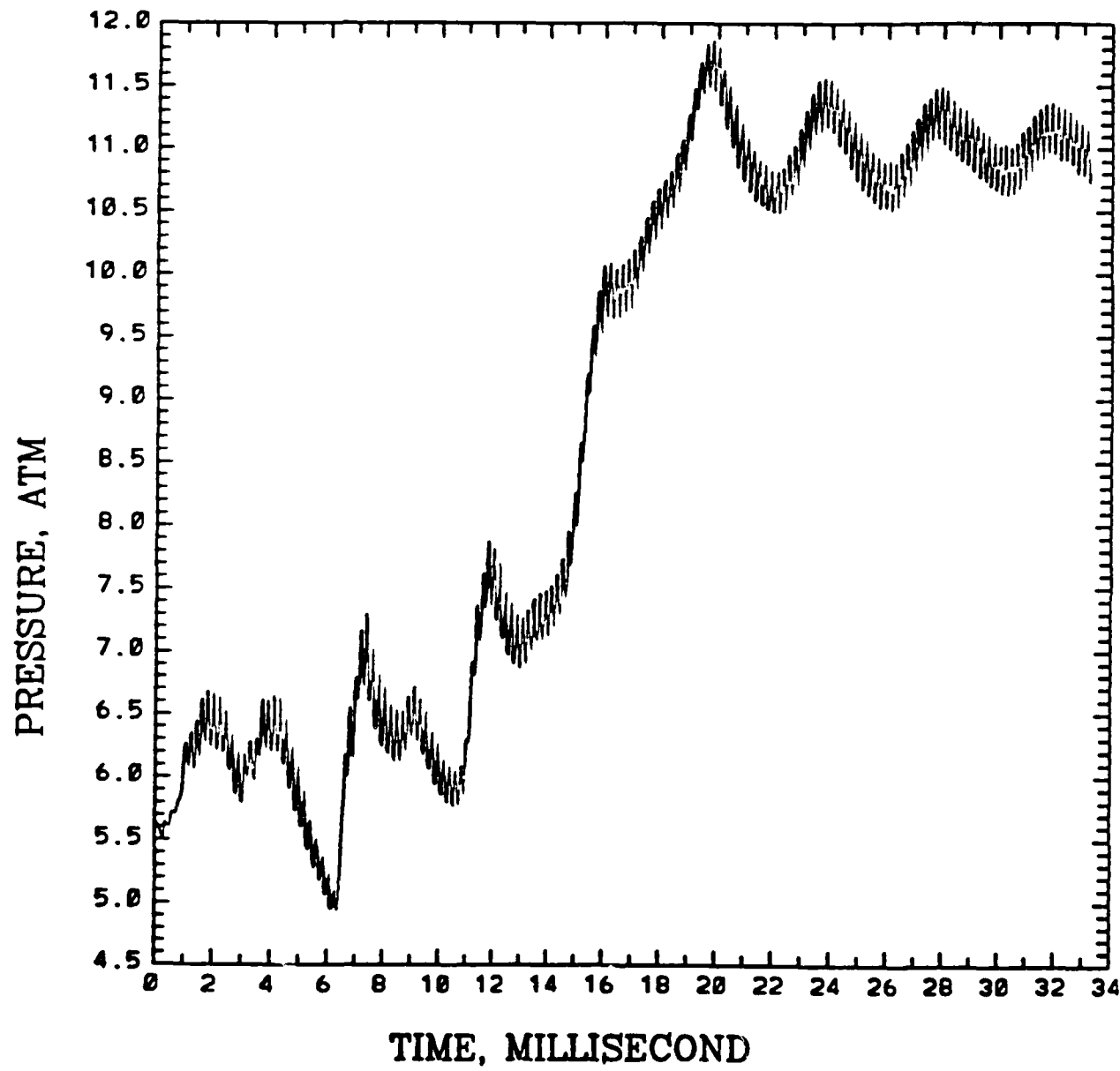


Figure D.8: Pressure vs. time for the axisymmetric case, only Arrhenius kinetics considered, mesh size of 100 by 20, initial drop radius of 75 microns, combustor length of 2.0 meters, inlet temperature=900K, $x=0.1L$.

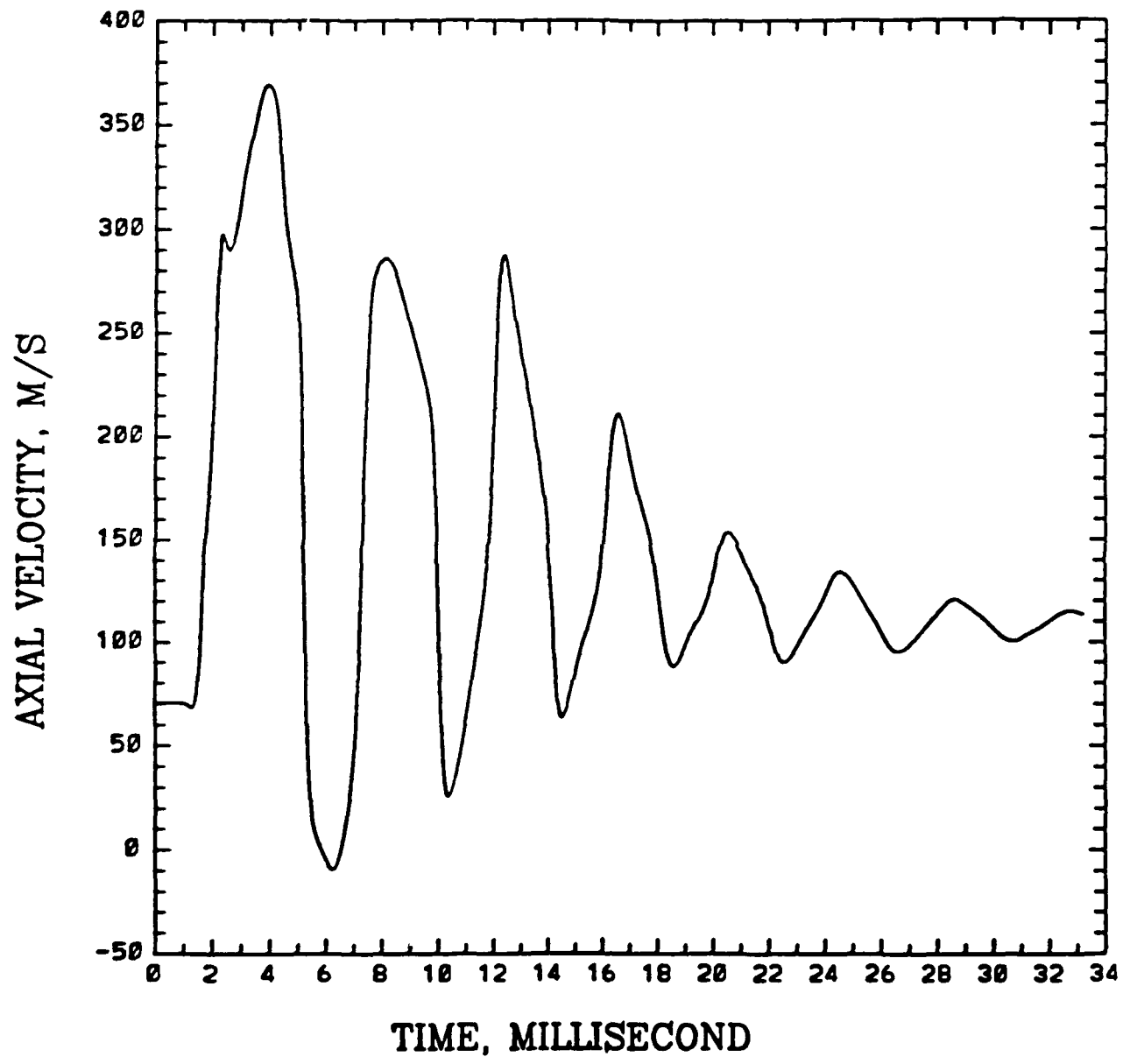


Figure D.9: Axial velocity vs. time for the axisymmetric case, only Arrhenius kinetics considered, mesh size of 100 by 20, initial drop radius of 50 microns, combustor length of 2.0 meters, inlet temperature=900K, $x=0.5L$.

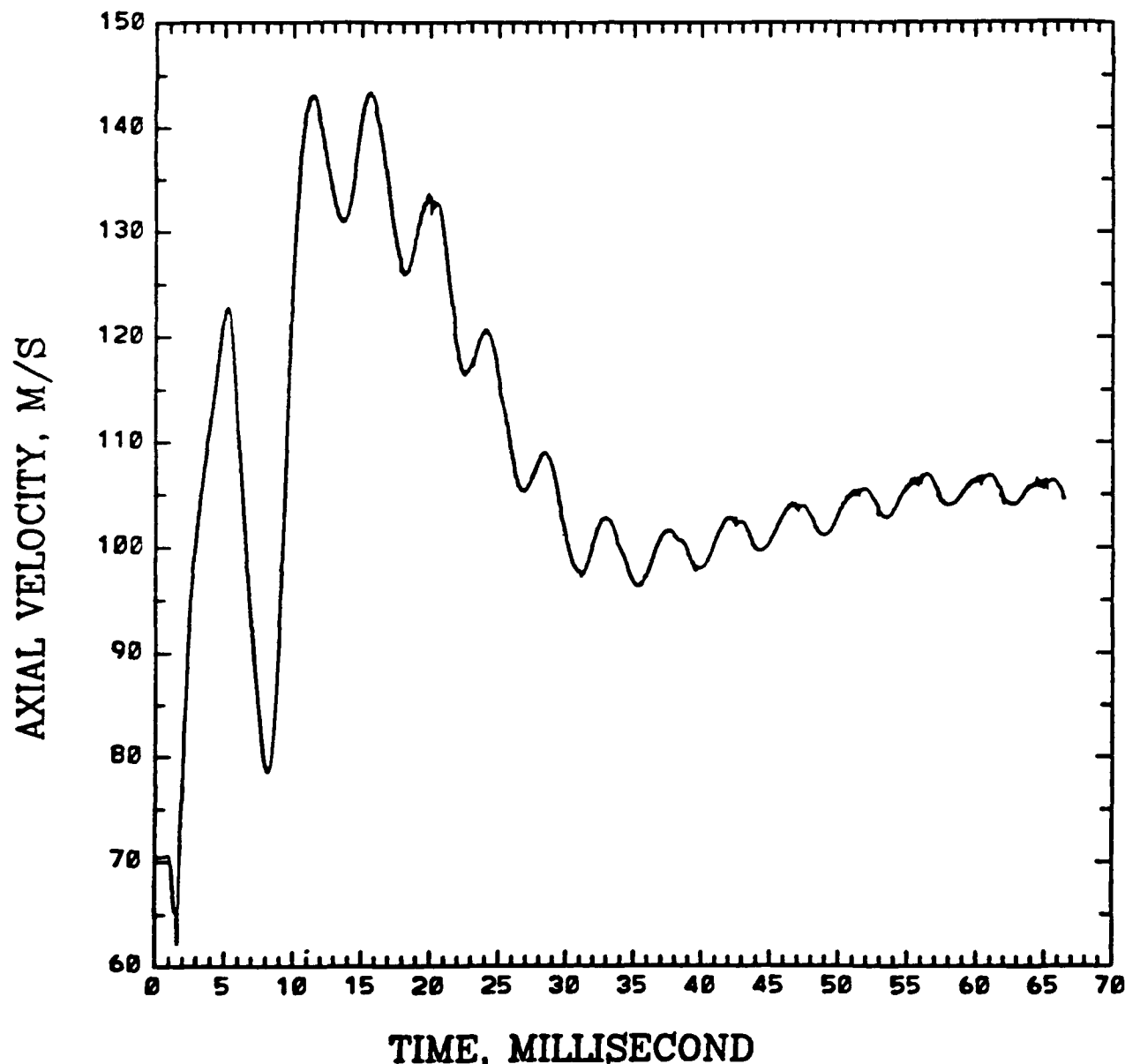


Figure D.10: Axial velocity vs. time for the axisymmetric case, both the Arrhenius kinetics and mixing effects considered, mesh size of 100 by 20, initial drop radius of 75 microns, combustor length of 2.0 meters, inlet temperature=900K, $x=0.5L$.

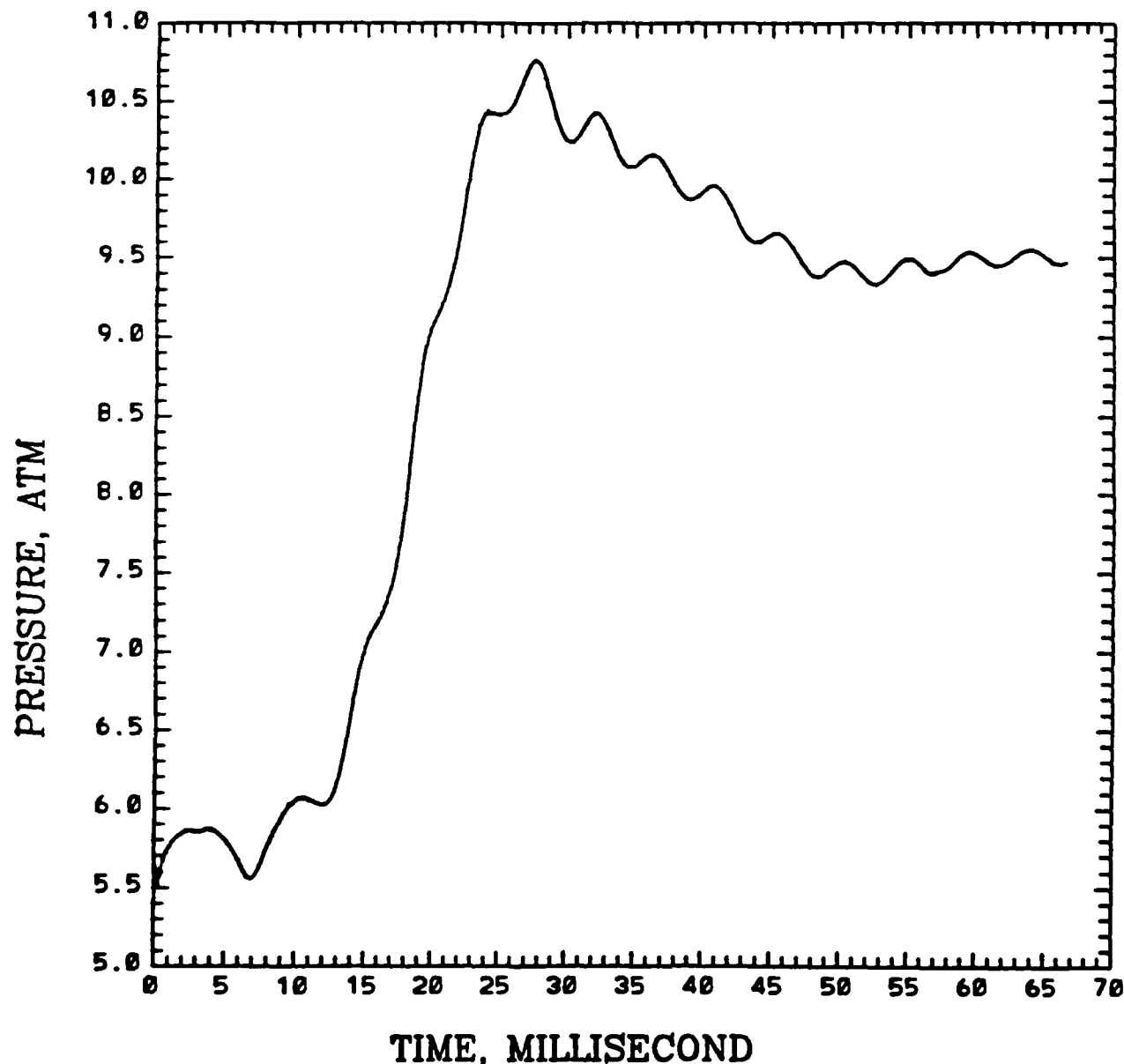


Figure D.11: Pressure vs. time for the axisymmetric case, both the Arrhenius kinetics and mixing effects considered, mesh size of 100 by 20, initial drop radius of 75 microns, combustor length of 2.0 meter, inlet temperature=900K, $x=0.1L$.